REALIZATION OF ALL OPTICAL SWITCH AND ROUTING DEVICES EXPLOITING THIRD ORDER NONLINEAR OPTICAL PROPERTIES

A Thesis Submitted to
the Graduate School of Engineering and Sciences of
Izmir Institute of Technology
in Partial Fulfillment of the Requirements for the Degree of

DOCTOR OF PHILOSOPHY

in Electronics and Communication Engineering

by
Osman AKIN

December 2012
IZMIR

We approve the thesis of **Osman AKIN**

Examining Committee Members:

Prof. Dr. M. Salih DİNLEYİCİ
Department of Electrical and Electronics Engineering/Izmir Institute of Technology

Prof. Dr. Necati ECEVİT
Department of Physics/Gebze Institute of Technology

Assoc. Prof. Dr. Alp KUŞTEPELİ
Department of Electrical and Electronics Engineering/Izmir Institute of Technology

Assoc. Prof. Dr. Sami SÖZÜER
Department of Physics/Izmir Institute of Technology

Assoc. Prof. Dr. Mustafa M. DEMİR
Department of Chemistry/Izmir Institute of Technology

17 December 2012

Prof. Dr. M. Salih DİNLEYİCİ
Supervisor
Department of Electrical and Electronics Engineering/Izmir Institute of Technology

Prof. Dr. F. Acar SAVACI
Head of the Department of Electrical and Electronics Engineering

Prof. Dr. R. Tuğrul SENGER
Dean of the Graduate School of Engineering and Sciences

ACKNOWLEDGMENTS

I would like to acknowledge the support of my thesis advisor Prof. Dr. M. Salih Dinleyici. Working with him as a PhD student I have had the possibility to see the whole path of a scientific work. He spent a significant amount of time and great effort for this work and always had time for my questions. I wish to thank him for his guidance, support and encouragement for both of scientific and non-scientific issues.

I am grateful to Assoc. Prof. Dr. Alp Kuştepeli and Assoc. Prof. Dr. Sami Sözüer for serving on my thesis committee.

I would like to express my sincere gratitude to Assoc. Prof. Dr. Mustafa M. Demir for allocating his laboratory for material preparation and involving to my thesis committee.

I would like to thank my parents for their unconditional support, patience and confidence.

Finally, I would like to express my special thanks to my wife, Fulya, for her endless love, patience, support and understanding throughout the years of this study.

ABSTRACT

REALIZATION OF
ALL OPTICAL SWITCH AND ROUTING DEVICES EXPLOITING
THIRD ORDER NONLINEAR OPTICAL PROPERTIES

In this thesis, we developed an in-fiber all optical switching device exploiting a transient grating as a control mechanism that was formed by interference of laser light beams via the Kerr effect. The switching device is designed by partial removal of the fiber cladding and replacing the polished cladding with a nonlinear polymer film (slab waveguide) that exhibits higher third order (Kerr) optical nonlinearity. The proposed device structure is analyzed considering Four Wave Mixing (FWM) of Gaussian beams of the grating and propagating modes of the optical fiber in the evanescent region where the nonlinear material is placed. The fields of modes and the grating forming beams interact in the nonlinear medium according to the matching conditions and evoke power transfer among the fiber modes. Thus, the coupling between the modes is directed by means of the transient grating. In the experimental part, polymeric thin films are prepared and linear refractive indices are measured using Fresnel diffraction method (developed in the laboratory) by matching the model with the experimental output. Then, z-scan method is employed to characterize the third order nonlinear optical properties of the thin films and pump-probe experiments are exploited to ensure existence of the transient grating and its diffraction capability. Finally, the side polished fiber is coated with the Methyl Red doped PVA composite polymer and by generating transient gratings on the polymer film, the switching capability of the device is introduced. The switching can be achieved either by a bulk refractive index change (no grating) or a transient grating between the modes of the optical fiber.

ÖZET

ÜÇÜNCÜ DERECEDEN DOĞRUSAL OLMAYAN OPTİK ÖZELLİKLER KULLANARAK TAMAMEN OPTİK ANAHTAR VE YÖNLENDİRİCİLERİN GERÇEKLEŞTİRİLMESİ

Bu tezde, geçici ızgara yardımıyla fiber üzerinde tamamen optic anahtarlama yapabilen bir aygıt geliştirildi. Geçici ızgara lazer ışınlarının giriştirilmesiyle Kerr etkisine bağlı olarak oluştu. Anahtarlama aygıtı, fiber kılıfının kısmi olarak kazınması ve yerine üçüncü dereceden optic doğrusalsızlık özelliğine sahip bir polimerin yerleştirilmesiyle oluşturuldu. Önerilen cihaz analitik olarak incelenirken, ızgarayı oluşturan iki lazer hüzmesi ve fiberin ilerleyen modunun etkileşimi Dört Dalga Karışımı olarak ele alındı. Buna gore fiber modu ile lazer hüzmeleri üçüncü dereceden doğrusalsızlık özelliğine sahip bir ortamda etkileştiklerinde, faz eşleme sağlanması durumunda fiber modları arasında güç transferi gerçekleşmektedir. Dolayısıyla, modlar arası güç aktarımı geçici izgara tarafından sağlanmaktadır. Çalışmanın deneysel bölümünde öncelikle polimer film hazırlandı ve Fresnel kırınımı metodu kullanılarak polimerin doğrusal kırılma indisi bulundu. Z tarama yöntemi kullanılarak bu polimer ile oluşturulan ince filmin üçüncü dereceden doğrusalsızlık karakteristiği elde edildi ve "pump probe" tekniği kullanılarak geçici ızgaranın varlığı ve onun kırınım özelliği araştırıldı.Son olarak, fiberin kazınmış yüzeyi kompozit polymer film ile kaplandı ve filmde oluşturulan geçici kırınım ızgaraları ile aygıtın anahtarlama yeteneği ortaya çıkarıldı. Anahtarlama özelliği, farklı mekanizmalar sonucu, hem geçici kırılma indisi değişimi(ızgara oluşturulmadan), hem de ızgara oluşturularak modlar arasında güç transferi ile gerçekleştirilebildiği gösterildi.

TABLE OF CONTENTS

LIST OF FIGURES

LIST OF TABLES

CHAPTER 1

INTRODUCTION

Dramatic increase of data traffic in current communication networks leads to a huge demand for higher bandwidth and faster all optical signal processing elements in the physical layer of the optical networks. The fourth generation telecommunication networks, triple play multimedia services and many other digital communication services like IPTV and video streaming website are examples of these high capacity systems. While the speed of electronic systems is limited to 120 Gbit/sec [1], optical systems provide nearly unlimited bandwidth (>Terahertz) and ultrafast response for optical signal processing applications. Recently many all optical devices have been presented to control/process the flow of information in photonic systems [2]. The most common and easiest way to introduce an optical device is to insert a bulk element like grating, lens or mirror on the path of the optical data. However, the integration of these components into the backbone requires interruption of the optical fiber that leads to high insertion loss, power loss due to reflections and poor mechanical integrity. Another method is the realization of in-fiber optical devices that are based on altering the light guiding properties of the waveguide. The implementation of the optical function is based mainly on creating a disturbance: instantaneous change in refractive index, absorption, polarization, etc. of host materials provided by an applied optical control signal. Because of linearity of the Maxwell's equations, all optical devices require nonlinear interaction between light and matter. Thus, to provide control of light with light, all of the host materials should exhibit optical nonlinearities.

Designing a faster all optical routing components is one of the most desired goals in the field of all-optical information processing. The invention of high-power lasers made it possible to realize photonic components based on optical nonlinearities requiring high power densities. However, researchers are investigating novel approaches in all optical switching requiring low light level optical processing. Another limitation in developing optical switches is finding an appropriate material with high nonlinearity, small nonlinear absorption and ultrafast response. Although there are many literature works about characterization of nonlinear materials for potential application in all optical switching devices, there has been no commercial integration as a complete all optical routing/switching instruments.

Optical switching technologies may be classified in many ways. They can be roughly divided into groups according to the domains [3]: space, wavelength and time domains. The classification may also be realized by considering the physical effect and material used in device fabrication. Although nonlinear optics is a hot topic since 1960's, there has not been a convergence on the material set that best suits the needs of all optical devices. Currently, optical switching is achieved by means of rare earth–doped optical fiber amplifiers, semiconductor optical amplifiers [4], semiconductors and nonlinear crystals. Applications include all optical switches based on optical patterns created in nonlinear medium [2], modulators [5], wavelength converter [6], grating based in-fiber optical switch [7] and optical gates based on third order nonlinearity [8] for integrated photonic circuits, all optical flip-flops fabricated on a Silicon-on-Insulator (SOI) platforms [9]. However, most of these devices are far from being satisfactory for the current requirements of optical packet switching. These requirements include low switching power, scalability, high switching efficiency, high switching rate and low power consumption,

Traditional in-fiber devices are composed of a structure on the light path (fiber core) that induces phase shift, wavelength selection or blocking function on the propagating wave. There are numerous publications for all-optical switching based on stationary gratings externally written on the fiber core [10]. Mach Zehnder interferometers [11] and Sagnac interferometers [12] are also common structures in all optical switching implementations. However, in some publications it was proposed that a periodic perturbation created in the cladding can affect the fundamental core mode and demonstrated that perturbations created in the cladding offer lower attenuation and flexible spectral characteristics in comparison with traditional fiber core index modulated grating [13].

On the material side, organic polymeric materials exhibits strong optical nonlinearities and may be good candidates for all optical switching devices. Third order optical nonlinear processes (Kerr type) in polymeric materials offer great advantages in terms of response time, high nonlinearity and processing simplicity [4]. Kerr effect is known as one of the fastest phenomena that can be exploited to design a high speed all-optical switching mechanism [14].

The stimulus of my thesis arises from these considerations: we have utilized nonlinear polymer to realize all optical in-fiber switching device based on a mode vulnerability that has great potential to be used as fast switching mechanism. In this dissertation, we demonstrate an ultrafast all-optical switch based on a coupler structure that consists of a side polished single mode fiber and the nonlinear polymer slab waveguide as shown in figure 1.1.

The refractive index of the dye doped polymer slab waveguide can locally be altered with a transient grating generated by interference of control laser pulses.

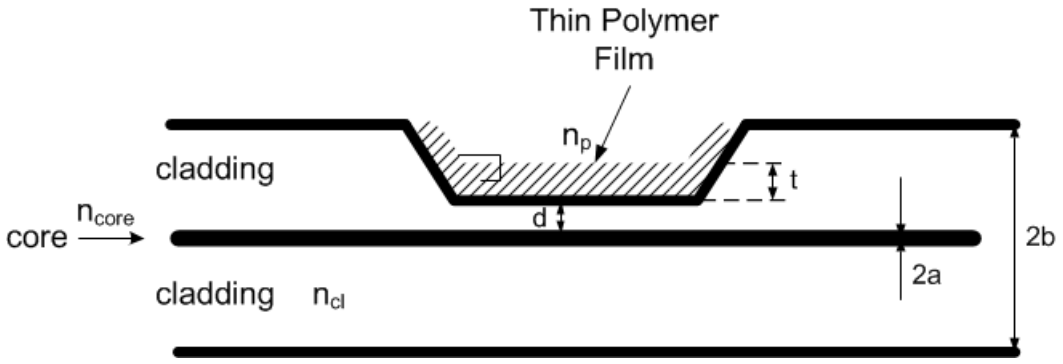

Figure 1.1. Geometry of the Switching Device with Polymeric Layer

Refractive index modulation arising from intensity dependent Kerr effect becomes in the shape of the control beams interference pattern profile. The nonlinear medium enables the interaction of the propagating mode with the grating forming laser control light in the evanescent region of the waveguide that results in all optical switching as result of Four Wave Mixing (FWM). Due to fast response time (fs) of Kerr type materials this method gives possibility to achieve high optical switching rates of about tens of Gbits/s that is suitable for recent optical communication systems.

CHAPTER 2

MATHEMATICAL MODEL FOR ALL OPTICAL SWITCHING MECHANISM

This chapter provides theoretical foundation of the in-fiber all optical switching device that is capable of realizing the fast all optical switching. In this study we investigate the mode switching capability of a transient laser-induced grating formed by interference of Gaussian beams at the core cladding boundary of a waveguide. Although this mathematical model is about power coupling from fundamental mode into higher order modes due to Four Wave Mixing (FWM) interactions, it is also useful for investigation of power coupling between different wavelengths that satisfy FWM conditions. Furthermore, we look for the transient grating parameters that maximize the conversion efficiency and investigate the spectral characteristics of the switch. Finally, we determine the tuning parameters of the transient grating that affect the transmission efficiency of the whole system.

2.1 Third Order Optical Nonlinearity

The origin of the optical nonlinearity lies in the nonlinear response of an optical material to an applied strong optical field (laser beam). The properties of a dielectric medium through which an optical wave propagates can be described by the relation between the polarization $\mathcal{P}$ and the electric field vector $\mathcal{E}$ expressed in Taylor series expression in the form [12], [20]

$$\mathcal{P} = \varepsilon_0 \chi \mathcal{E} + 2d\mathcal{E}^2 + 4\chi^{(3)}\mathcal{E}^3 + \cdots = \mathcal{P}_L + \mathcal{P}_{NL} \tag{2.1}$$

where χ is the linear susceptibility, d and $\chi^{(3)}$ are second-order and third-order nonlinear optical susceptibilities, respectively.

The propagation of light beams in a nonlinear medium is provided by wave equation given as

$$\nabla^2 \mathcal{E}(r,t) - \frac{1}{c^2}\frac{\partial^2 \mathcal{E}(r,t)}{\partial t^2} = \mu_0 \frac{\partial^2 \mathcal{P}_{NL}(r,t)}{\partial t^2} \tag{2.2}$$

Second order nonlinearity does not exist in centrosymmetric media, thus third order nonlinearity is the dominant effect and the nonlinear polarization can be written as

$$\mathcal{P}_{NL}(r,t) = 4\chi^{(3)}\mathcal{E}^3(r,t) \tag{2.3}$$

The response of a third order nonlinear medium to a monochromatic wave $\mathcal{E}(r,t) = Re\{E(r)\exp(j\omega t)\}$ yields polarization components at frequencies ω and 3ω given by $\mathcal{P}_{NL}(\omega) = 3\chi^{(3)}|E|^2E$ and $\mathcal{P}_{NL}(3\omega) = \chi^{(3)}E^3$. The existence of a component with frequency ω corresponds to a change of the susceptibility given by [12]

$$\varepsilon_0 \Delta\chi = \frac{\mathcal{P}_{NL}(\omega)}{E} = 3\chi^{(3)}|E|^2 = 6\chi^{(3)}\eta I \tag{2.4}$$

where optical intensity is given by $I = \frac{|E|^2}{2\eta}$. Refractive index is related to susceptibility by $n^2 = 1 + \chi$ which gives $2n\Delta n = \Delta\chi$ and leads to

$$\Delta n = \frac{3\eta}{\varepsilon_0 n}\chi^{(3)} I \equiv n_2 I \tag{2.5}$$

where n_2 is the optical Kerr coefficient and defined as

$$n_2 = \frac{3\eta_0}{n^2\varepsilon_0}\chi^{(3)} \tag{2.6}$$

The total refractive index in the material is given by

$$n(I) = n + n_2 I \tag{2.7}$$

As can be seen from the eq. (2.7), the total refractive index of the material depends on the intensity of the applied field. This effect is known as optical Kerr effect. During the derivation of this coefficient, we assume that the medium is non-resonant, that is, the energy of photons of applied optical field is much smaller than the band gap energy. The materials having this non-resonant nonlinear property exhibit a nearly instantaneous response time typically on the order of femtoseconds.

Table 2.1. Optical susceptibilities and response time of materials

Material	$\chi^{(3)}$	*Response Time*
Air	1.2×10^{-17}	
Carbon Disulfide	1.9×10^{-12}	2 ps
GaAs	6.5×10^{-4}	20 ns
GaAs / GaAlAs (MQW)	0.04	20 ns
Indium antimonide	0.3	400 ns
Semiconductor doped glass	10^{-8}	30 ps
Optical glasses	$(1- 100) \times 10^{-14}$	Very fast
Polydiacetylene	2.5×10^{-10}	Very fast

2.2 Four Wave Mixing (FWM)

Four-wave mixing is an essential third order nonlinear effect that will be exploited to realize the switching in the nonlinear region of the waveguide. For the description, the monochromatic plane wave can be written as

$$\mathcal{E}(r,t) = \frac{1}{2}(E(r)exp(-j\omega t) + c.c.) \tag{2.8}$$

where

$$E(r) = E_0 \exp\left(-j\vec{k}\cdot\vec{r}\right) \tag{2.9}$$

The effect of four wave mixing (FWM) can be understood by considering the response of the nonlinear medium to an optical field that consists of waves of frequencies ω_1, ω_2, ω_3 and ω_4 given by

$$\begin{aligned}\mathcal{E}(r,t) &= \sum_{q=1,2,3,4} Re\left\{E_q(r)exp\left(-j\omega_q t\right)\right\} \\ &= \sum_{q=\pm1,\pm2,\pm3,\pm4} \frac{1}{2}E_q(r)exp\left(-j\omega_q t\right)\end{aligned} \tag{2.10}$$

Wave propagation in third order nonlinear material is governed by the wave equation given by eq. (2.2) and third order nonlinearity is characterized by eq. (2.3). It is convenient to refine the wave equation as following

$$\nabla^2 \mathcal{E}(r,t) - \frac{1}{c^2}\frac{\partial^2 \mathcal{E}(r,t)}{\partial t^2} = -\mathcal{S}(r,t) \tag{2.11}$$

Where $\mathcal{S}$ is regarded as source of radiation given by

$$\mathcal{S}(r,t) = -\mu_0 \frac{\partial^2 \mathcal{P}_{NL}(r,t)}{\partial t^2} \tag{2.12}$$

After placing eq. (2.10) into eq. (2.12), corresponding source of radiation can be written as a sum of $8^3 = 512$ terms

$$\mathcal{S} = \frac{1}{2}\mu_0 \chi^{(3)} \sum_{q,p,r=\pm1,\pm2,\pm3,\pm4} \left(\omega_q + \omega_p + \omega_r\right)^2 \; E_q E_p E_r \times exp\left[j\left(\omega_q + \omega_p + \omega_r\right)t\right] \tag{2.13}$$

Substituting eq. (2.10) and eq. (2.13) into wave equation (2.11) results in four Helmholtz equations

$$\nabla^2 \mathcal{E} + k_q^2 \mathcal{E} = -\mathcal{S}_q\,, \quad q = 1,2,3,4 \tag{2.14}$$

where $\mathcal{S}_q$ is the amplitude of the component of $\mathcal{S}$ at frequency ω_q. In order for the wave to be coupled, their frequencies and phases must be matched. Consider the case shown

in figure 2.1 where three waves with frequencies ω_1, ω_2 and ω_3 recombine to form a new wave with frequency ω_4

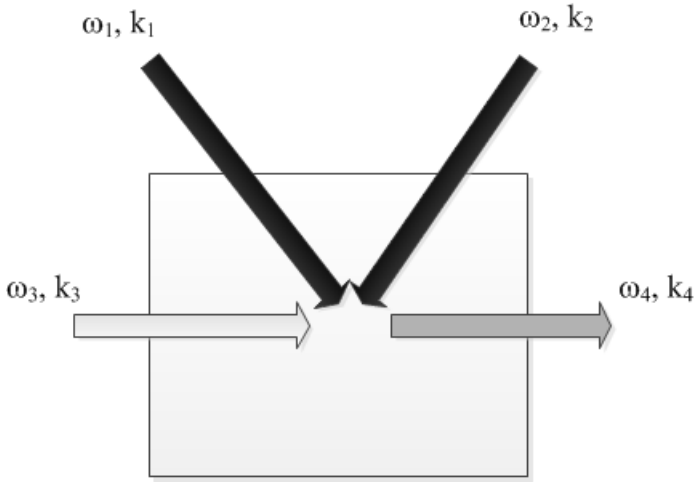

Figure 2.1. Four Wave Mixing in a nonlinear media

The frequency and phase conditions for efficient interaction are given by

$$\omega_4 = \omega_1 + \omega_2 - \omega_3 \tag{2.15}$$

$$\vec{k}_4 = \vec{k}_1 + \vec{k}_2 - \vec{k}_3 \tag{2.16}$$

The radiation source for each wave can be written as following

$$\mathcal{S}_1 = \mu_0 \omega_1^2 \chi^{(3)} \{6E_3 E_4 E_2^* + 3E_1[|E_1|^2 + 2|E_2|^2 + 2|E_3|^2 + 2|E_4|^2]\} \tag{2.17}$$

$$\mathcal{S}_2 = \mu_0 \omega_2^2 \chi^{(3)} \{6E_3 E_4 E_1^* + 3E_2[|E_2|^2 + 2|E_1|^2 + 2|E_3|^2 + 2|E_4|^2]\} \tag{2.18}$$

$$\mathcal{S}_3 = \mu_0 \omega_3^2 \chi^{(3)} \{6E_1 E_2 E_4^* + 3E_3[|E_3|^2 + 2|E_2|^2 + 2|E_1|^2 + 2|E_4|^2]\} \quad (2.19)$$

$$\mathcal{S}_4 = \mu_0 \omega_4^2 \chi^{(3)} \{6E_1 E_2 E_3^* + 3E_4[|E_4|^2 + 2|E_1|^2 + 2|E_2|^2 + 2|E_3|^2]\} \quad (2.20)$$

Each source component consists of two distinct parts. The first part of the source compromises the effect of mixing of other three waves to form the aforementioned radiation source. The second part represents the self-coupling of each wave.

In order to separate the contribution of each part, the radiation sources can be rewritten as following

$$S_q = \overline{S_q} + \left(\omega_q / c_0\right)^2 \Delta\chi_q E_q, \quad q = 1,2,3,4 \quad (2.21)$$

Where

$$\overline{S_1} = 6\mu_0 \omega_1^2 \chi^{(3)} E_3 E_4 E_2^* \quad (2.22)$$

$$\overline{S_2} = 6\mu_0 \omega_2^2 \chi^{(3)} E_3 E_4 E_1^* \quad (2.23)$$

$$\overline{S_3} = 6\mu_0 \omega_3^2 \chi^{(3)} E_1 E_2 E_4^* \quad (2.24)$$

$$\overline{S_4} = 6\mu_0 \omega_4^2 \chi^{(3)} E_1 E_2 E_3^* \quad (2.25)$$

and

$$\Delta\chi_q = 6\frac{\eta}{\epsilon_0}\left(2I - I_q\right), \quad q = 1,2,3,4 \tag{2.26}$$

$I_q = \left|E_q\right|^2/2\eta$ represent the intensities of the waves, $I = I_1 + I_2 + I_3 + I_4$ is the total intensity and η is the impedance of the medium. Thus, the Helmholtz equation (2.14) can be rewritten as [12]

$$\left(\nabla^2 + \bar{k}_q^2\right)E_q = -\bar{\mathcal{S}}_q, \quad q = 1,2,3,4 \tag{2.27}$$

Where

$$\bar{k}_q = \bar{n}_q\frac{\omega_q}{c_0} \tag{2.28}$$

$$\bar{n}_q^2 = n^2 + 2nn_2\left(2I - I_q\right) \tag{2.29}$$

$$n_2 = \frac{3\eta_0}{\epsilon_0 n^2}\chi^{(3)} \tag{2.30}$$

These equations are used to generate nonlinear coupling equations that may be solved for different boundary conditions. This approach can be applied to analyze a case of interaction of four waves in the evanescent region of the waveguide described in the next section.

2.3 All Optical Switching Using FWM Interactions

In this work we investigated a new in-fiber all optical switching device that consists of a transient grating formed by control laser beams according to the Kerr effect. The suggested device, shown in figure 2.2, is created by partial removal of the cladding and placing a material with high third order nonlinearity instead of a cladding material. The nonlinear medium enables the interaction of the propagating modes with the transient grating which is formed by the laser control light pulses. In this method, the existence of transient grating satisfies the switching operation, while the laser beam intensity is the control parameter. The switching efficiency can be controlled via total intensity. Additionally, higher Kerr coefficient of the cladding material implies lower intensity required for switching operation. Recent developments in polymer science can make it possible to realize this instantaneous switching with low level control light [4], [19].

The waveguide structure can be analyzed by considering Four Wave Mixing (FWM) of two Gaussian beams and the propagating mode in the region of core-cladding boundary where the fields of modes and grating forming fields are interacting in the

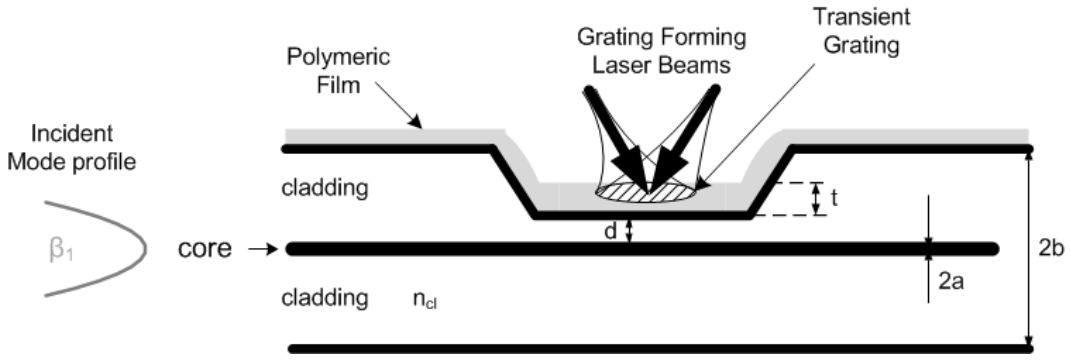

Figure 2.2. Schematic of optical switch based on transient grating

evanescent region of the waveguide and where nonlinear material is placed. The formed structure is close enough to the core-cladding boundary so that it may perturbate the guiding properties of the waveguide. In other words, the temporary grating destroys the

transverse resonance of the mode and couples the fundamental fiber mode into higher-order modes. Thus, this structure can be treated as a photonic crystal with a stop band allowing the propagation of only certain modes. Hereafter, the coupled wave equations for the propagating modes are obtained in the existence of the transient grating. Due to fast response time (fs) of Kerr type materials this method gives possibility to achieve high optical switching rates of about tens of Gbits/s for recent optical communication systems.

To begin with, consider a Two Mode Slab Waveguide with a cladding composed of third-order nonlinear material given in figure 2.3. The fundamental mode propagating in the waveguide is represented by U_3 with a propagation constant β_3 and higher order mode U_4 with propagation constant β_4. Furthermore, the grating forming Gaussian beams U_1 and U_2 at wavelength λ_L cross at half angle θ at the cladding side of the core-cladding boundary. The interaction of the propagating mode with the transient grating can be considered as a Four Wave Mixing (FWM) process in which grating forming beams U_1, U_2 and the propagating waveguide mode U_3 interact with each other and a fourth wave U_4 is formed as a result of this FWM interaction.

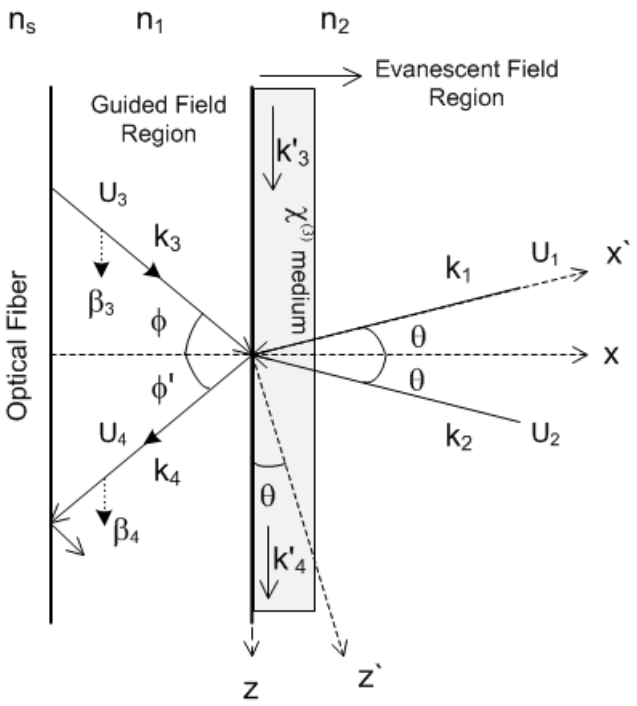

Figure 2.3. Four Wave Mixing at the core cladding boundary

This interaction permits a real time ultrafast switching capability considering the outward mode properties. Figure 2.3 shows the geometry of the interaction and the fields that are involved in the FWM process.

For the waves to be coupled, frequency and phase matching requirements are given by

$$\omega_1 + \omega_3 = \omega_2 + \omega_4 \tag{2.31}$$

$$\overrightarrow{k_1} + \overrightarrow{k_3} = \overrightarrow{k_2} + \overrightarrow{k_4} \tag{2.32}$$

where $\omega_1 = \omega_2$ and $\omega_3 = \omega_4$.

Because the light-matter interaction in this case results in a weak refractive index perturbation, the overall interaction process in the cladding can be analyzed using "Coupled Mode Theory". The detailed derivation of the coupled mode theory in the nonlinear medium can be found in Saleh [12], Boyd [20] and Yariv [21]. By using FWM matching conditions defined by (2.31) and (2.32), the Helmholtz equations given by eq. (2.27) takes the following form for incident and outgoing waves written as

$$\left(\nabla^2 + k_3^2\right)U_3 = -\zeta_3 \Psi U_4 - \gamma_3 U_3 \tag{2.33}$$

$$\left(\nabla^2 + k_4^2\right)U_4 = -\zeta_4 \Psi^* U_3 - \gamma_4 U_4 \tag{2.34}$$

where $\zeta_{3,4} = 6\mu_0 \omega_{3,4}^2 \chi^{(3)}$, $\gamma_{3,4} = 2n_{cl} n_2 \frac{\omega_{3,4}^2}{c_o^2}(2I - I_{3,4})$, n_{cl} is the cladding refractive index, n_2 is the Kerr coefficient, $I = I_1 + I_2 + I_3 + I_4$ is the total intensity and $I_{3,4} = \frac{\left|U_{3,4}\right|^2}{2\eta_0}$, $\chi^{(3)}$ is the third order nonlinear susceptibility and $\Psi = U_1^* U_2$ where U_1 and U_2 are the grating forming fields of the Gaussian beams.

In the interaction geometry shown in figure 2.3, the grating is formed by two

Gaussian beams traveling in the $-x'$ direction and beams' initial plane is $x' = L$. A Gaussian beam can also be expressed in terms of the propagation angle θ in (x, y, z) coordinate system. Using coordinate transformation and considering the paraxial approximation that involves small intersection angle θ, i.e., $\cos\theta = 1$ and $\sin\theta = \theta$, any traveling Gaussian beam can be written as:

$$U = \frac{A}{\rho(x,z,\theta)} \exp(jk\eta) \exp\left(-jk \frac{\Phi^2}{2\rho(x,z,\theta)}\right) \exp\{-j\omega t\} \tag{2.35}$$

where

$$\Phi^2 = \begin{cases} \Phi_+^2 = y^2 + (x\theta + z)^2, & \theta > 0 \\ \Phi_-^2 = y^2 + (-x\theta + z)^2, & \theta < 0 \end{cases} \tag{2.36}$$

$$\eta = \begin{cases} \eta_+ = x - z\theta - L, & \theta > 0 \\ \eta_- = x + z\theta - L, & \theta < 0 \end{cases} \tag{2.37}$$

If $x - L >> z\theta$, then $\rho = \rho_+ = \rho_- = x - L + jx_0$. In these equations A is a constant, x_0 is the Rayleigh range which is estimated by $\frac{\pi}{\lambda_L} W_0^2$, λ_L is the laser wavelength, W_0 is the minimum waist of Gaussian beam and Φ is the radial distance.

Assuming that both grating writing beams are originating from the same source; their wavelengths, beam magnitudes and waists can be considered equal. Although the interference equation consists of traveling and standing waves, a grating pattern is created by the stationary wave pattern given as [22]:

$$\Psi(x,y,z)=\frac{A^2}{|\rho|^2}\exp\left(-k_L x_0\frac{y^2+\left(x\sin(\theta)\right)^2+z^2}{|\rho|^2}\right)\cdot\cos\left[2k_L\sin\theta\left(1-x\frac{x-L}{|\rho|^2}\right)z\right] \quad (2.38)$$

where $|\rho|^2=|x''-L|^2+|x_0|^2$, $k_L=\frac{2\pi}{\lambda_L}$ and x'' is the intersection plane $x=x''$. The exponential part of this equation defines a Gaussian profile for the grating. The coefficient $k_L\frac{x_0}{|q|^2}$ acts like a diminishing factor in three dimensions, while grating period in the z direction depends on the intersection angle θ, writing beam wavelength λ_L and the interference plane ($x=0$). When the beam interference occurs at the plane $x=0$, the grating period along z direction can be written as $\Lambda=\frac{\lambda_L}{2\sin(\theta)}$, however the length of the grating pattern is bounded by the envelope function $-k_L x_0\frac{z^2}{|\rho|^2}$, which is a very convenient tool for tuning purposes.

2.4 Mode Conversion Switching by Means of Transient Grating

The total field in the interaction region can be written as the superposition of the ideal modes, as follows

$$U_3=\sum_m A_m(z)E_m(x,y)\exp\{-j\beta_m z\} \quad (2.39)$$

$$U_4=\sum_n B_n(z)E_n(x,y)\exp\{-j\beta_n z\} \quad (2.40)$$

where A_m and B_n are slowly varying amplitudes. E_m is the transverse field distribution of incident (fundamental) mode (m) and E_n is the transverse field distributions of the output (higher order) mode (n).

When we substitute (2.39) and (2.40) into (2.33) and (2.34), we obtain coupled mode equations for every mode:

$$\frac{dA_m}{dz} = -j\mathrm{K}_m(z)B_n(z)\exp\{-j(\beta_n-\beta_m)z\} + j\left(-\frac{\gamma_3}{2\beta_m}\right)A_m(z) \tag{2.41}$$

$$\frac{dB_n}{dz} = -j\mathrm{K}_n(z)A_m(z)\exp\{j(\beta_n-\beta_m)z\} + j\left(-\frac{\gamma_4}{2\beta_n}\right)B_n(z) \tag{2.42}$$

where K_m and K_n are mode coupling coefficients denoted as:

$$\mathrm{K}_m(z) = \frac{|\beta_m|}{\beta_m}\frac{1}{4\omega\mu}\zeta_3 C_{mn}(z)\ ,\ \mathrm{K}_n(z) = \frac{|\beta_n|}{\beta_n}\frac{1}{4\omega\mu}\zeta_4 C_{nm}(z) \tag{2.43}$$

and C_{nm} is the overlap integral coefficient, which can be written as:

$$C_{nm}(z) = \iint_S \Psi(x,y,z)E_m(x,y)E_n^*(x,y)dxdy \tag{2.44}$$

where $\Psi(x,y,z)$ is the corrugation (grating) function that disrupts the orthogonality of transverse fields. This function results from the interference of Gaussian beams described in (2.38).

The exact solution of coupled wave equations (2.41) and (2.42) is possible only for uniform grating structures. Non-uniform gratings can be analyzed using numerical approximations. Generalized transfer matrix method [23], effective index method [24], Bloch Wave Analysis [25], Rouard's method [26] are the best known approaches for

analyzing non-uniform grating structures. In this study, we prefer expanding the non-uniform grating function into Fourier series. Considering the length of the grating as L_g grating depth as L_{int} and the period of the grating in the z- direction as $\Lambda = \frac{\lambda_L}{2\sin\theta}$, the waveguide corrugation function can be written as:

$$\Psi(x,y,z) = \frac{A^2}{|\rho|^2}\exp\left(-k_L x_0 \frac{y^2}{|\rho|^2}\right)\mathrm{H}(x,z) \tag{2.45}$$

where $\mathrm{H}(x,z)$ can be expressed in terms of Fourier series as

$$\mathrm{H}(x,z) = \sum_{p,r} F_{p,r}\exp\left(i\frac{2\pi p}{L_g}z\right)\exp\left(i\frac{2\pi r}{L_{\text{int}}}x\right) \tag{2.46}$$

Fourier coefficient $F_{p,r}$ is the solution to the integral

$$F_{p,r} = \frac{1}{L_g L_{int}}\int_{-\frac{L_g}{2}}^{\frac{L_g}{2}}\int_{-\frac{L_{int}}{2}}^{\frac{L_{int}}{2}} exp\left(-k_L x_0\frac{(x\sin\theta)^2+z^2}{|\rho|^2}\right)\times\cos\left[2k_L\sin\theta\left(1 - x\frac{x-L}{|\rho|^2}\right)z\right] exp\left(-i\frac{2\pi r}{L_{int}}x\right)\exp\left(-i\frac{2\pi p}{L_g}z\right)dxdz \tag{2.47}$$

The definition of the interaction length L_{int} of the beams can be found in [24], where it is given by $L_{\text{int}} = \frac{W_0}{\theta} = \frac{\pi W_0^2}{N_f \lambda_L}$ and $\mathrm{N_f}$ is the number of interference fringes.

Considering the solution of the coupled equations (2.41) and (2.42) for each

harmonic q corresponding to each Fourier coefficient parameter (p, r) related to the grating function (2.45), total amplitudes of the propagating modes in the waveguide can be written as:

$$A_m(z) = \sum_q A_q(z) = \sum_{p,r} A_{p,r}(z) \tag{2.48}$$

$$B_n(z) = \sum_q B_q(z) = \sum_{p,r} B_{p,r}(z) \tag{2.49}$$

Applying boundary conditions $A(0) = A_{0,p,r}$, $B(0) = 0$ and assuming that total optical power is conserved within the waveguide $\left[\frac{d}{dz}\left(|A_m|^2 + |B_n|^2\right) = 0\right]$, the solution for each harmonic can be written as:

$$A_{p,r}(z) = \left[A_{0,p,r}\cos\left(Q_{p,r}z\right) + j\frac{A_{0,p,r}}{Q_{p,r}}\hat{\delta}_{p,r}\sin\left(Q_{p,r}z\right)\right]\cdot\exp\left(-j\delta_{p,r}z + j\frac{\alpha_a+\alpha_b}{2}z\right) \tag{2.50}$$

$$B_{p,r}(z) = -j\frac{\mathrm{K}_{n,p,r}}{Q_{p,r}}A_{0,p,r}\sin\left(Q_{p,r}z\right)\cdot\exp\left(j\delta_{p,r}z + j\frac{\alpha_a+\alpha_b}{2}z\right) \tag{2.51}$$

where $\mathrm{K}_{m,p,r}$ and $\mathrm{K}_{n,p,r}$ are the amplitudes of coupling coefficients $\mathrm{K}_{m(n),p,r}(z) = \mathrm{K}_{m(n),p,r}\exp\left(i\frac{2\pi p}{L_g}z\right)$ for each harmonic of modes (m) and (n), respectively. These coefficients can be written as:

$$\mathrm{K}_{m,p,r} = \frac{|\beta_3|}{\beta_3}\frac{1}{4\omega\mu}\zeta_3 C_{mn,p,r} \tag{2.52}$$

$$\mathrm{K}_{n,p,r} = \frac{|\beta_4|}{\beta_4}\frac{1}{4\omega\mu}\zeta_4 C_{nm,p,r} \tag{2.53}$$

$C_{nm,p,r}$ and $C_{mn,p,r}$ are the integral coefficients related with the orthogonality of the propagating modes and they are given by ($C_{nm,p,r} = C_{mn,p,r}$):

$$C_{p,r} = \iint_S \frac{A^2}{\rho^2} F_{p,r} \exp\left(-k_L x_0 \frac{y^2}{|\rho|^2}\right) \cdot \exp\left(i\frac{2\pi r}{L_{\text{int}}}x\right) E_m(x,y) E_n^*(x,y)\, dxdy \tag{2.54}$$

where $F_{p,r}$ is defined in (2.34).

Assuming $\mathrm{K}_{p,r} = \mathrm{K}_{m,p,r} = \mathrm{K}_{n,p,r}$, we find the Q parameter as $Q_{p,r}^2 = \mathrm{K}_{p,r}^2 + \hat{\delta}_{p,r}^2$, where the detuning parameter $\hat{\delta}_{p,r}$ is written in terms of the phase matching parameter $\delta_{p,r}$ and self-coupling coefficients α_a and α_{b} as $\hat{\delta}_{p,r} = \delta_{p,r} + \frac{\alpha_a - \alpha_b}{2}$. Self-coupling coefficients arise from the third order nonlinearity and depend on the Kerr nonlinearity and total intensity I. These coefficients can be written as:

$$\alpha_{a,b} = -\frac{2n_{cl}n_2\frac{\omega_{3,4}^2}{c_0^2}(2I - I_{3,4})}{2\beta_{3,4}} \tag{2.55}$$

If we assume that grating forming beams are traveling in x-z plane, then the grating profile in y-direction has the Gaussian profile centered at $y = 0$ and has a solely effect

on breaking the mode orthogonality as specified in (2.54). This is also the case for the r-components in x-direction, which mainly affect resonance breaking mechanism. Hence, phase matching parameter $\delta_{p,r}$ can be written in terms of mode propagation constants β_3 and β_4, grating length L_g and Fourier coefficient parameter p (pointing spatial frequency along z direction) as follows:

$$\delta_{p,r} = \frac{1}{2}\left(\beta_4 - \beta_3\right) + \frac{\pi p}{L_g} \tag{2.56}$$

where L_g is the grating length. Considering the mode amplitudes given by (2.50) and (2.51), total mode conversion efficiency resulting from transient grating is:

$$\eta = \frac{\left|B_n\left(L_g\right)\right|^2}{\left|A_m\left(0\right)\right|^2} = \sum_{p,r} \frac{\mathrm{K}_{p,r}{}^2}{Q_{p,r}^2} \sin^2\left(Q_{p,r} L_g\right) \tag{2.57}$$

The maximum efficiency can be obtained when detuning parameter $\hat{\delta}_{p,r} = 0$. Satisfying this condition leads to the following simple relation:

$$\beta_4\left(1 + n_{cl}\frac{\Delta n_4}{n_{eff\,4}^2}\right) = \beta_3\left(1 + n_{cl}\frac{\Delta n_3}{n_{eff\,3}^2}\right) - \frac{2\pi}{L_g} p \tag{2.58}$$

where $\Delta n_{3,4} = n_2\left(2I - I_{3,4}\right)$, n_{eff} is the effective refractive index of the related mode and mode propagation constants can be written as $\beta_{3,4} = \frac{2\pi}{\lambda} n_{eff\,3,eff\,4}$. Since Δn depends on intensity I, the conversion process can be tuned by varying the total intensity and

therefore it can be used as a control parameter to provide perfect phase matching. However, interference half angle θ and material nonlinearity $\chi^{(3)}$ are parameters that can be used as design parameters to obtain high index variation Δn. Assuming that phase matching requirement is met, then maximum efficiency can be obtained by satisfying $Q_{p,r} L_g = K_{p,r} L_g = \frac{\pi}{2}$ for each component of the mode.

2.5 Mathematical Model Simulation Results

Consider an asymmetric slab waveguide that allows only two modes to propagate at communication wavelength $\lambda = 1550\, nm$. Assume that cladding is made of polymeric nonlinear material with refractive index $n_{cl} = 2.32$ and the core refractive index is $n_{core} = 2.4$. Using the dispersion relation for planar dielectric waveguide given in [12], the propagation constants of fundamental mode and higher order mode are calculated as $\beta_3 = 9.708 \times 10^6$ and $\beta_4 = 9.6 \times 10^6$ for $\omega = 1203.2 \times 10^{12}$ rad/s. By taking the slab thickness as 2 μm only two modes are allowed to propagate and introducing a cladding thickness of 750 μm, approximately 4% of the total power flows in the cladding region. The beam minimum waist is $W_0 = 1\, mm$ and the distance between laser minimum waist location and intersection point is $L = 1\, mm$. The period of the resulting grating is $\Lambda = 25.4\ \mu$m as shown in figure 2.4. This structure can also be regarded as a one dimensional periodic medium placed in the waveguide cladding, where refractive indices of the successive stacks are n_{cl} and $n_{cl} + \Delta n$.

When no grating is present in the proposed structure, most of the power is concentrated in the fundamental mode. The formation of index variation at the cladding region yields a power exchange between the two existing modes that can be analyzed using Coupled Mode Theory. In other words, the formation of the grating causes a periodic structure at the cladding that produces a forbidden region for the propagating modes. If the cladding index variation is $\Delta n = 0.007$, the dispersion relation provides the upper and the lower frequency limits of the forbidden gap which lies between

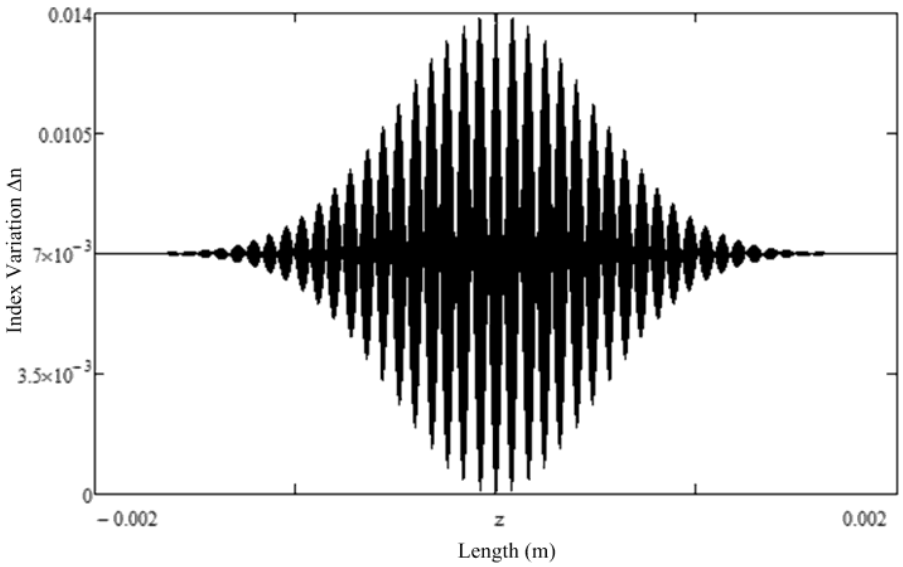

(a)

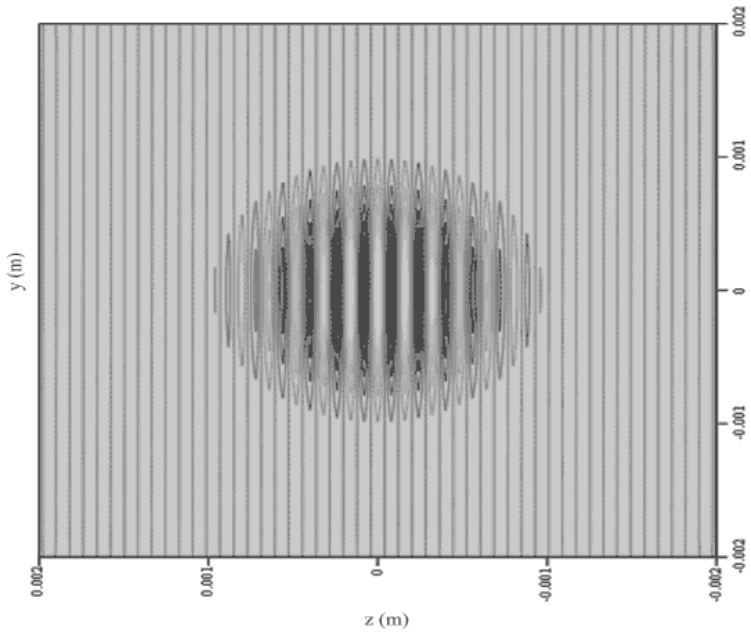

(b)

Figure 2.4. a-) Intensity-dependent refractive index grating pattern in z- direction with a DC Value b-) Interference fringes in the y-z plane (x = 0)

As can be seen, the propagation constant of the fundamental mode falls into the local forbidden region, thus in existence of a transient grating it is not allowed to propagate. In contrary, higher order mode propagation constant is out of the band gap regime, i.e., it lies on the dispersion line and it is in the propagation regime. $11994.05\times10^{12} \le \omega_B \le 1200.167\times10^{12}$. In this band structure the spatial width of the layers is $\Lambda/2$ and the index difference between the layers is equal to the amplitude of the transient grating, i.e., Δn. The relation of the mode propagation constants with the band structure is shown in figure 2.5.

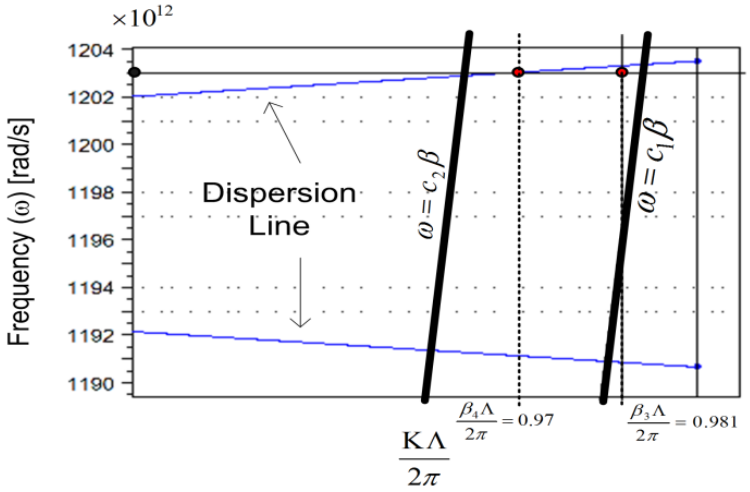

Figure 2.5. Dispersion diagram of periodic medium placed in evanescent region, where the refractive indices of successive stacks are $n_{cl} = 2.32$ and $n_{cl} + \Delta n = 2.327$

The amplitudes of the fundamental mode (m) and the higher-order mode (n) is governed by (2.41) and (2.42). By expanding the grating function into a 2-D Fourier series along x and z directions as given by (2.45), (2.46), (2.47) and assuming effective grating length $L_g = 1mm$, the Fourier coefficients $F_{p,r}$ and corresponding harmonics can be found easily.

When the perfect phase matching condition is satisfied (detuning parameter $\hat{\delta}_{p,r} = 0$) a power conversion efficiency of about 67% is obtained at the end of the grating. Such an interaction is not so sensitive to the grating length, which allows relaxation in critical

length adjustment.

The perfect phase matching condition is given by (2.58), where intensity can be regarded as the phase matching tuning parameter due to its effect on Δn . Because of the limited variation in Δn , it is not an easy task to provide steady perfect phase matching. In this case, if the magnitude of the coupling coefficient is comparable to the magnitude of the phase mismatch (detuning parameter $\hat{\delta}$), the coupling between the propagating modes is limited and most of the power remains in the fundamental mode. In this situation, the coupling efficiency remains at about 33% as shown in figure 2.6.

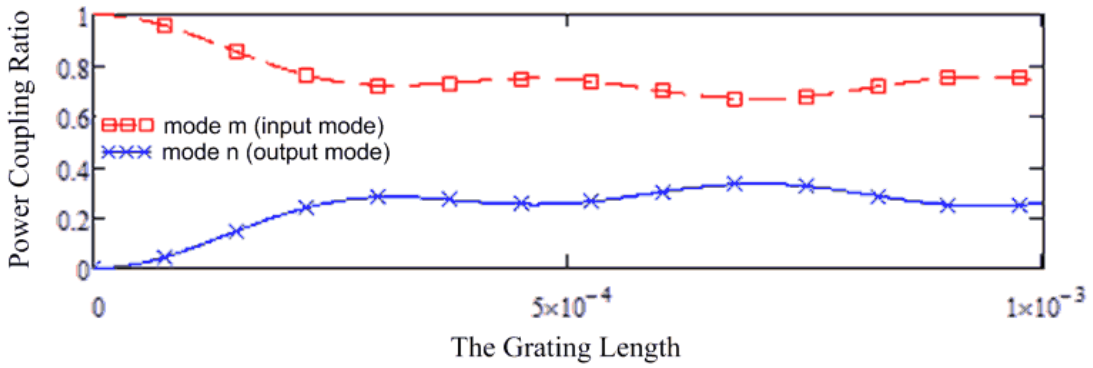

Figure 2.6. Input and output power in the case of under coupling (no phase matching: $K \cong \hat{\delta}$)

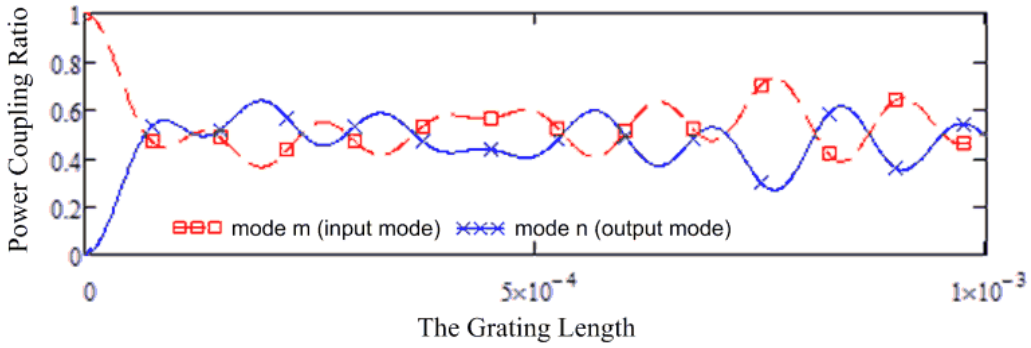

Figure 2.7. The power coupling in the case of over coupling ($|K| >> |\hat{\delta}|$)

Another way of getting strong coupling into higher order mode is to ensure over coupling, i.e. In such a case, an instantaneous power coupling occurs at the beginning of the transient grating and there exist some fluctuations through the grating leading to an average conversion efficiency of about 48%, calculated at the end of the grating as shown in figure 2.7.

On the other hand, third order optical nonlinearity is another important factor that has a major influence on mode conversion efficiency. The coupling efficiency as a function of nonlinearity is depicted in figure 2.8 for both transient non-uniform and transient sinusoidal gratings and the efficiency is compared for different types of nonlinear materials and phase matching situations.

The third order nonlinear susceptibility of the optical glasses is typically about $(1-100)\times10^{-14}$ esu [20], while this value is in the order of $(2.4\pm0.8)\times10^{-13}$ esu for Lithium Niobate [28] and about 2×10^{-7} esu for polymers [29]. If we take a closer look to the relation between power coupling efficiency and third order nonlinear susceptibility, we see that the coupling efficiency is much higher for both sinusoidal grating and non-periodic grating if the phase matching condition is satisfied. A further increase in the susceptibility (using polymer with susceptibility of about 10^{-7} esu instead of optical glass) enhances the efficiency of the non-periodic grating. When the susceptibility is below some threshold value (about $10^{-9}\,m^2/W$), there is a linear relation between nonlinearity and efficiency. Efficiency reaches saturation for the non-uniform grating and gets nearly constant values above threshold, while there are large efficiency fluctuations for sinusoidal gratings. When the nonlinearity is weak, the satisfaction of phase matching is the fundamental factor that has an influence on the efficiency, but a further increase in the nonlinearity may result in over coupling, i.e. $|\mathrm{K}| >> \hat{\delta}$, which diminishes the effect of phase matching.

Considering the spectral characteristics of the grating, the maximum power coupling between the modes occurs in the case of perfect phase matching at the wavelengths satisfying (2.45). Alternatively, maximum coupling occurs when $Q_{p,r}L_g = \frac{\pi}{2}$, which can be optimized for different wavelengths by choosing appropriate design parameters (interference half angle, grating period) and waveguide parameters. Normalized spectral characteristics of the non-uniform grating for phase-mismatched coupling ( ) with the parameters given above is shown in figure 2.9.

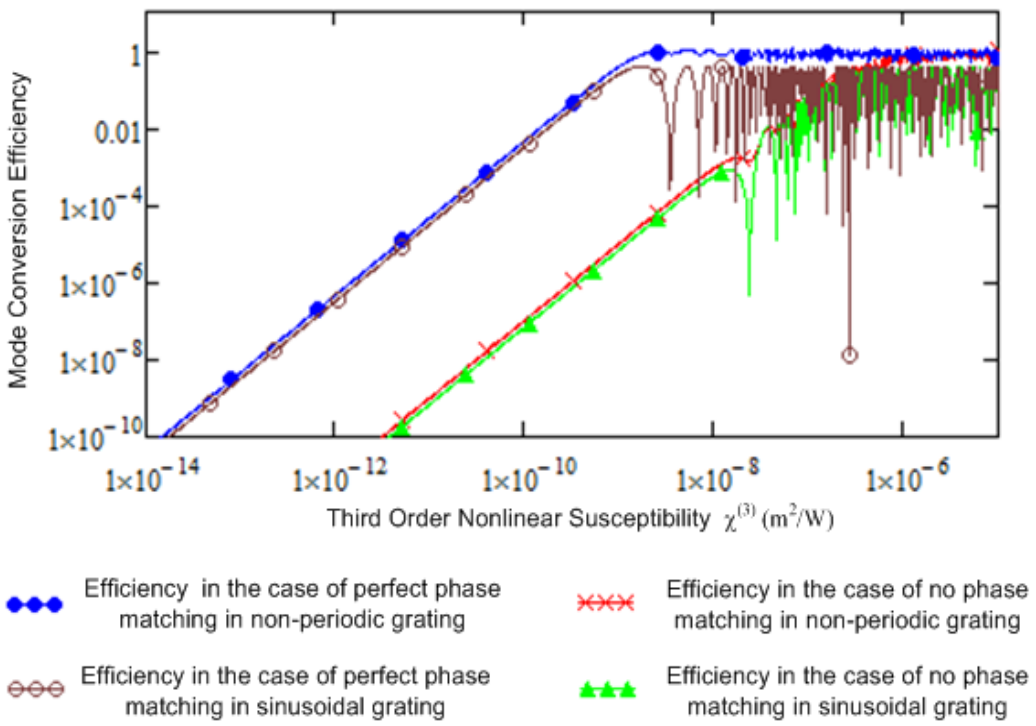

Figure 2.8. Graphical representation of efficiency vs. third order optical susceptibility (grating length constant)

For the selected set of parameters, there is 1 nm spacing between the maximum conversion peaks in the spectrum. In contrary, there are deeps at wavelengths 1541.6 nm, 1544.5 nm and 1548.5 nm, where the power efficiency drops about 40 dB and the mode coupling is completely suppressed. Using the tuning parameters of the transient

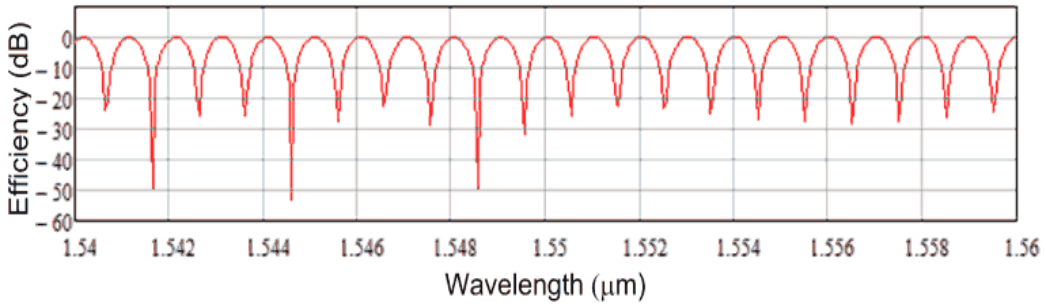

Figure 2.9. Spectral transmission characteristic of the grating

grating such as interference angle and laser wavelength, the efficiency can be maximized for the desired modes. This optimization will ensure the utilization of the system in DWDM applications such as a tunable mode coupler or drop filter.

CHAPTER 3

NONLINEAR POLYMERIC MATERIALS FOR ALL OPTICAL SWITCHING APPLICATIONS

Current optical communication components are being redesigned to achieve faster all optical signal processing functions for all-optical networks. Along with fundamental research for material properties, applied research is carried out for optimal use of these materials in light induced processes for all optical applications. Nonlinear optical polymers possess a great potential for use in photonic systems, including optical switches [4], high density storage devices [56] and ultrafast optical modulators [57]. Third order optical nonlinear processes (Kerr type) in polymeric materials offer great advantages in terms of response time, high nonlinearity and processing simplicity. All-optical switching applications require materials with large third-order nonlinearities, low nonlinear optical losses and fast response time.

To create an in-fiber device, light in the fiber must interact with the nonlinear material that forms the basis of the switching device realized in this thesis. For applications in evanescent region of the fiber, a section of cladding is removed and polymeric thin film is placed in the polished region so that some amount of field propagating in core reaches nonlinear material. By placing the material in a cladding region we allow the control of propagating mode by another light signal applied externally to the material. The feasibility of this method is also supported by other researches. It has been discovered that a periodic perturbation created in cladding can affect the fundamental core mode and demonstrated that perturbations created in cladding offer lower attenuation and flexible spectral characteristics in comparison with traditional fiber core index modulated grating [13]. Additionally, successful results were obtained by implementing Kerr type material in pump probe experiments and efficient power transfer into higher diffraction orders in nearly instantaneous response times were observed [16]. Placing the device in the fiber eliminates the need for light to be taken out of the fiber and coupled back in, that reduces insertion losses.

3.1 Requirements of Polymers for Photonic Applications

In order for a nonlinear material to be useful in optical signal processing devices, it must satisfy the following conditions [30]:

1. The excitation time of the nonlinear effect must be less than the pulse width of the excitation source and the sum of excitation and the relaxation times must be shorter than the pulse spacing
2. The effect of linear absorption must be weak compared to the effect of nonlinearity. This condition is specified in terms of the figure of merit Ψ as

$$\Psi = \frac{\Delta n}{\alpha_0 \lambda} > 1 \tag{3.1}$$

where $\Delta n = n_2 I$ is the induced index change, α_0 is the linear absorption and λ is the wavelength of light.

3. The effect of two-photon absorption must be weak compared to the nonlinear effect. This condition is specified in terms of the figure of merit T as

$$T = \frac{2\beta_2 \lambda}{n_2} < 1 \tag{3.2}$$

where β_2 is the two-photon absorption coefficient $\left({}^{cm}/_{W}\right)$.

3.2 Polymers for All-Optical Switching Applications

For a potential material in all optical switching, we have searched for polymeric nonlinear optical materials with large third order optical nonlinearities and fast response. We have developed scenarios for different polymer composites as a grating layer. According to our design specifications the candidate material should additionally exhibit following properties due to pump source available at the Lightwave Lab:

1. The polymeric material should exhibit strong nonlinearity at 532 nm.
2. The nonlinearity should depend on electronic transition which will satisfy the short response time of the material.
3. Figure of merits defined in the section 3.1, i.e., $T < 1$ and $\Psi > 1$ must be satisfied at 532 nm wavelength. This will ensure the capability of the material to be used in a photonic device.

After a detailed literature search, a material composition given by He et al [31] was decided to be used as a nonlinear platform for the switching device. In the mentioned study Polyvinyl Alcohol (PVA) and Methyl Red (MR) are employed to form a composite film with high nonlinear property. Both of these polymers are commercially available from Sigma Aldrich.

PVA is a commercially available polymer that can be found in various molecular weights and degree of hydrolysis. Molecular weight is an important parameter that directly affects the material thickness. PVA with high average molecular weights have long polymer chains and when dissolved in water, solution with high viscosity is obtained which results in great material thickness. Also, this situation gives rise to a high light dispersion. Additionally, there are some experimental works that examine the role of the molecular weight on transmission and diffraction efficiencies. These works indicate that high losses due to absorption and dispersion of light occur in PVA with molecular weight $M_w = 195\,000$ as compared with PVA of molecular weight $M_w = 130\,000$. However, in the literature there exists another comparative study, in which PVA with low molecular weight ($M_w = 20\,000 - 70\,000$) and PVA with molecular weight of $M_w = 130\,000$ is compared and similar results is obtained for both of diffraction and transmission efficiency [32].

Methyl red (MR) is a kind of important azobenzene molecule, and there have been many researches about the nonlinear optical characteristic and optical storage of this molecule, most of which are investigated by CW-laser as excitation source. Although the third-order nonlinearity of materials using CW-laser is large, it is not applicable for high-bandwidth optical signal processing due to long excitation and relaxation times: μs – ms for the former and μs – minutes for the latter.

He et al. [31] investigated third order coefficients of Methyl Orange (MO) and Methyl Red (MR) doped PVA films using pulsed laser in Z-scan experimental study. In this study, the third-order nonlinear refractive indices are given as $n_2 = -1.23\times10^{-9} esu$ and $n_2 = -1.18\times10^{-9} esu$ for MO and MR doped PVA films, respectively. According to these results, by exploiting the 532 nm pulsed laser with 5 W mean power and 15 ns pulse duration that exist in our laboratory; it would be possible to obtain refractive index variations of $\Delta n = 0.01845$ for MO doped PVA film and $\Delta n = 0.0177$ for MR doped PVA film, theoretically. Under 532 nm excitation the figures of merit for MO and MR doped PVA films were calculated as $\Psi_1 = 2.34$ and $\Psi_2 = 2.05$, respectively, with corresponding $T_{1,2} = 0$.

According to the experimental data given in the abovementioned research study, the absorption spectrum of PVA doped composite materials is shown in figure 3.1, where the absorption peak of MR is centered at 449 nm. Although nonlinear and absorption coefficients are investigated by He et al. [31], these parameters strongly depend on the concentration of each polymer in the composite. Therefore, absorption and nonlinearity properties must be examined for the polymeric solution used in this thesis. Additionally, refractive index of the polymeric film is another primary parameter that has a direct effect on coupling and loss mechanism in the switching structure. Although there are several values for the refractive index of the PVA based films, then composite nonlinear film refractive index must be measured for given concentration values. In the next section, the composite nonlinear film is characterized for refractive index, nonlinear coefficient and absorption coefficient.

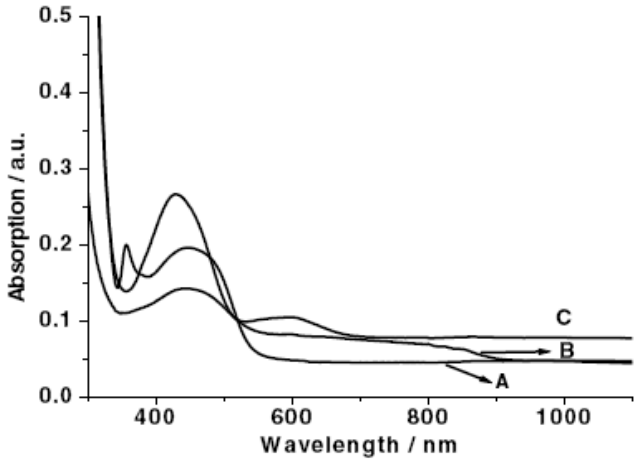

Figure 3.1. Absorption spectra of thin films: (A) MO doped PVA; (B) PDBAA Doped PVA; (C) MR doped PVA

3.3 Characterization of Polymers for Switching Applications

The polymeric film employed in the switching device is prepared using %90 hydrolyzed PVA with molecular weight $M_w = 70\,000$ and Methyl Red (MR), which are supplied by Sigma Aldrich. The solution consist of 9.09% w/v PVA and 0.018% w/v MR. PVA and MR is dissolved separately in distilled water and mixed completely. The solution is stirred for 12 hour. Acquired mixture is filtered to eliminate the unwanted particles, coated onto microscopic glass by Doctor Blade method and dried approximately 24h at room temperature.

Figure 3.2 shows the cross-sectional SEM image of the polymeric film with thickness of about 17.83 μm. The thickness of the polymer layer is directly related to the viscosity of the polymer. For efficient grating formation, the film thickness must be less than the coherence length of the pump laser. On the other hand, polymeric film refractive index is an unknown parameter at this stage and need to be measured before exploiting on the fiber device.

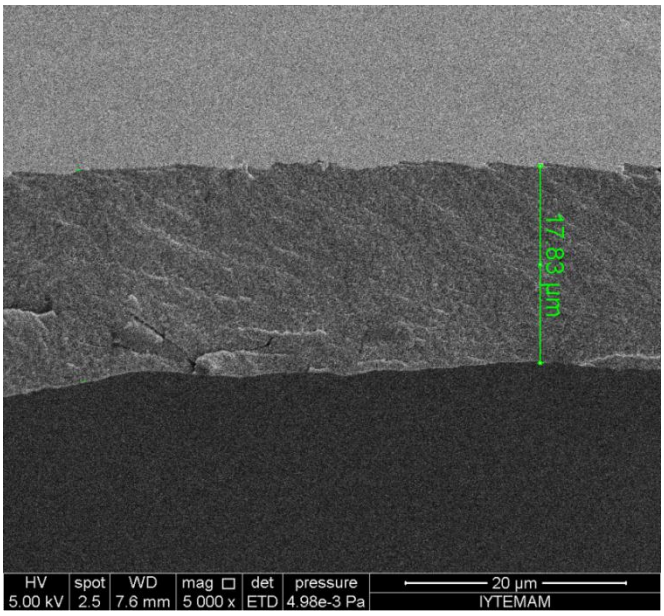

Figure 3.2. SEM image of the thin film

3.3.1 Measurement of Refractive Index of Polymer Films

The refractive index of the film was measured using Fresnel diffraction based nondestructive measurement method [33], [34]. Fiber with well-known parameters is immersed into the polymer thin film and far field diffraction pattern is recorded as shown in figure 3.3.

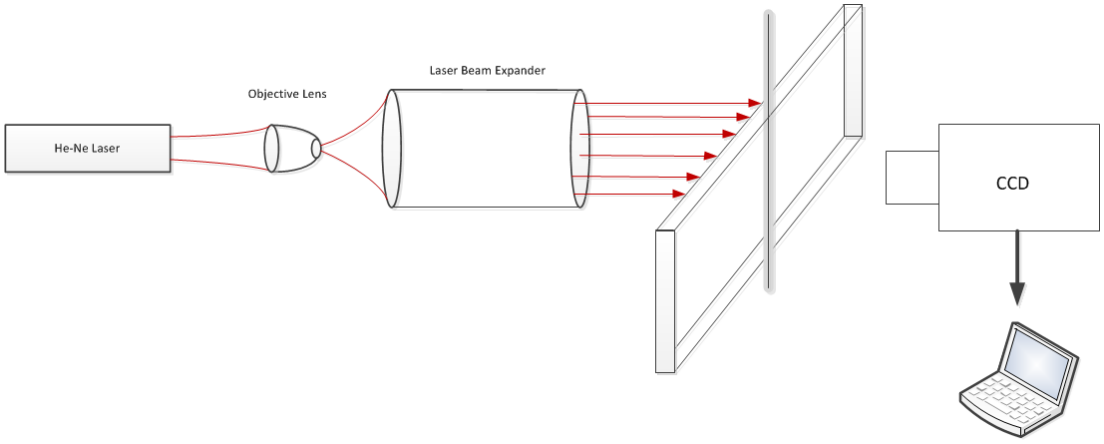

Figure 3.3. Setup for recording far field diffraction pattern

Theoretical intensity distribution on the Fresnel diffraction pattern of a fiber is formulated in [33] using the Fresnel-Kirchhoff integral. This approximation was used to find the refractive index of the polymeric film. Using paraxial distribution, the far field distribution in observation plane can written in the following form

$$\begin{aligned} U = \frac{K'\exp(-i\varphi_p)}{B}\Bigg\{ & 1 + C(\alpha) - C(\beta) + i[1 + S(\alpha) - S(\beta)] \\ & + B\left[\int_{-b}^{-a} exp(-i\varphi_{cl}(x'))\, exp\left(ik\frac{(x-x')^2}{2z'}\right)dx'\right. \\ & + \int_{-a}^{a} exp\{-i[\varphi_{cl}(x') \\ & + \varphi_{co}(x')]\} exp\left[ik\frac{(x-x')^2}{2z'}\right]dx' \\ & \left. + \int_{a}^{b} exp(-i\varphi_{cl}(x'))\, exp\left(ik\frac{(x-x')^2}{2z'}\right)dx'\right]\Bigg\} \end{aligned} \tag{3.3}$$

where

$$\varphi_p = 2kbn_p\,, \qquad |x'| > b \tag{3.4}$$

$$\varphi_1 = 2k\left[\left(b - \sqrt{b^2 - x'^2}\right)n_p + \left(b - \sqrt{b^2 - x'^2}\right)n_{cl}\right], \quad a < |x'| < b \tag{3.5}$$

$$\varphi_2 = 2k\left[\left(b - \sqrt{b^2 - x'^2}\right)n_p + \left(\sqrt{b^2 - x'^2} - \sqrt{a^2 - x'^2}\right)n_{cl} + \sqrt{a^2 - x'^2}n_{co}\right], \quad |x'| < a \tag{3.6}$$

where n_p, n_{cl}, n_{co}, and k are the refractive indices of the polymeric film, the cladding, the core, and wave number, respectively.

$$\varphi_{cl} = 2k\left(n_{cl} - n_p\right)\sqrt{b^2 - x'^2} \tag{3.7}$$

$$\varphi_{co} = 2k\left(n_{cl} - n_p\right)\sqrt{a^2 - x'^2} \tag{3.8}$$

$$\varphi_1 = \varphi_p + \varphi_{cl} \tag{3.9}$$

$$\varphi_2 = \varphi_p + \varphi_{cl} + \varphi_{co} \tag{3.10}$$

where $K' = K\frac{exp(iz')}{\sqrt{z'}}$, $B = \frac{2}{\sqrt{\lambda z'}}$ $\alpha = B(x-b)$ and $\beta = B(x+b)$.

$C(\alpha)$ and $S(\alpha)$ are Fresnel integrals given by $C(\alpha) = \int_0^a cos\left(\frac{\pi v^2}{2}\right)dv$ and $S(\alpha) = \int_0^a \cos\left(\frac{\pi v^2}{2}\right)dv$

The acrylate coating of the Nufern 780HP fiber was stripped and bare fiber was immersed into liquid polymer and left for 24h in room temperature to allow the polymer to dry. Dried film has a thickness of 125 μm. Single mode step index fiber is characterized by core diameter $2a = 5\ \mu m$, core refractive index $n_{co} = 1.4591$, cladding diameter $2b = 125\ \mu m$ and cladding refractive index $n_{cl} = 1.4537$. A beam from 632.8 nm He-Ne laser was expanded into plane wave and used to illuminate the thin film structure. The diffraction pattern was recorded on CCD that has pixel size of 11 μm × 11 μm. Intensity diffraction pattern is shown in figure 3.4.

The theoretical intensity distribution is fitted on the corresponding experimental intensity distribution by trying different values of the substrate index. Finally, linear refractive

index of the thin film obtained from this solution was estimated as $n = 1.4995$. The tolerance of the measurement method is given as 5×10^{-5} .

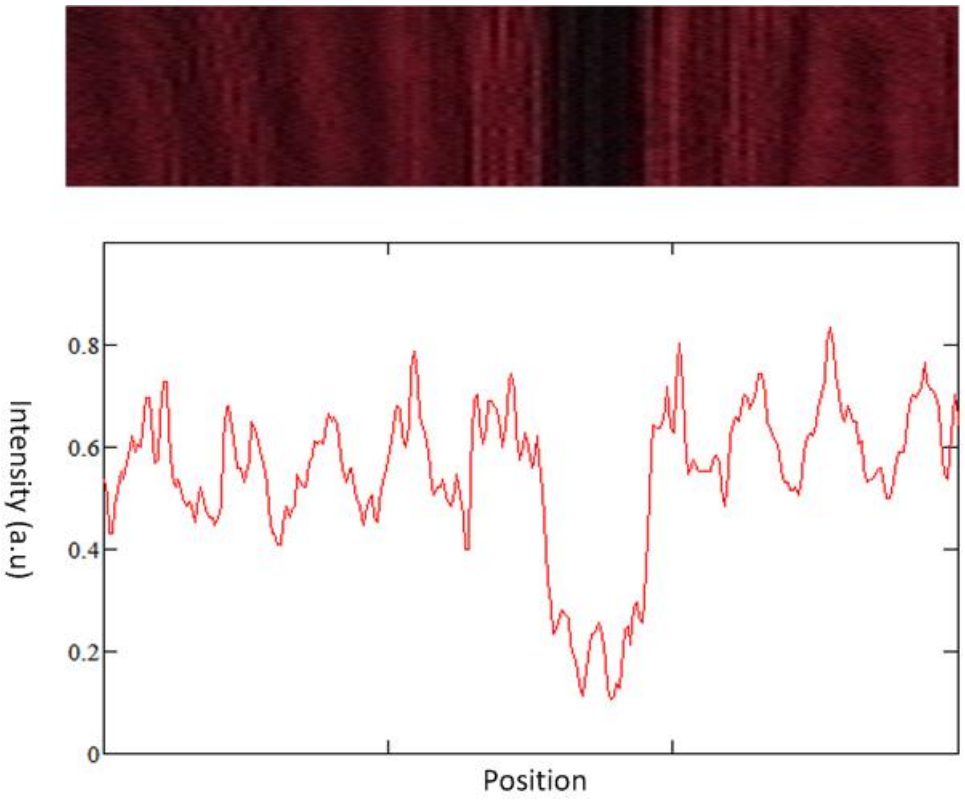

Figure 3.4. Experimental result on the diffraction of laser beam from single mode fiber

3.3.2 Measurement of Third Order Optical Nonlinearity

There exist several techniques to measure the nonlinear refractive index of the material. Some of these methods are degenerate four wave mixing [52], nonlinear interferometry [53] and ellipse rotation [54]. The "Z-scan" method, developed by the Eric Van Stryland has become the standard technique for determining the nonlinear absorption (open aperture) and nonlinear refraction coefficient (closed aperture) of materials [35]. The z-scan technique is performed by translating a sample through the beam waist of a focused beam and then measuring the power transmitted through the sample. As the sample moves through the beam focus, the beam wave front phase is

modified due to self-focusing and de-focusing. If the beam experiences any nonlinear phase shift due to the sample as it is translated through the focal region, then the fraction of detected light will vary due to the Kerr lens generated in the material by the intense laser beam.

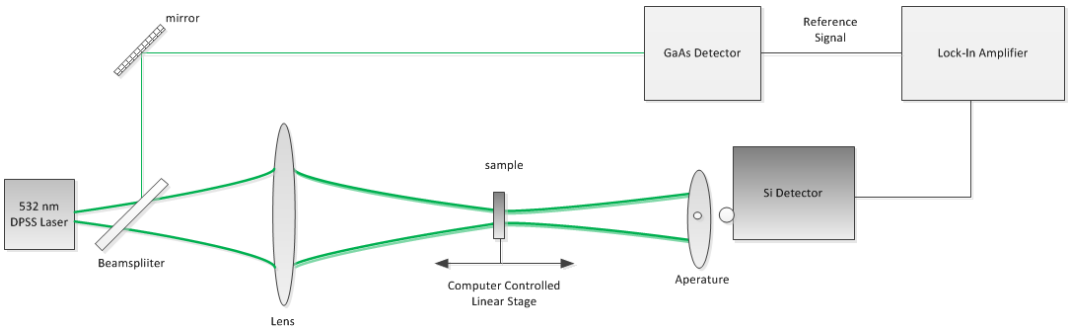

Figure 3.5. Illustration of the experimental setup for z-scan

To figure out how the Z-scan transmittance as a function of z is related to the nonlinear refraction of the sample, let us assume a medium with a negative nonlinear refraction index and a thickness smaller than the diffraction length of the focused beam. This can be considered as a thin lens of variable focal length. Beginning far from the focus ($z < 0$), the beam irradiance is low and nonlinear refraction is negligible. In this condition, the measured transmittance remains constant (z-independent). As the sample approaches the beam focus, irradiance increases that leads to self-lensing in the sample. A negative self-lens before the focal plane will tend to collimate the beam on the aperture in the far field, increasing the transmittance measured at the iris position.

Self-defocusing increases the beam divergence, leading to a widening of the beam at the iris and thus reducing the measured transmittance. Far from focus (z > 0), the nonlinear refraction is low, resulting in a transmittance z-independent. A pre-focal transmittance maximum (peak), followed by a post-focal transmittance minimum (valley) is a Z-scan signature of a negative nonlinearity. An inverse Z-scan curve (a valley followed by a peak) characterizes a positive nonlinearity.

Considering centro-symmetric media, intensity dependent refractive index n and absorption coefficient α can be written as following [36].

$$n(I) = n_0 + \gamma I \tag{3.11}$$

and

$$\alpha(I) = \alpha_0 + \beta I \tag{3.12}$$

Where n_0 and α_0 are the linear refractive index and linear absorption coefficient, respectively.

Nonlinear refractive index and absorption coefficients are associated with third order electric susceptibility in the following form

$$\gamma = \frac{1}{2n_0^2\varepsilon_0 c} Re\{\chi^{(3)}\} \tag{3.13}$$

$$\beta = \frac{\omega}{n_0^2\varepsilon_0 c^2} Im\{\chi^{(3)}\} \tag{3.14}$$

The transmittance as a function of the position z is given by

$$T = \frac{S(z)}{S(z \to \infty)} = 1 + \Delta\Phi_0 \frac{4x}{(x^2+1)(x^2+9)} \tag{3.15}$$

Where S is the photodetector signal at position z, $\Delta\Phi_0$ is the on-axis nonlinear phase shift at focus, $x = \frac{z}{z_0}$ and z_0 is the Rayleigh range of the Gaussian beam.

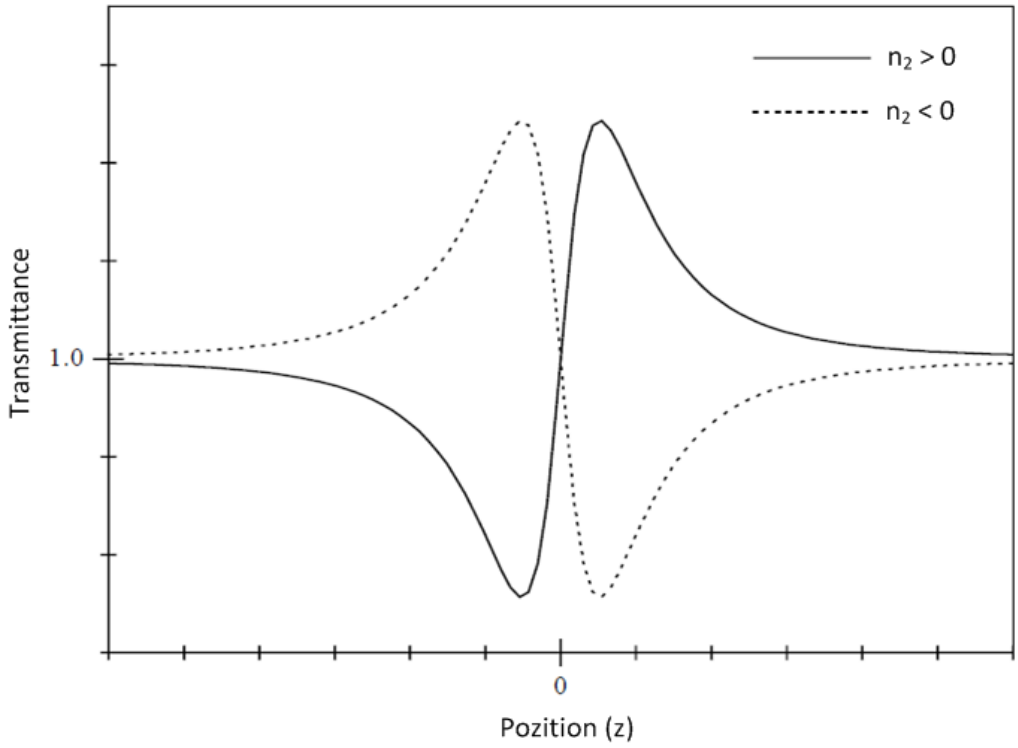

Figure 3.6. Z-scan curve as a function of position z

The position of the peak and valley, relative to the Z-axis, depends on the sign of the nonlinear phase shift, $\Delta\Phi_0$, as depicted in figure 3.6. If the phase shift is positive (self-focusing occurs), then the peak will trail the valley. If the phase shift is negative, then the valley will trail the peak (self-defocusing). The magnitude of the phase shift can be determined from the change in normalized transmittance between peak and valley, ΔT_{pv} using the relation [37]

$$|\Delta\Phi_0| = \frac{\Delta T_{pv}}{0.406(1-S)^{0.27}} \tag{3.16}$$

where S is the fraction of beam transmitted through the aperture. The nonlinear index, n_2 can be found from the phase shift using

$$n_2 = \left(\frac{\lambda}{2\pi}\right)\frac{\Delta\Phi_0}{I_0 L_{eff}} \tag{3.17}$$

where I_0 is the peak on-axis irradiance at focus. The refractive index at a given point on the material depends only on the light intensity at the same point.

In order to find the third order optical nonlinear coefficient of the polymeric film, a number of experiments are performed. To begin with, an experimental setup constructed to measure the nonlinear coefficient of polymeric film is shown in figure 3.5. The film is prepared with 9.09% w/v PVA and 0.018% w/v Methyl Red. The beam emerging from the 532 nm DPSS laser with pulse duration of 14 ns is focused onto the 17 μm thick polymeric film sample by a lens with focal length of 2 cm. As the sample moves through focal point, the transmitted intensity is measured using Si detector, connected to the Lock-In amplifier and the normalized intensity as a function of the sample position (right side of the focal point) is given in figure 3.7.

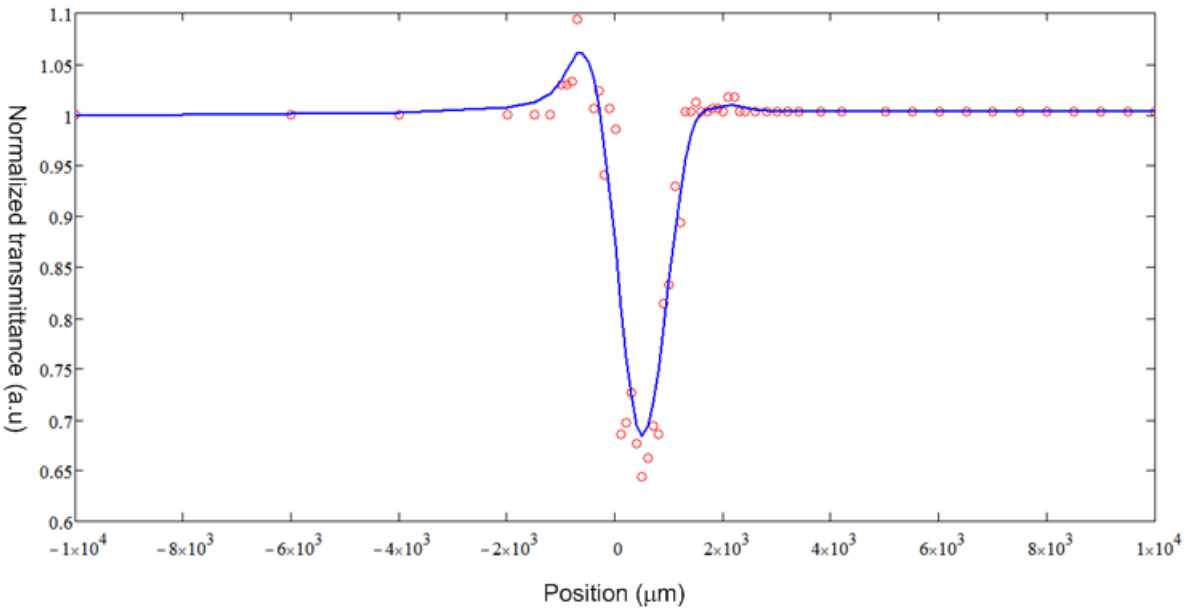

Figure 3.7. Z-scan data for nonlinear coefficient of MR doped PVA

The peak intensity at focus is measured as $I_0 = 1.846 \times 10^9 \frac{W}{cm^2}$ and the spot size at focal point is $1\,\mu m$ in diameter. According to the experimental results third order nonlinear coefficient of the film is found as $n_2 = -4.02 \times 10^{-11}\ {}^{cm^2}/_{W}$. The valley in the left side of the origin indicates the negative nonlinear coefficient, which results from self-defocusing. In the research carried by T. He [31], the nonlinear coefficient is estimated as $n_2 = -3.21 \times 10^{-12}\ {}^{cm^2}/_{W}$. This difference between the two experimental results arises from the difference of the mixture ratio of the PVA and MR used in the production of composite material. In the aforementioned reference, the mixture ratio is not defined. However, in our study trial and error method was used to obtain optimal mixture ratio.

Figure 3.8 depicts the absorption curve for the same sample which is obtained with open aperture placed in front of the detector.

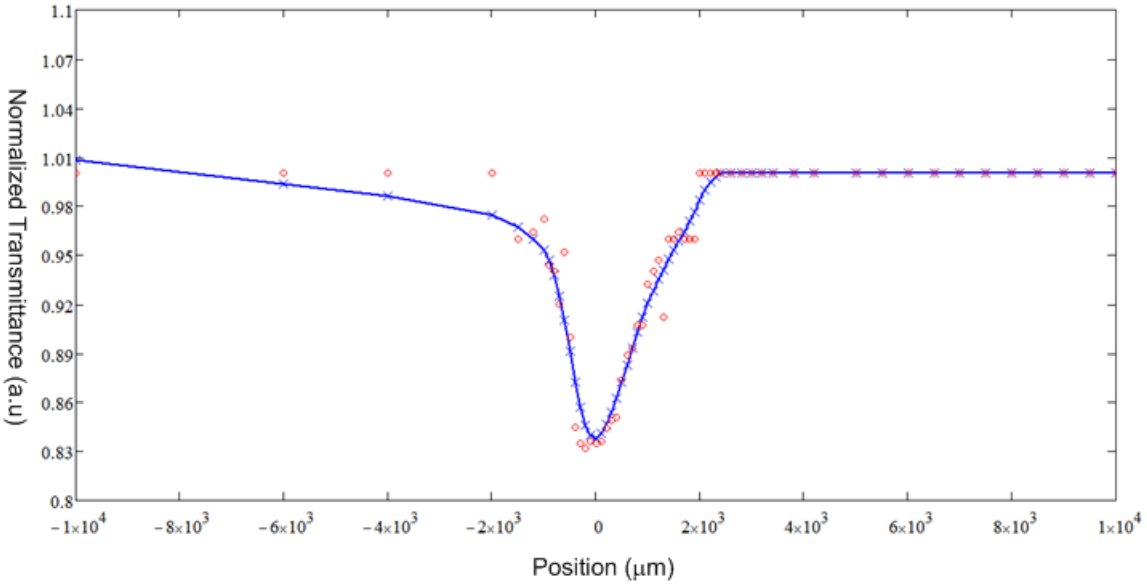

Figure 3.8. Z-scan data for absorption of MR doped PVA

Comparative graph depicted from the experimental data of the nonlinear refraction and nonlinear absorption experiments is given in figure 3.9.

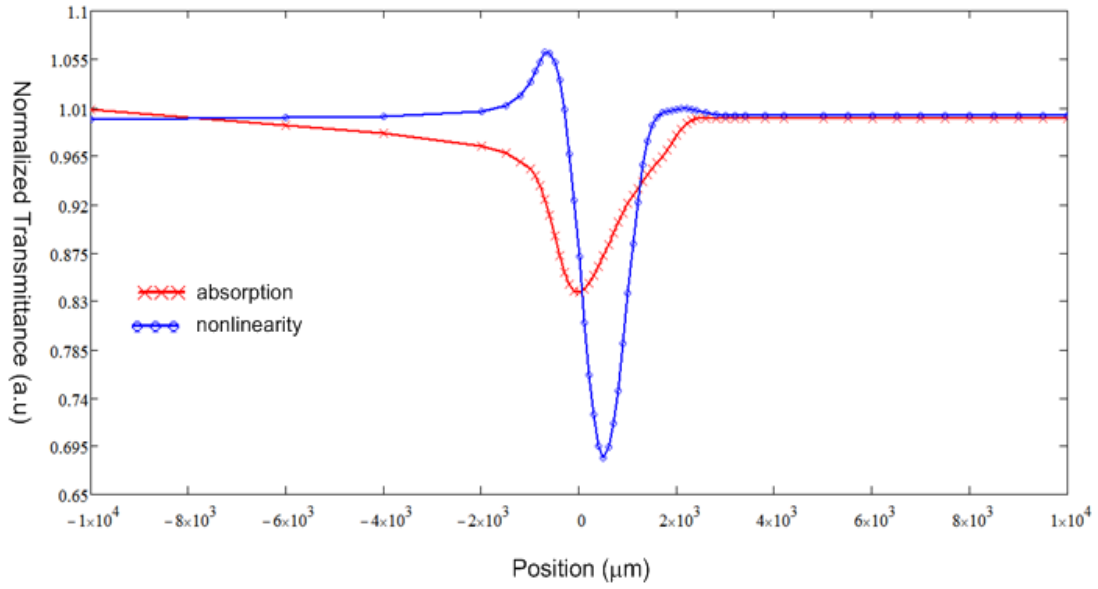

Figure 3.9. Open aperture and closed aperture Z scan result for MR Doped PVA

These two experiments are repeated for different peak intensities at focal point. At smaller intensities, peak-valley characteristic of the nonlinearity is not observed. On the other hand, increasing intensity results in thermal damaging of the sample.

The film characterized in this chapter is going to be coated on the flat side of the polished fiber. The linear refractive index of the polymeric film, as stated above, is measured as $n_p = 1.4995$. However, the refractive index of the fiber cladding is the $n_{cl} = 1.4507(@980\,nm)$. Because $n_p >> n_{cl}$, some of the light propagating in the fiber radiates to the external medium [49] and only small portion of the mode continues to propagate in the fiber. To reduce the radiation power, the index difference $n_p - n_{cl}$ should be reduced, that can be achieved by decreasing the polymer refractive index. The first solution is the adding a fluoropolymer based material into PVA and MR solution. Fluoropolymers have low refractive index of about 1.3 and adding this material will reduce the film refractive index. However the nonlinearity properties of these polymers are unknown and there are not any experimental data on the nonlinearity characteristics of fluoropolymers. On the other hand, some researches have shown that adding nanoparticles enhances optical nonlinearity. Although most researches investigate gold and silver nanoparticles, silicon nanoparticles are also suitable for that purpose [38]. SiO_2 nano particles with 20 nm diameter are provided by Alfa Aesar

(Pr.No.12727) and own refractive index of 1.46. To fabricate the composite film, SiO2 particles are added to the mixture of PVA and dye solutions such that nanoparticles and PVA weight equally (SiO_2- %7.35, PVA- %7.42, Methyl Red - % 0.014). The mixture is coated onto microscope glass and dried approximately for 24h at room temperature. The third order nonlinearity and absorption property of the thin film are investigated by Z-scan experiment. The closed aperture (nonlinearity) curve is depicted in figure 3.10.

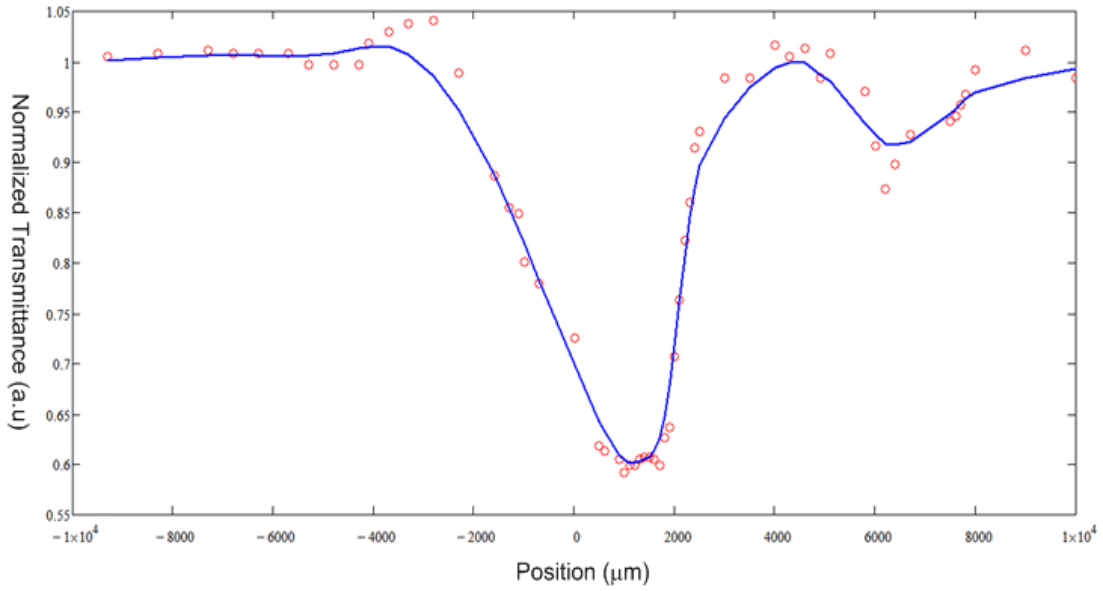

Figure 3.10. Z scan data for optical nonlinearity of MR and nanoparticle doped PVA

According to the experimental results, third order nonlinear coefficient of the film is found using eq. (3.16) and eq. (3.17) as $n_2 = -4.616 \times 10^{-11}\ {}^{cm^2}/_{W}$.

The absorption curve is depicted in figure 3.11.

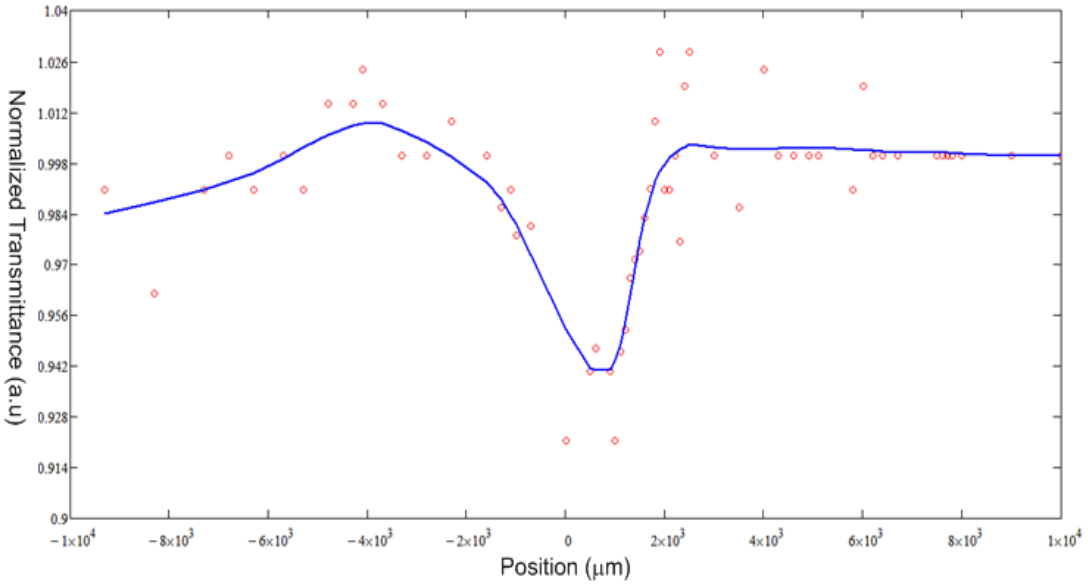

Figure 3.11. Z scan data for absorption of MR and nanoparticle doped PVA

Comparative graph depicted from the experimental data of the nonlinear refraction and nonlinear absorption experiments is given in figure 3.12.

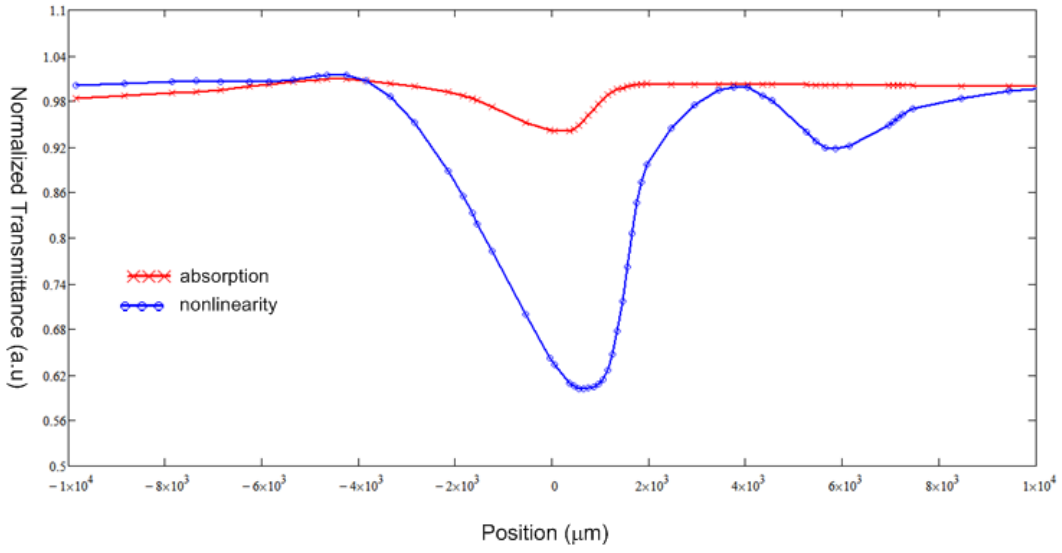

Figure 3.12. Open aperture and closed aperture Z scan result for MR and nanoparticle doped PVA

From the analysis of experimental data given in figure 3.9 and figure 3.12, it is apparent that the absorption values of the films are in decent value and the figures of merit $W \approx 2 > 1$ and $T = 0 < 1$ are satisfied at 532 nm. The large optical nonlinearity, satisfaction of figure of merits and fast response time enables this material to be a good candidate for high-speed switching applications.

CHAPTER 4

CHARACTERIZATION OF TRANSIENT GRATINGS IN POLYMERIC MATERIALS USING PUMP-PROBE TECHNIQUE

Laser-induced gratings arise from the nonlinear interaction between a medium and the radiation from an interference structure generated by two crossed laser beams. This interaction leads to a periodic modulation of the refractive index, i.e. to the formation of a dynamic optical grating by various mechanisms. The optical properties of matter such as the refractive index and the absorption coefficient become spatially modulated in the interference region. The spatial modulation of the optical material properties acts as a diffraction grating. Dynamics of the formed grating may be analyzed using two color pump and probe technique. The main principle of this technique is to diffract a third beam off the laser induced transient grating and to monitor the diffraction efficiency of the probe beam. The diffracted beam can be made to propagate in different directions, which allows the detection of a signal in the ‘‘background-free” area, which is considered as a big advantage of the pump-probe technique [39].

4.1 Pump Probe Technique

Laser-induced gratings are formed in a polymeric medium by various mechanisms such as photorefractive and Kerr effects as a response to the spatially modulated light field that arises from the interference of two beams. Their total electric field produces some material excitation, which then leads to a change of the optical properties such as complex refractive index that depends on the incident-light intensity. Conventional pump-probe experimental set-up in a slab material is illustrated in figure 4.1. The basic structure of the interaction of the pump and probe beams can be understand by considering the interaction in a small volume of the sample.

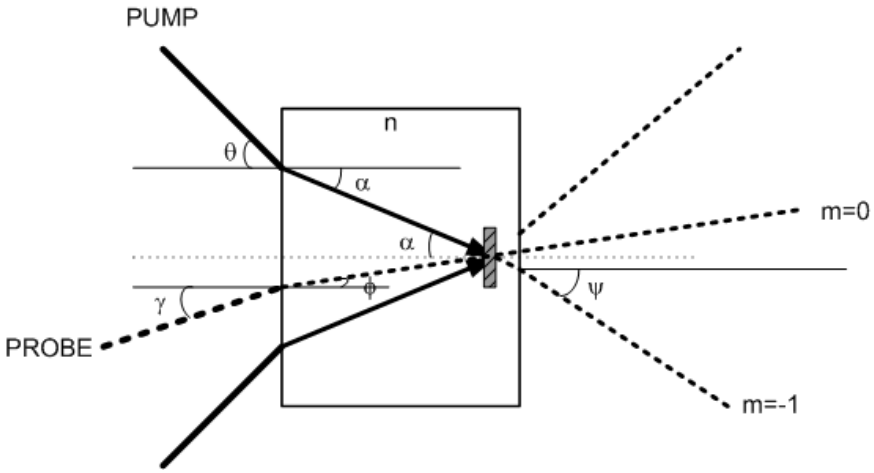

Figure 4.1. Schematic diagram of the pump-probe arrangement

The relation between the incident angle θ of the pump beam and the half intersection angle α is defined by Snell's law, given by

$$\alpha = \text{asin}\left(\frac{\sin\theta}{n}\right) \tag{4.1}$$

where n is the linear refractive index of the material. The period of the formed grating is defined as

$$\Lambda = \frac{\lambda}{2n\sin\alpha} \tag{4.2}$$

where λ is the pump beam wavelength. The probe beam travelling at angle γ in air with respect to the surface normal refracts in the boundary and enters the transient grating with an angle of ϕ given by

$$\phi = \sin^{-1}\frac{\sin\gamma}{n} \tag{4.3}$$

If the grating vector matches with wave vector of the incident beam, then the probe beam is efficiently diffracted into many orders, where the angle of each order is given by

$$\chi = \sin^{-1}\left(\sin(\phi) + m \times \frac{\lambda_p}{\Lambda \times n}\right) \tag{4.4}$$

m is the diffraction order. Finally the diffracted beams leave out the material at an angle

$$\psi = \sin^{-1}(n \sin\chi) \tag{4.5}$$

4.1.1 Diffraction Efficiency of Thick Gratings

Laser-induced gratings can be probed by detecting the diffracted light from a third laser beam, having a wavelength different from that one of the grating beams. According to the sample thickness, wavelength and grating period, the formed diffraction structure can be classified as thick and thin diffraction elements. The efficient probing of thick grating, illustrated in figure 4.2, ensures the Bragg condition defined by [55]

$$\vec{k}_{pr} - \vec{k}_l = m\vec{K} \tag{4.6}$$

where k_{pr} represents wave vector of the probe beam, k_l is the wave vector of the diffracted beam and K is the grating vector defined as

$$K = \frac{2\pi}{\Lambda} \tag{4.7}$$

Diffraction efficiency of the grating is defined as the power diffracted into the first Bragg order with respect to total incident power in the material.

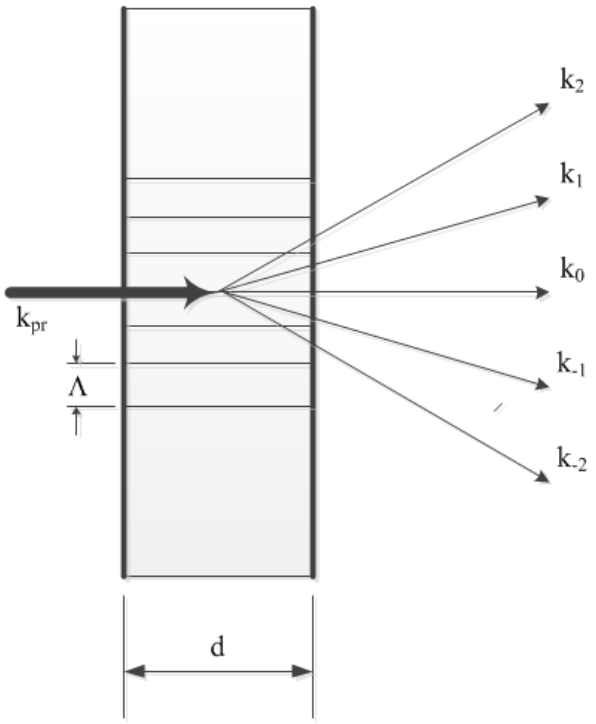

Figure 4.2. Illustration of the diffraction of the probe beam

Those gratings characterized by a large grating thickness compared to the fringe spacing, are called thick gratings. The condition for thick grating is defined by the thickness parameter Q which is a function of probe wavelength λ, linear refractive index n and grating period Λ [40].

$$Q = \frac{2\pi\lambda d}{n\Lambda^2} > 1 \tag{4.8}$$

and

$$\rho = \frac{\lambda^2}{n\Lambda^2\Delta n} \geq 10 \tag{4.9}$$

where d is the thickness of the medium and Δn is the amplitude of the index modulation. Diffraction efficiency, that is power diffracted from the incident probe beam into the first order, is defined by

$$\eta = \frac{\left(\sin\left(\upsilon^2 + \xi^2\right)^{\frac{1}{2}}\right)^2}{1 + \frac{\xi^2}{\upsilon^2}} \tag{4.10}$$

In this calculation, the absorption of the material is ignored. The parameter υ is related to the grating strength and given by

$$\upsilon = \frac{\pi\Delta n d}{\lambda \cos\varphi} \tag{4.11}$$

where

$$\varphi = \cos^{-1}\left((\cos\phi\cos\chi)^{\frac{1}{2}}\right) \tag{4.12}$$

According to the setup shown in figure 4.1, the parameter ξ describes the angular mismatch parameter defined by

$$\xi = \frac{\Delta\upsilon K d}{2} \tag{4.13}$$

$$\Delta\upsilon = \upsilon - \upsilon_0 \tag{4.14}$$

where K is the magnitude of the grating vector given as by eq. (4.7), υ_0 is the Bragg angle for which phase matching is completely satisfied, defined by

$$\upsilon_0 = \sin^{-1}\left(\frac{\lambda}{2\pi\Lambda}\right) \tag{4.15}$$

In thick gratings light is only diffracted if angle of incidence is close to the Bragg angle and Eq. (4.10) for the diffraction efficiency is valid for gratings with small Δn.

4.1.2 Thin Transient Grating Diffraction Efficiency

The diffraction efficiency for a thin transient grating can be written in the following form [41]

$$\eta = \eta_0 f_G exp\left(-\left(\frac{2\Delta t}{\Psi}\right)^2\right) \tag{4.16}$$

Where η_0 is the diffraction efficiency for monochromatic Bragg matched waves and it is given by

$$\eta_0 = \left(\frac{2\pi d}{\lambda_r}\right)^2 I_1 I_2 \left(n_2^2 + \left(\frac{\beta_r \lambda_r}{4\pi}\right)^2\right) \tag{4.17}$$

f_G is the geometric factor that takes into account the diameters of the pump beam and the probe beam. That factor is written as

$$f_G = \frac{D_p^2}{D_p^2 + 2D_r^2} \times \frac{1}{(3 + 14q^2)^{1/2}} \tag{4.18}$$

Where D_p is the pump beam diameter and D_r is the probe beam diameter, q is the dimensionless angular parameter given by

$$q = \frac{\theta_p \times D_\psi}{\nu \Psi} \tag{4.19}$$

θ_p is the pump half angle, υ is the beam velocity, Ψ is the temporal width of the pump pulses, D_ψ is the effective diameter given by

$$D_{\psi} = \frac{D_p D_r}{\left(D_p^2 + 2D_r^2\right)^{\frac{1}{2}}} \tag{4.20}$$

4.2 Diffraction From Transient Gratings

To set up the grating a strong pulsed laser and a continuous wave (CW) laser to read out the grating are required. Diode pumped solid state (DPSS) lasers with nanosecond pulse width are proper choice due to their compactness and high intensity output. For the application of laser induced dynamic gratings, the characteristics of the optical sources are very important because these characteristics affect the profound results. First of all, most of these lasers have a coherence time that is shorter than their pulse length. Therefore the optical path length of the excitation beams must be carefully adjusted to obtain good interference and thus a high diffraction efficiency of the laser induced grating. The influence of this feature upon a generated signal is presented and discussed in the following section 4.2.1. Additionally, the relative high output intensity of this pulsed laser must be controlled since the nature of the induced grating depends on it. High laser intensities can lead to physical changes of the sample and damage materials of the used optics.

4.2.1 Coherence and Diffraction Contrast

The concepts of spatial and temporal coherence are important in discussing the phase characteristics of optical systems. In general, the concept of coherence is related to the predictability of phase. Spatial coherence describes the correlation between signals at different points in space. Temporal coherence describes the correlation between signals observed at different moments in time.

Since the coherence time is inversely proportional to the bandwidth, in general, multimode lasers have a short coherence time. For example, the DPSS pulsed laser that was used in the experiments carried out in this thesis has a bandwidth of about 100 MHz and has coherence time of about 11 ns. If the duration of the excitation pulses is much longer than the coherence time of the excitation laser one has to account for the

time dependence of the excitation fields to correctly describe the diffraction efficiency η of a grating generated by partially coherent excitation beams. For a most of the pulsed DPSS laser, the coherence time is smaller than the pulse duration and, therefore, in order to obtain high grating diffraction efficiency, it is crucial to reduce the optical path difference of the excitation beams to a small fraction of the coherence length of the laser source.

Due to random nature of intensity as a function of time and position, it is more convenient to use statistical average to introduce the concept of coherence. At a given position r and time t the intensities of the two waves are $I_1 = \langle |U_1|^2 \rangle$ and $I_2 = \langle |U_2|^2 \rangle$, and their cross-correlation is described by the statistical average $G_{12} = \langle U_1 * U_2 \rangle$ and its normalized version is given by [12]

$$g_{12} = \frac{\langle U_1 * U_2 \rangle}{\sqrt{I_1 I_2}} \tag{4.21}$$

When the waves U_1 and U_2 are interfered, the intensity can be written as

$$I = I_1 + I_2 + 2\sqrt{I_1 I_2}|g_{12}| \cos\varphi \tag{4.22}$$

where φ is the phase of g_{12}. Thus, for completely correlated waves with $|g_{12}| = 1$ we obtain the classical interference equation. For two uncorrelated waves with $|g_{12}| = 0$, interference equation is $I = I_1 + I_2$, which means that there is no interference.
The strength of the interference is measured by the visibility $\mathcal{V}$ given by

$$\mathcal{V} = \frac{I_{max} - I_{min}}{I_{max} + I_{min}} = \frac{2\sqrt{I_1 I_2}}{I_1 + I_2}|g_{12}| \tag{4.23}$$

For a Gaussian wave the spectral width is given by

$$\Delta \upsilon_c = \frac{c}{\lambda^2} \Delta\lambda \tag{4.24}$$

where $\Delta\lambda$ is the bandwidth of the laser. The coherence time is the inverse of the spectral width, and can be written in the form

$$\tau_c = \frac{1}{\Delta \upsilon_c} \tag{4.25}$$

In this case the coherence length is calculated as

$$l_c = c\tau_c \tag{4.26}$$

If the optical path difference between the interfering waves is Δd, then the time delay is written as

$$\tau = \frac{\Delta d}{c} \tag{4.27}$$

Interference has a maximum value when $\tau = 0$ and vanishes for $\tau \gg \tau_c$.

To understand the spatial coherence, consider a plane travelling in z direction given by

$$U(r,t) = a\left(t - \frac{z}{c}\right) exp\left(j\omega_0\left(\tau - \frac{z}{c}\right)\right) \tag{4.28}$$

where $a(t)$ is a random function. The mutual coherence function is defined as

$$G(r_1, r_2, \tau) = G_a\left(\tau - \frac{z_2 - z_1}{c}\right) exp\left(\tau - \frac{z_2 - z_1}{c}\right) \tag{4.29}$$

Where the autocorrelation function of $a(t)$ can be written as

$$G_a(\tau) = \langle a^*(t)a(t+\tau)\rangle \tag{4.30}$$

The spatial coherence is described by

$$G(r_1, r_2, 0) = G_a\left(\frac{z_2 - z_1}{c}\right) exp\left(\frac{z_2 - z_1}{c}\right) \tag{4.31}$$

If two points r_1 and r_2 lies in the same transverse plane, then

$$|G(r_1, r_2, 0)| = |G_a(0)| = 1 \tag{4.32}$$

This means that fluctuations at points on a waveform are correlated.

The axial (longitudinal) spatial coherence of the wave has a one-to-one correspondence with the temporal coherence. The ratio of the coherence length $l_c = c\tau_c$ to the optical

path difference Δd in the system governs the coherence. If $l_c > \Delta d$, then the wave is completely coherent.

4.3 Thin Film Fabrication

The detailed description of preparation of the composite film was given in chapter 3. The polymeric film employed in the switching device is prepared using %90 hydrolyzed PVA with molecular weight $M_w = 70\,000$ and Methyl Red (MR), which are supplied by Sigma Aldrich. The concentration of the MR in the composite film directly affects the nonlinearity of the material. Thus, we have prepared two kinds of solution by varying MR ratio. The first solution is prepared with 9.09% w/v PVA and 0.018% w/v MR and it is named MR1. The second solution consists of 14.28% w/v PVA and 0.028% w/v MR and it is called MR2. Both of the solutions are dissolved separately in distilled water and mixed completely.

Table 4.1. The characteristic of thin films

	Material	**Rotation Speed (rev/min)**	**Spinning Time (sec)**	**Film Thickness (μm)**
Film 1	MR1	1000	60	0.460
Film 2	MR2	1000	60	0.460
Film 3	MR1	1500	30	2.7
Film 4	MR2	1500	30	2.7
Film 5	MR2	2000	30	2

The solutions are stirred for at least 12 hour and then filtered to eliminate the unwanted particles.

In addition to the concentration of MR in solution, the effect of film thickness on the diffraction efficiency is also unknown parameter. According to material ingredients and film thicknesses, five different polymeric films are prepared. These films are given

in table 4.1. The thickness of the film is arranged using rotation speed and spin time of the spin coater. SEM is used to measure the film thicknesses.

4.4 Experimental Results on Diffraction from Transient Grating

To begin with investigating the gratings, the pump-probe arrangement shown in figure 4.3 is set-up. DPSS laser producing 532 nm light pulses with 15 ns pulse width is employed as a pump source. The beam emerging from the laser is split up into two beams and the pump beams are focused onto the sample, where they interfere and form interference pattern.

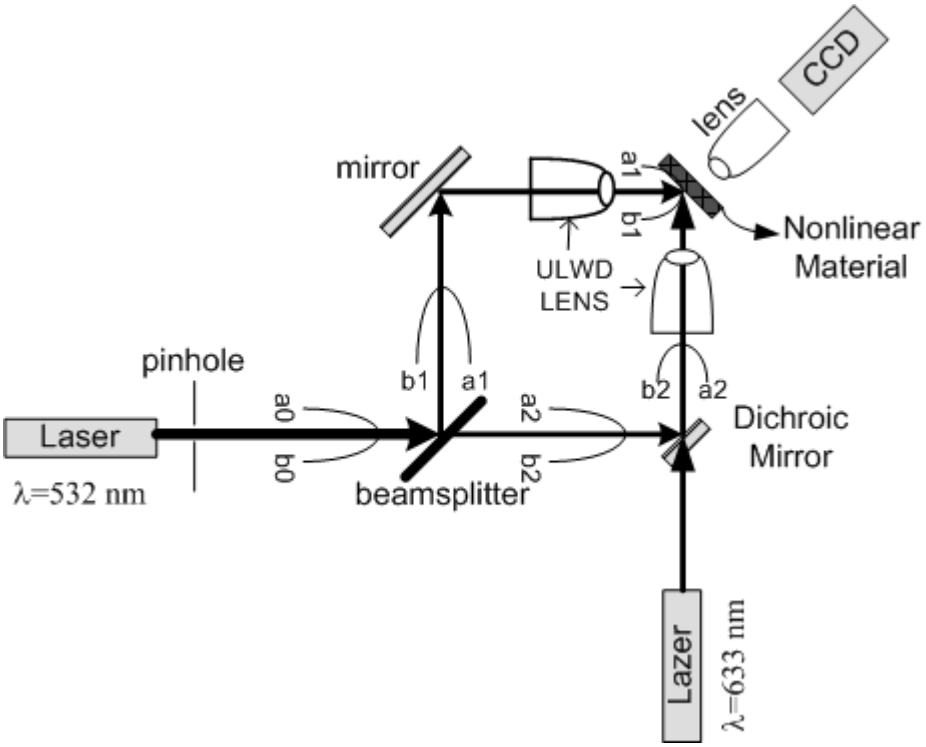

Figure 4.3. Pump Probe Experiment

The interference pattern formed by the pump beams on the material causes fringes shown in figure 4.4. Objective lens with Numerical Aperture of 0.9 and magnification x90 is used to resolve the fringes.

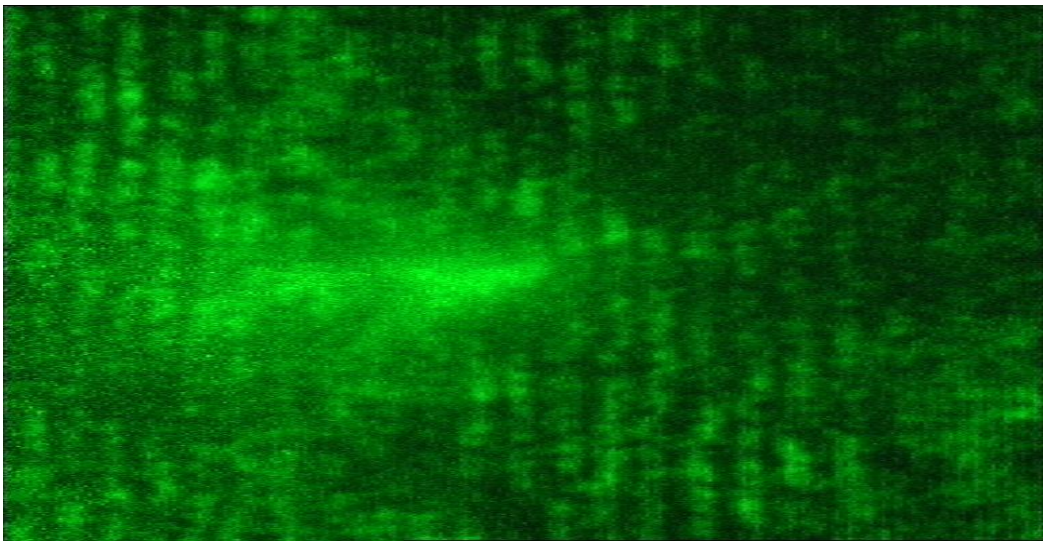

Figure 4.4. Interference fringes on the MR doped PVA polymeric composite

After observing the interference pattern, probe beam of 632.8 nm with 15 mW output power was applied to detect the diffraction from transient grating. However, we were not able to observe any diffraction pattern on the CCD recorder. Although an interference pattern with contrast higher than 50% have been observed, we failed to measure any power at the diffraction orders $m = 1$ or $m = -1$. In order to improve the interaction mechanism, we developed more enhanced experimental setup.

In a Mach-Zehnder interferometry setup, described in figure 4.3, the output of the laser is split into two excitation beams B1 with lobes b1:a1 and B2 with lobes a2:b2. By tracing the excitation pumps it is easy to observe that in the interference plane; a1 side of the beam B1 interacts with b2 of the beam B2 and b1 side of the beam B1 interacts with a2 of the beam B1. In case of pure Gaussian output profile of the laser this spatial relation does not have a crucial effect on grating formation, but in some imbalances this occasion reduces fringe visibility due to phase incompatibility. Figure 4.5 shows the modified version of the experimental setup, where each of the beams is interfering with their counterpart.

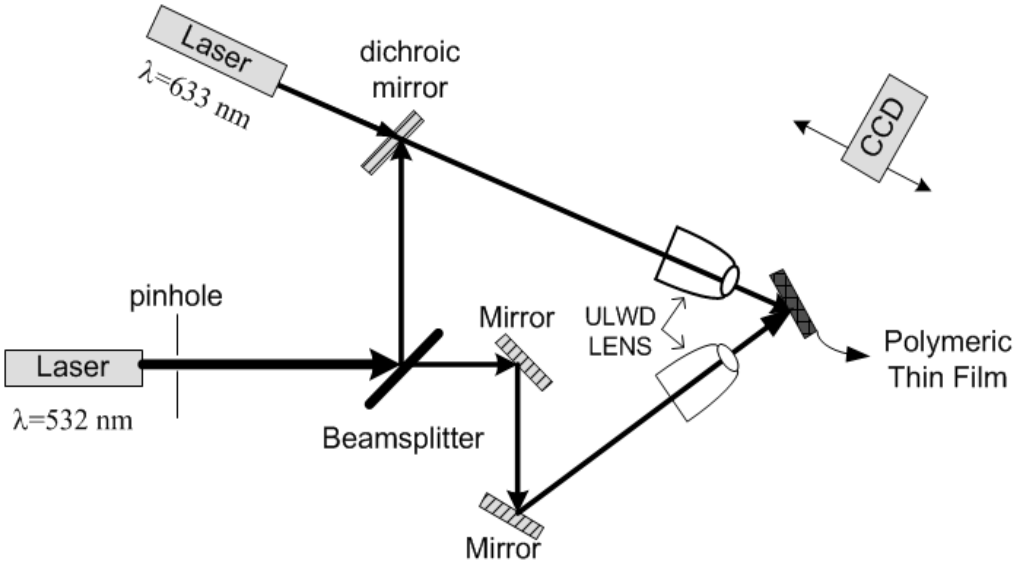

Figure 4.5. Diffraction from the transient grating

In addition to phase concerns, coherent length is another important parameter that has to be taken into account during the measurements. The bandwidth of the DPSS laser is measured as $\Delta\lambda = 3\,nm$ which corresponds to coherence coherent length of $94\,\mu m$. The path difference of the two beams should be carefully arranged and reduced below the coherence length.

The experimental setup shown in figure 4.5 is constructed using polymeric films given in table 4.1. Pump beams are crossed at half intersection angle of 45° by Ultra Long Working Distance lenses with focal length of 2 cm (NA: 0.42, x50) and 632.8 nm He-Ne laser is used as a probe beam. The spot size of the pump beams at the intersection plane is about 1 mm in diameter. The angle of first-order diffraction is estimated using eq. (4.5) and CCD is placed to observe the diffracted probe beam. CCD is sensitive to the minimum power variation of about 1 nW. In order to avoid the recording of pump beams in CCD, laser line filter with 632.8 nm central wavelength and 10 nm band pass bandwidth is placed in front of the CCD. The results for each film are given in the following figures. To explain the experimental data we used the following terminology:

1. *"0^{th} order total intensity variation"*

The total intensity I_t is obtained by summing the values of all pixels when pump exist. Intensity I_0 is obtained by summing the values of all pixels when pump is not applied. The difference $I_t - I_0$ is total intensity variation. This is an important parameter that points the grating existence because some of the power is transferred into other diffraction orders and total intensity at that order falls down.

2. *"First order total intensity"*

Total intensity in the first diffraction order ($m = -1$) obtained by summing the values of all pixels.

3. *"0^{th} order peak intensity variation"*

This parameter indicates the difference of peak value of intensity for $m = 0$ when grating exist and does not exist.

4. *"First order peak intensity variation"*

This parameter indicates the difference of peak value of intensity for $m = -1$ when grating exist and does not exist.

Experimental Results with Film 1

When the surface of the film 1 was inspected under microscope, many particles with diameter similar to pump wavelength was observed. Although there is 10% variation in the 0^{th} order at 29 A laser diode current, this power is not transferred to the other diffraction orders. The further increase in laser power does not result in any diffraction.

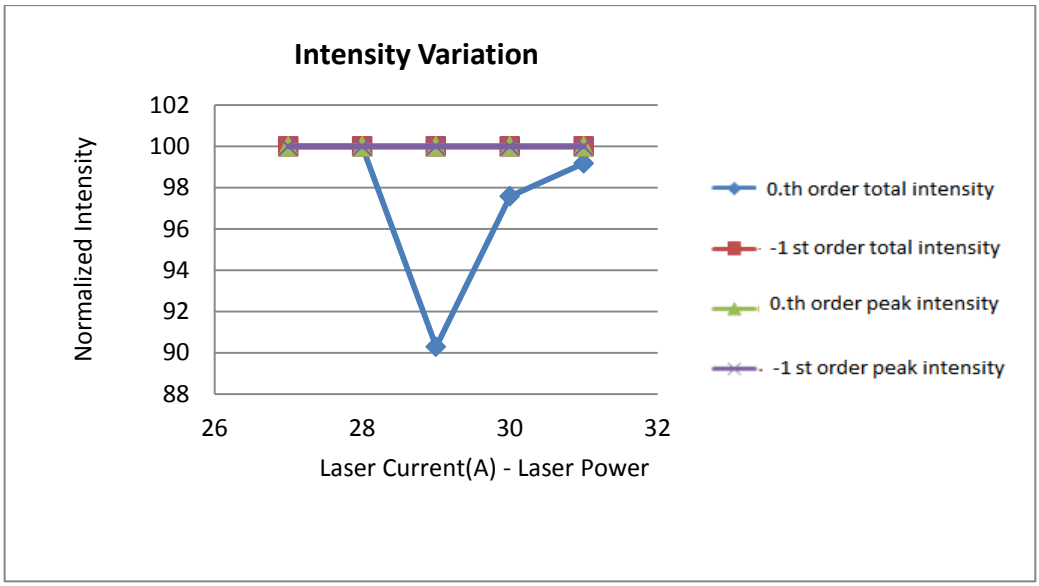

Figure 4.6. Intensity variations due to transient grating for film 1

Experimental Results with Fim 2

A diffraction pattern is observed when the laser diode current is arranged to 30A. At this laser power, the 0^{th} order power decreases 4% and this power is coupled to the first diffraction order, i.e. $m = -1$.

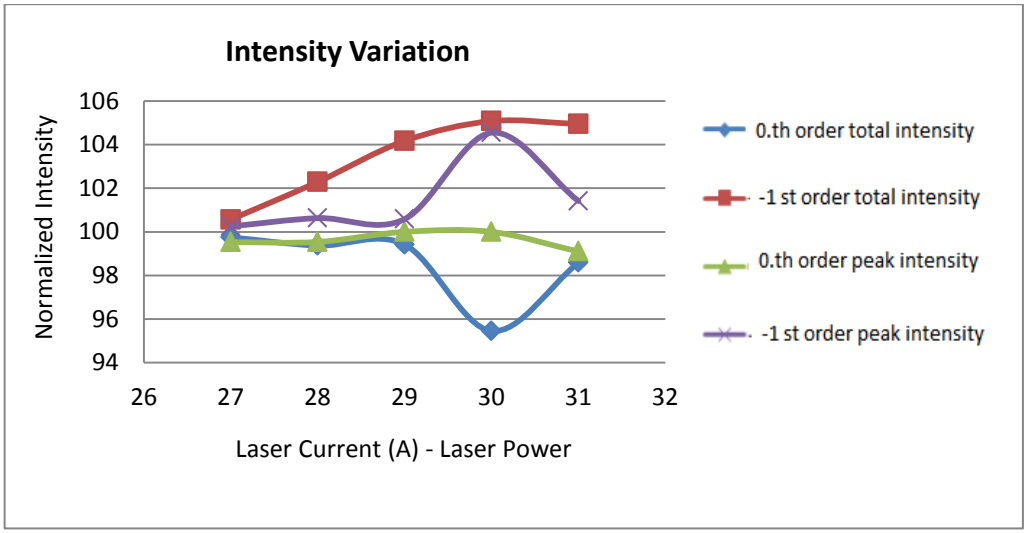

Figure 4.7. Intensity variations due to transient grating for film 2

Experimental Results with Film 3

The maximum power transfer into first diffraction order is observed in laser diode current of 30A. At this pump power rate, the 15% of the probe beam is diffracted into the order $m = -1$

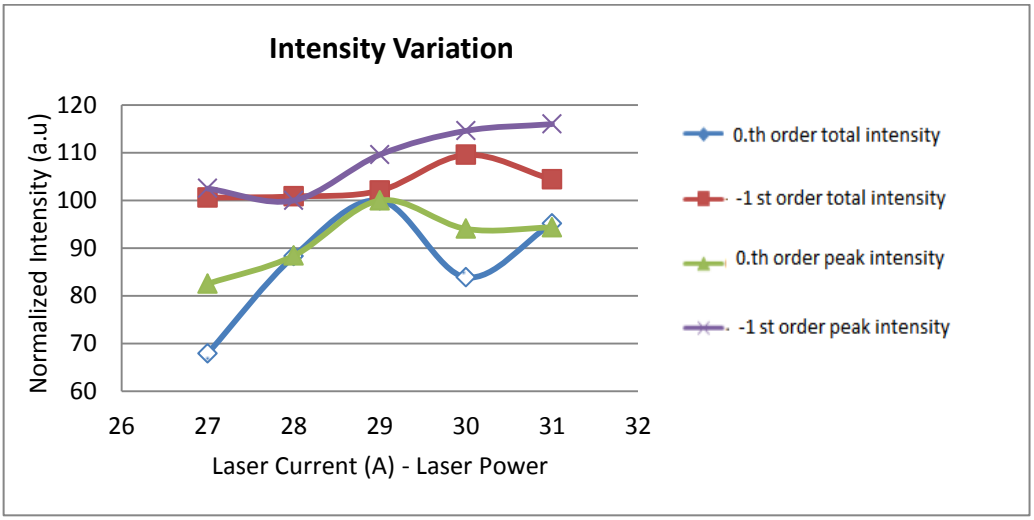

Figure 4.8. Intensity variations due to the transient grating for film 3

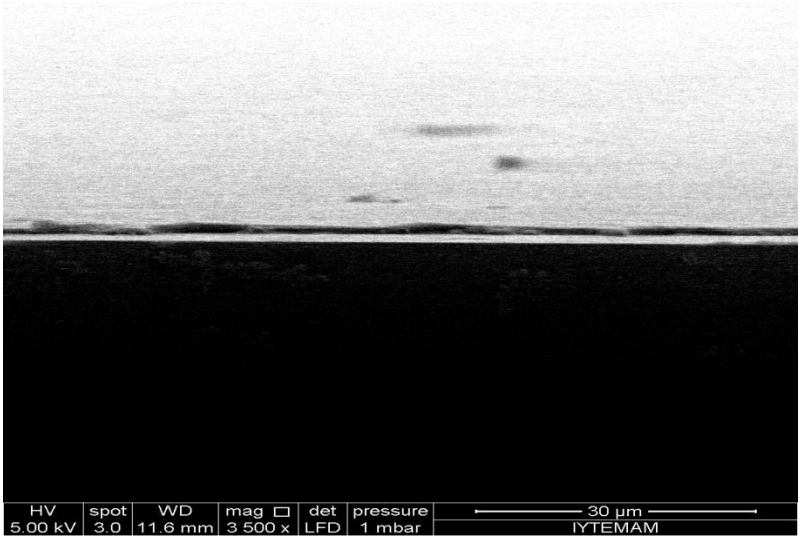

Figure 4.9. SEM picture of film 3

Experimental Results with Film 4

In this sample, although a 10% variation in the 0^{th} order is observed, we were not able to measure any power changes in the diffraction order $m = -1$.

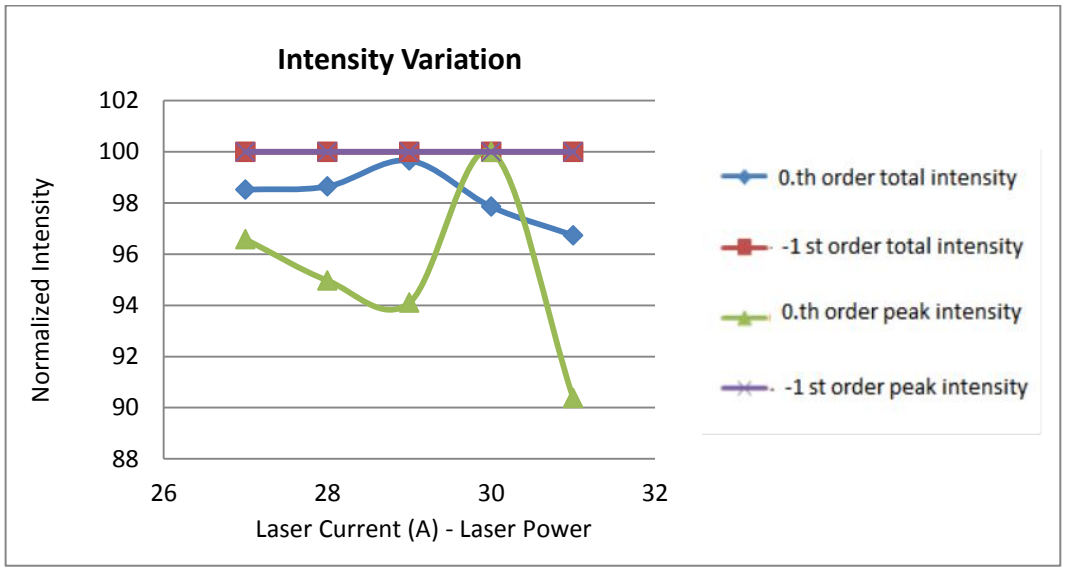

Figure 4.10. Intensity variations due to the transient grating for film 4

Experimental Results with Film 5

In this sample 4% of the power of the probe beam is diffracted in to the first order $m = -1$. In contrast to the other other films, this power transfer occurs at higher pump powers(Laser diode current: 31A)

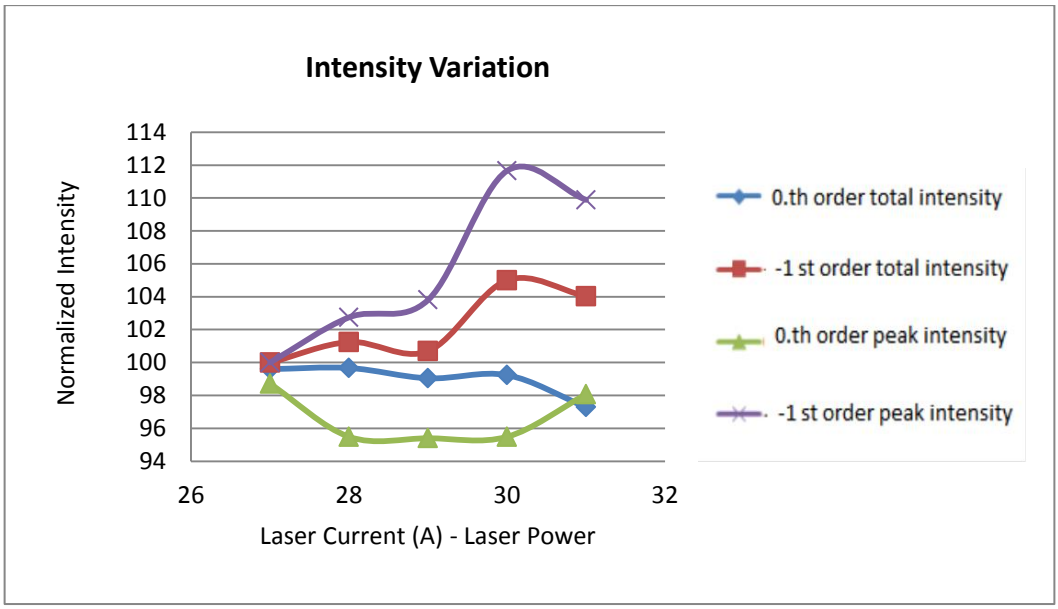

Figure 4.11. Intensity variations due to the transient grating for film 5

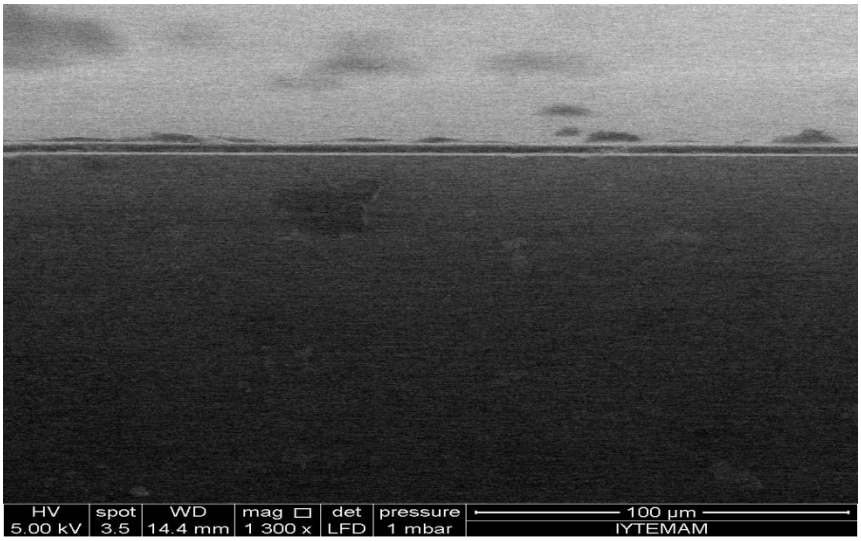

Figure 4.12. SEM picture of film 5

In order to summarize the experimental data, figure 4.13 and figure 4.14 shows 0^{th} order and 1^{st} order diffraction efficiencies, respectively.

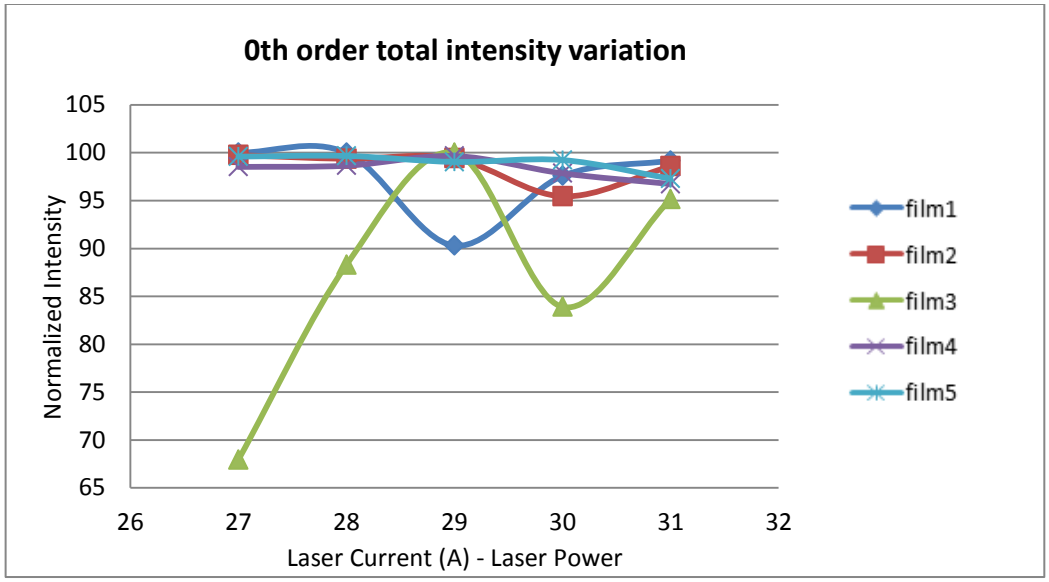

Figure 4.13. 0^{th} order intensity variations for all films

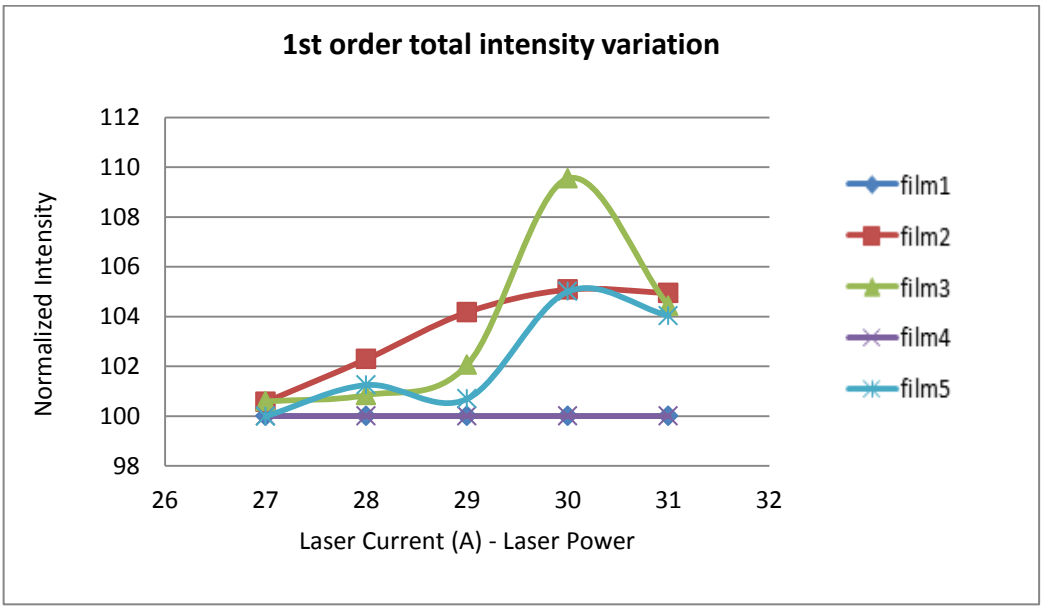

Figure 4.14. 1^{st} order intensity variations for all films

According to the experimental data, using the film3 as a nonlinear material with thickness of 2.7 μm gives best diffraction efficiency of about 10%. Although film2 and film5 are also suitable for optical applications, they show a weaker diffraction property of about %5 in comparison to film 3. As a consequence of these experimental results, we decided to use the formulation of MR1 as the film material for the switching device realized in the thesis.

CHAPTER 5

EXPERIMENTAL RESULTS OF ALL OPTICAL SWITCHING DEVICES

Third order optical processes (Kerr type) in nonlinear polymeric materials offer great advantages in terms of response time, high nonlinearity and processing simplicity [4]. The refractive index of dye doped polymer slab waveguide can locally be altered by applying a control pulse that results in pulse controlled power transfer from the fiber to the slab waveguide. The refractive index modulation arising from intensity dependent Kerr effect is in the form of control beam intensity profile or interference pattern profile.

Characteristics of directional coupler structures are extensively investigated for various waveguide structures (slab/slab, fiber/slab, fiber/fiber). The coupling between a fiber and a high index planar waveguide has been evaluated by Dinleyici [42] using a vector modal solution method. Alternatively, this structure has also been analyzed by a generalized method using Coupled Mode Theory (CMT) [43], including a four layer model of side polished fiber structures. Fiber/Slab Coupler has been investigated numerically investigated using Beam Propagation Methods [44], [45]. The switching structure, called "*fiber device*", that demonstrates the use of coupling mechanism

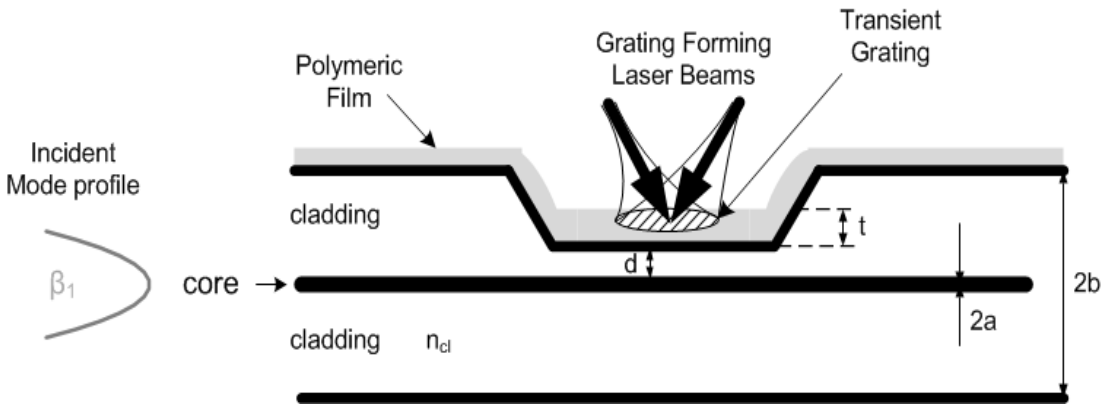

Figure 5.1. Illustration of the *fiber switching device*

realized in this thesis is shown in figure 5.1. This is a structure formed by polishing the single mode fiber cladding, replaced with thin polymeric film. The length of the fiber (Corning HI1060) is 2 m and the polished cladding part is created just in the middle of the fiber and the length of the flattened region is about 10 mm, which is shown in figure 5.2. The distance between core and flat side of the fiber is approximately 9.22 μm.

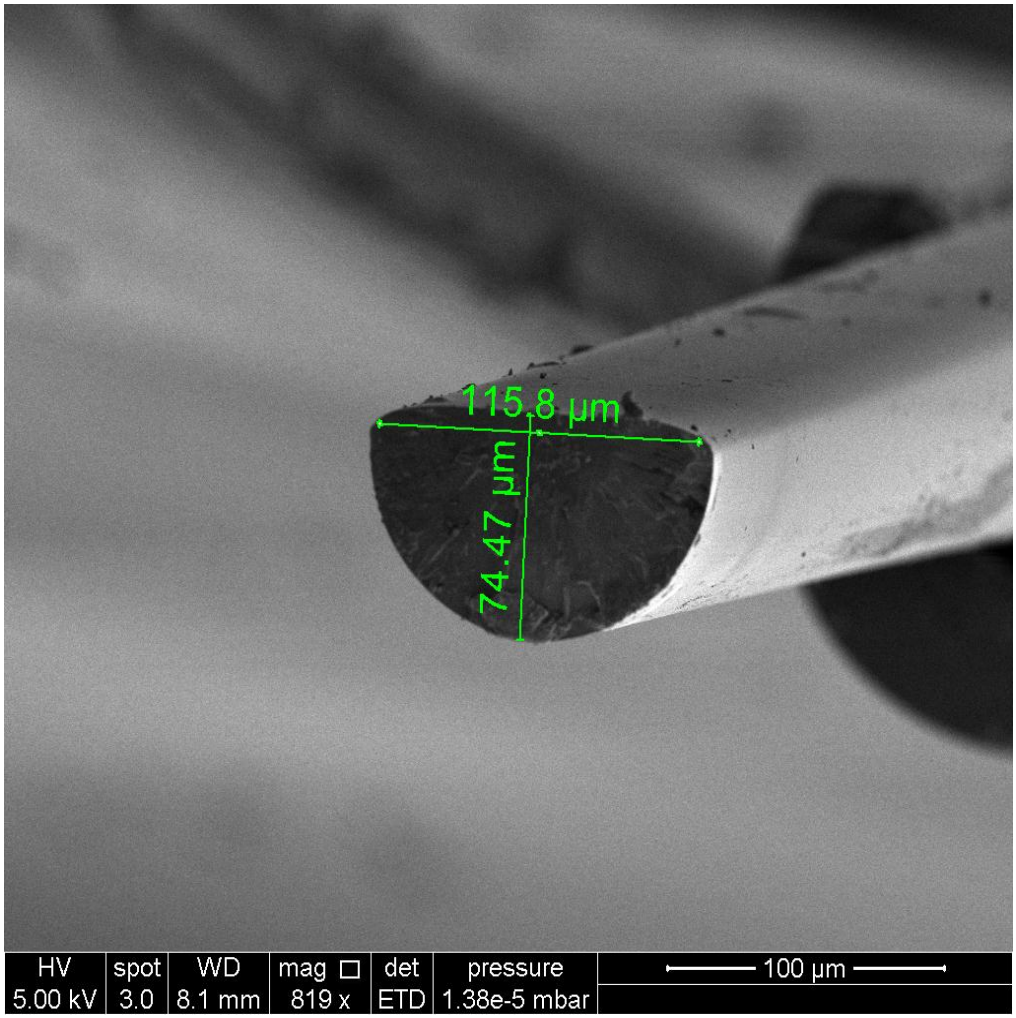

Figure 5.2. SEM image of the polished part of the fiber

The preparation of the nonlinear film used to form slab waveguide layer is described in detail in chapter 3. The thin film has linear refractive index $n = 1.4995$ which was estimated experimentally using Fresnel diffraction based nondestructive measurement method [33]. To increase the nonlinearity and reduce the linear refractive

index of the film, 20 nm SiO_2 particles [Alfa Aesar-Pr.No.12727] were added to the mixture of PVA and dye solutions such that nanoparticles and PVA weight equally (SiO2 - %7.35, PVA- %7.42, Methyl Red - % 0.014). Acquired mixture is coated onto polished part of the fiber by Doctor Blade method and dried approximately 24h at room temperature. The resulting film, as shown in figure 5.3, has approximate thickness of 17.83 µm.

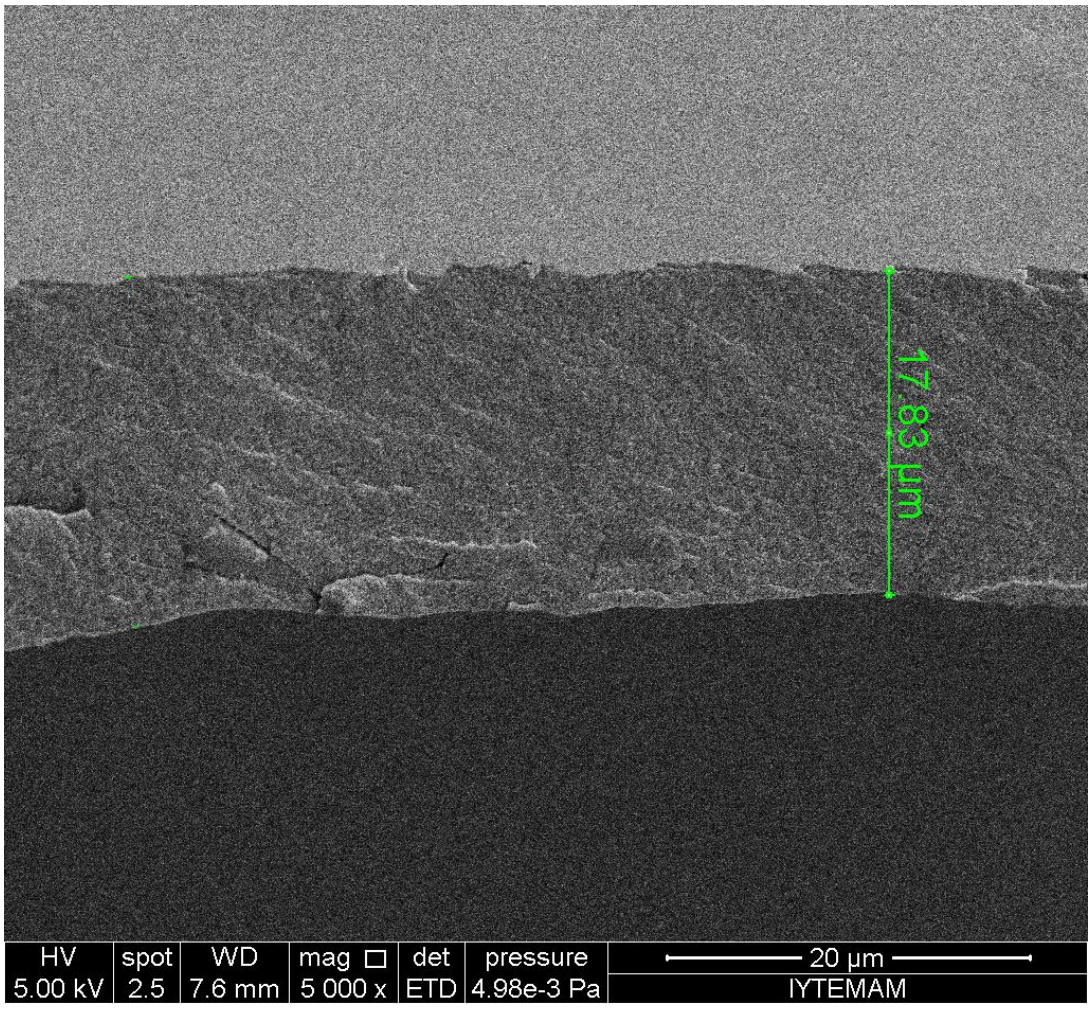

Figure 5.3. SEM image of the polymeric film

Before using in the fiber device, the mixture was coated onto microscope glass in order to investigate the absorption and third order nonlinear properties of the thin film. Z-scan experiment was performed and Kerr coefficient was measured as $n_2 = -4.616 \times$

10^{-11} cm^2/W. The linear refractive index of the nonlinear film affects the propagation characteristics of the light in coupling structure and it is discussed in the next section

5.1 Loss in Side Polished Fibers

The presence of the external medium the polished side of the fiber can be interpreted as a perturbation of the unpolished fiber, where the propagating mode guided by the unpolished fiber is the LP_{01} mode. The characteristics of the propagating mode can be described in terms of the normalized frequency V given in unpolished fiber [49]

$$V = ka\sqrt{n_{co}^2 - n_{cl}^2} \tag{5.1}$$

Where a, n_{co} and n_{cl} are the core radius, core and cladding refractive indices, respectively, and k is the wave number in free space. The effective index of refraction, n_{eff} is related to normalized refractive index b as given below

$$b = \frac{n_{eff}^2 - n_{cl}^2}{n_{co}^2 - n_{cl}^2} \tag{5.2}$$

For the geometry given in figure 5.1, the fiber cladding region $x > d$ is replaced by a polymeric film with refractive index n_p.

The existence of polymeric film has significant effect on propagation constant of the guided mode: if $n_p < n_{cl}$ mode confinement factor for the fundamental mode increases. If $n_p > n_{cl}$, power guided by the fiber is radiated at Cerenkov angle $\theta = \cos^{-1}\frac{n_{eff}}{n_{cl}}$. The power loss in fiber can be found in terms of normalized fiber parameters V, b, and

V_{ex}. A new normalized frequency V_{ex} is growing out after replacing cladding and it may be defined as

$$V_{ex} = ka\sqrt{n_p^2 - n_{cl}^2} \tag{5.3}$$

where V_{ex} is defined only for $n_p \geq n_{cl}$. In this case power guided by the fiber is radiated and the polymeric film acts like a mode sink. The attenuation constant α of the guided mode is a function of the n_p [49], [50]

$$\alpha \approx \frac{4(2\Delta)}{a(1+2b\Delta)} \frac{1-b}{K_1^2\left[V\left(\sqrt{b}\right)\right]} \frac{\left[b(V_{ex}^2 - bV^2)\right]^{1/2}}{V_{ex}^2} K_0\left[2\left(\sqrt{b}\right)V\frac{d}{a}\right] \tag{5.4}$$

where K_0 and K_1 are the modified Bessel function of second kind of the 0th and 1st order, respectively, and Δ is the fractional refractive index change given by

$$\Delta = \frac{n_{co} - n_{cl}}{n_{co}} \tag{5.5}$$

5.2 Coupler Based All Optical Switching/Modulating Device

In this dissertation, firstly, we have demonstrated an ultrafast optical switch/modulator based on a structure that evanescently couples the light from a side polished single mode fiber to the nonlinear polymer slab waveguide. The pulsed control beam emerged from the DPSS laser is focused on the polymer film and applied pulse alters the refractive index of the polymer according to the Kerr effect. This is a local

effect and limited with the control pulse duration. The basic experimental setup illustrated in figure 5.4 shows the implementation of the "*fiber device"*

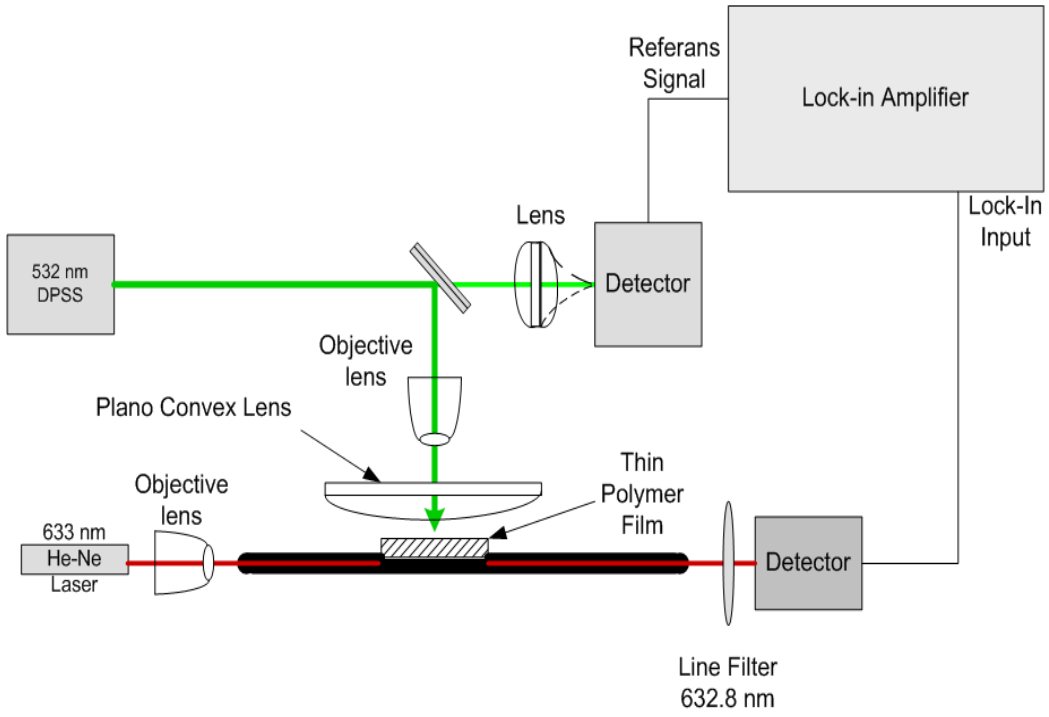

Figure 5.4. Design of the experimental setup

The light emerged from the CW 632.8 nm He-Ne laser is launched into the "*fiber device"* using an objective lens with NA = 0.11. Far field mode profile, given in figure 5.5, is recorded using CCD to ensure the nearly single mode operation before and after coating the cladding region. The control pulse, shown in figure 5.6, has 14 ns pulse duration (FWHM) at 35 kHz repetition rate. The Gaussian like beam spot size at the laser output is measured as 1.43 mm as depicted in figure 5.7.

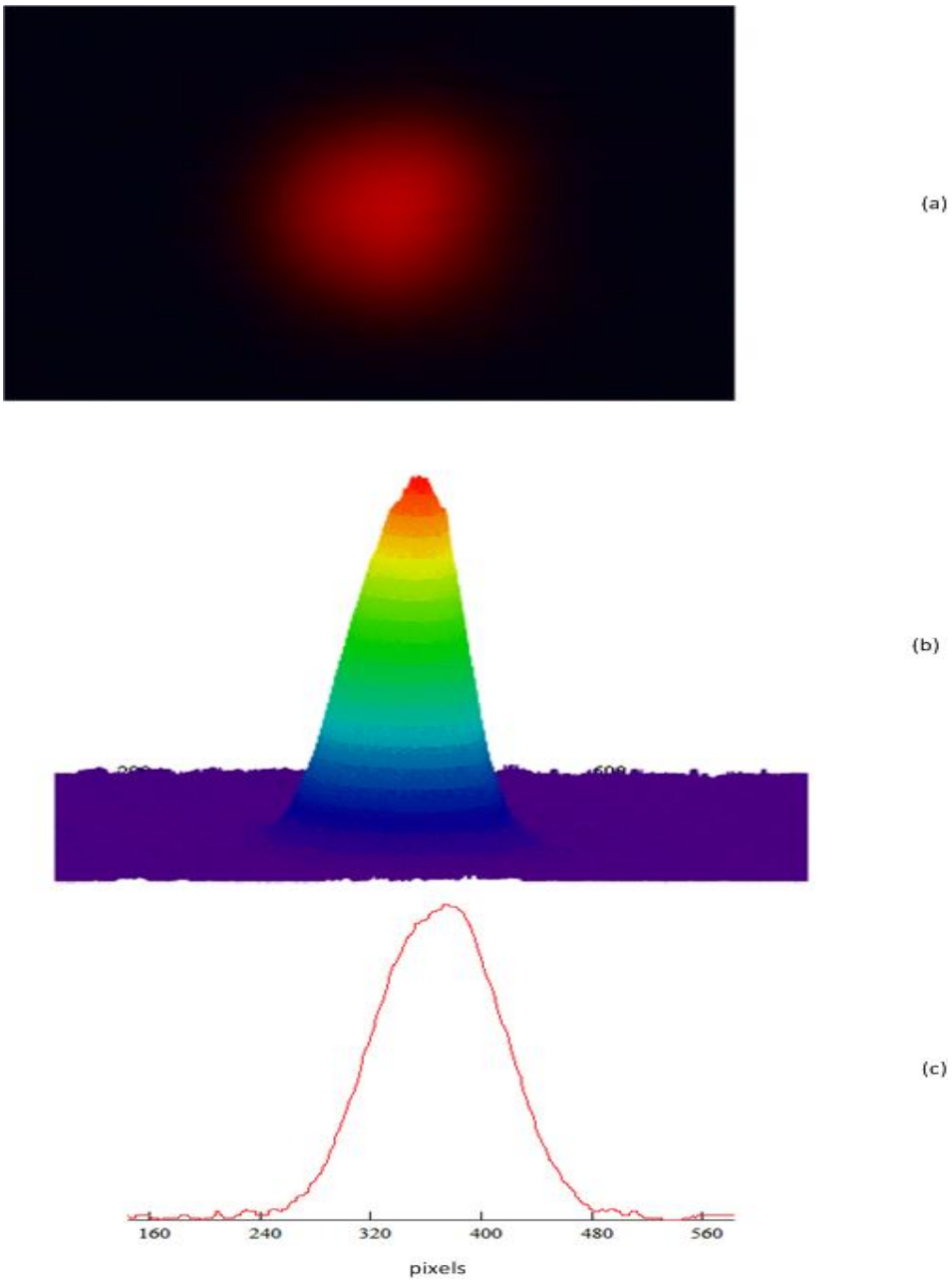

Figure 5.5. a) Far field profile of the beam radiated from fiber end b-) 3D visualization of the measured data c) 2D profile of the measured data

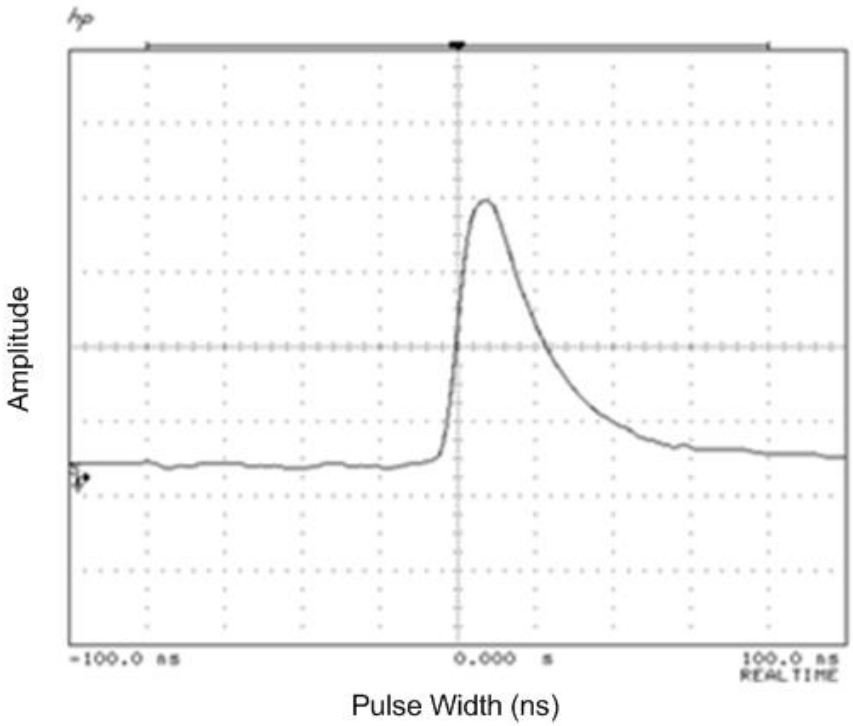

Figure 5.6. Temporal pump pulse profile

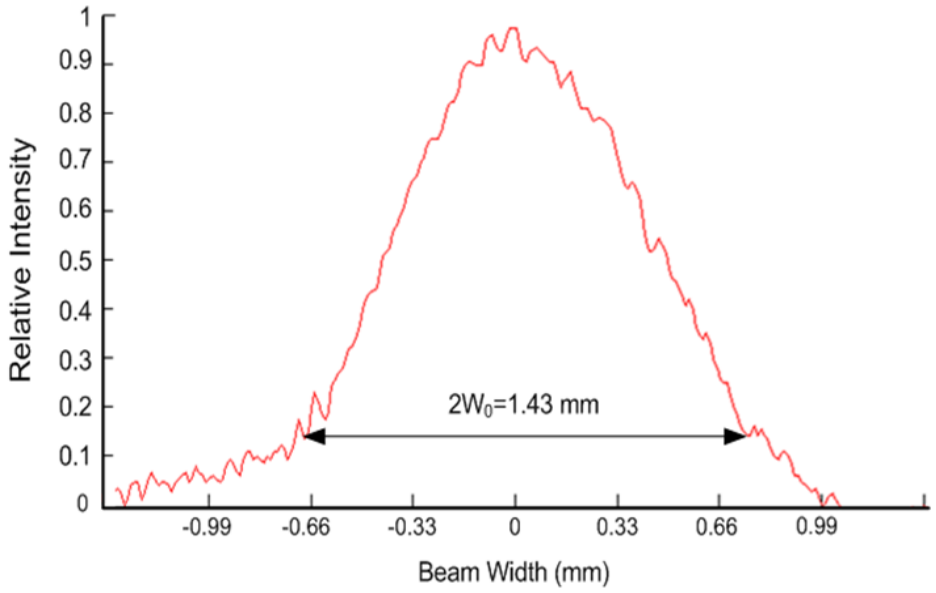

Figure 5.7. Spatial beam profile

The control pulses were focused to an elliptical spot onto the slab waveguide at normal incidence by using Plano convex and objective lenses (NA: 0.11, x4). The ellipsoidal spot has a minor axis of about 0.5 mm and the major axis was about 2 mm and the arrangement was made such that major axis coincides with the optical axis of the fiber core. It should be noted that the spot size of the beam plays an important role in switching mechanism since these temporal and spatial profiles cast into a refractive index modulation. It is desirable to be as large as possible, but also it should contain enough power to harvest the Kerr nonlinearity. The output power of the fiber is measured using high speed Silicon PIN detector (Newport 818BB21) connected to Lock-In Amplifier (Stanford Research – SR830). In order to synchronize the system, the reference input of the lock-in amplifier was obtained from the output of another detector having the same speed.

In order to ascertain switching/modulating capability of the coupler, the output power of the fiber is observed with a lock-in amplifier when the control pulses are applied onto the film slab layer. At the beginning, in the absence of control pulse, the fiber output power remains at a constant level of 25 nW, measured with a power meter. Since the lock-in amplifier is operated in AC mode for all time and there was not any time varying signal to be locked, it reads zero. Then, the peak control power was consistently increased by tuning DPSS current and/or repetition rate parameters until some power changes were measured at the fiber output. The measurements show that until some threshold level of the control peak power, measured as 561 W ($\Delta n = -0.00000259$), there was no significant output change observed. When the control pulses reach 2.344 kW ($\Delta n = -0.0000108199$) peak power, the maximum signal modulation is obtained and the output power of 25.374 nW is measured at the fiber. The right side of figure 5.8 shows the peak power of the modulated fiber signal with respect to the peak power of the applied control pulse. When control pulses are applied on the film, refractive index of the film is locally decreased with the geometry of the beam profile (the film has negative Kerr coefficient) and some of the power propagating in the fiber is transferred to the slab waveguide modes. At this rate of power density, no thermal deformation is observed but further increasing the peak power of control pulse up to 3 kW results in disruption in the polymer film. In that case lock-in amplifier is not able to lock to the reference signal. Later investigation of the fiber under the microscope clearly shows the thermal damage beyond 3 kW peak power rate.

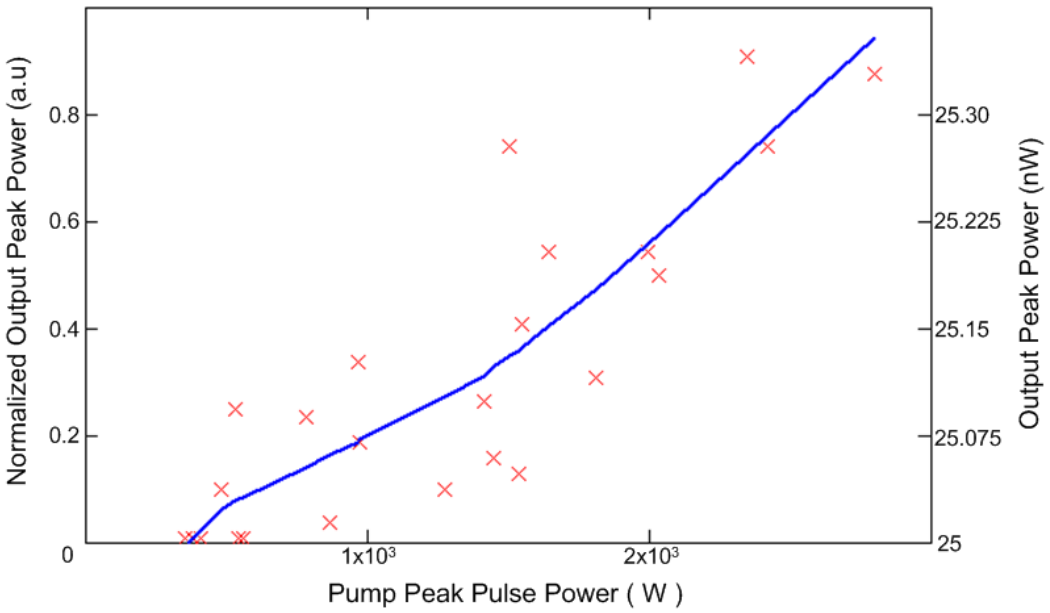

Figure 5.8. Fiber output peak power versus the control pulse peak power

Moreover, the application position of the control pulse is an important parameter for the coupling as shown in figure 5.9. The polished region was divided into three parts and each part, as shown in figure 5.9a, is illuminated with an elliptical beam with axis of 0.5 mm and 2 mm. The highest switching efficiency is observed when region 2 is illuminated and the output peak power is about 25.374nW. Although the refractive index modulation remains the same in all three regions, the effect of index modification is small in region 1 and region 3. The main reason for this result is probably the fiber core–flat side separation 'd', given in figure 5.9c [49]. The parameter 'd' determines the amount of power of the evanescent field that will interact with the index modulated region. When the separation distance 'd' is increased, the coupling coefficient is decreasing and the effect of index modulation on the ridge modes is diminishing [42], [44], [46]. Since the index modulation has the ellipsoidal like shape, rather than covering the whole film, the coupling among the modes (ridge modes, leaky modes and radiation modes) are quite complicated to track with mathematical methods; presumably, the experimental results are accumulation of all these coupling processes.

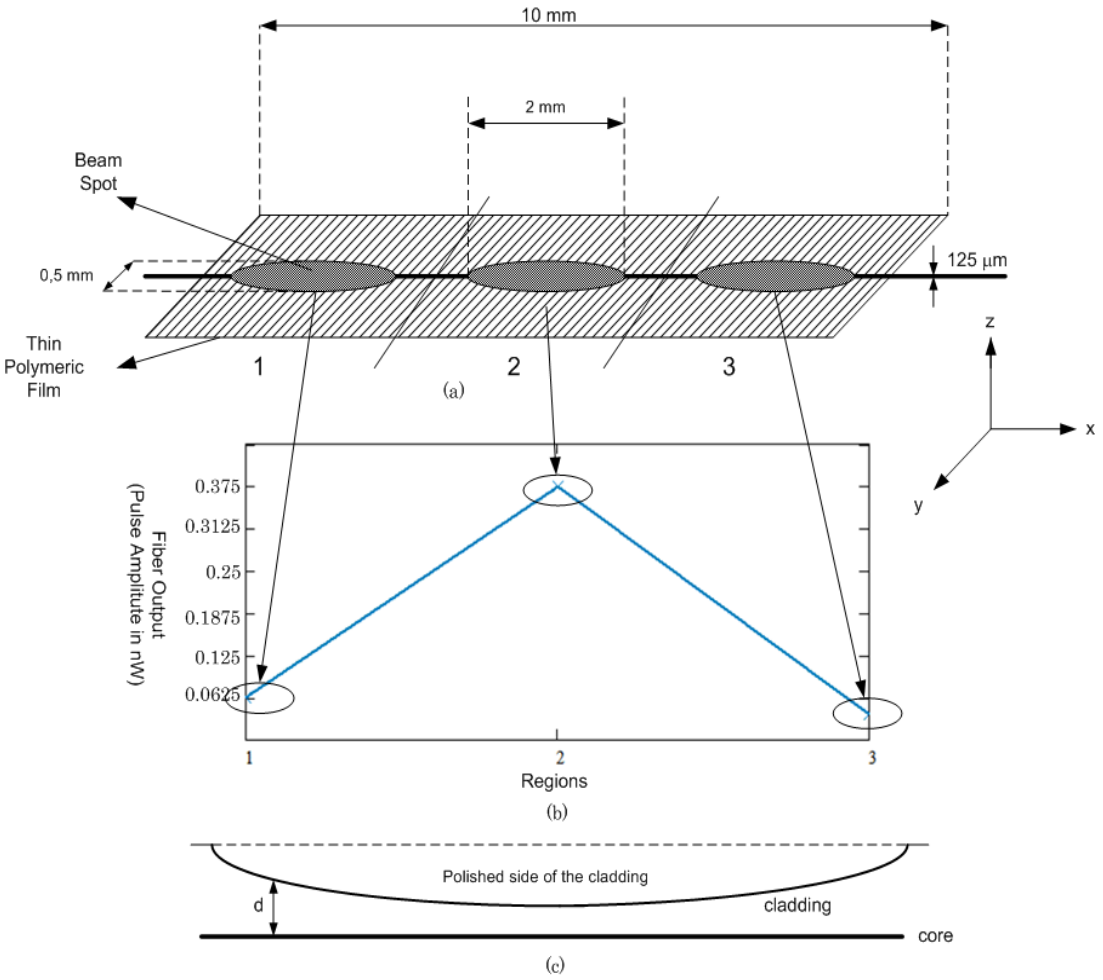

Figure 5.9. Switching efficiency dependence on the laser spot position

To understand the power modulation at the *fiber device* output, consider power loss mechanism in side polished fibers defined by eq. (5.4).

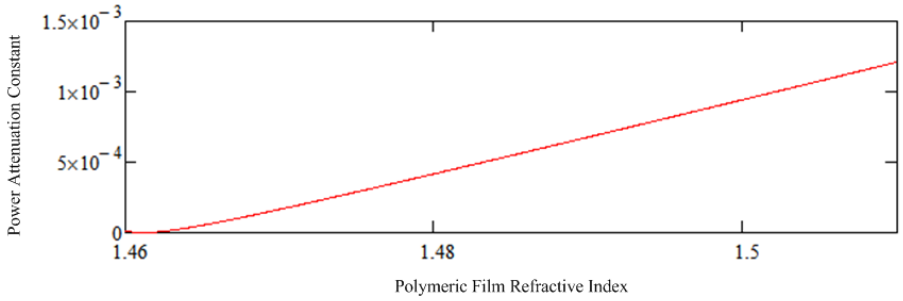

Figure 5.10. Power attenuation constant as a function of polymeric film index

Loss curve is ploted in figure 5.10. When pump pulses are applied as given in fig. 5.4, the refractive index of polymer film is decreasing due to Kerr effect and can be written as $n_p - \Delta n$, where n_p is the refractive index of the nonlinear cladding for no pulse case. Existence of pump pulse reduces the polymer refractive index and less power is radiated out of the fiber, which causes an increase in the output power. Thus, ultrafast power modulation is achived at the fiber output, even though the output power is very low.

5.3 All Optical Switching Based on a Transient Grating

5.3.1 Optical Switching by Mode Conversion

The refractive index of the dye doped polymer slab waveguide can locally be altered with a transient grating generated by interference of control laser pulses. The mathematical model describing the structure and switching efficiency was given in detail in chapter 2.

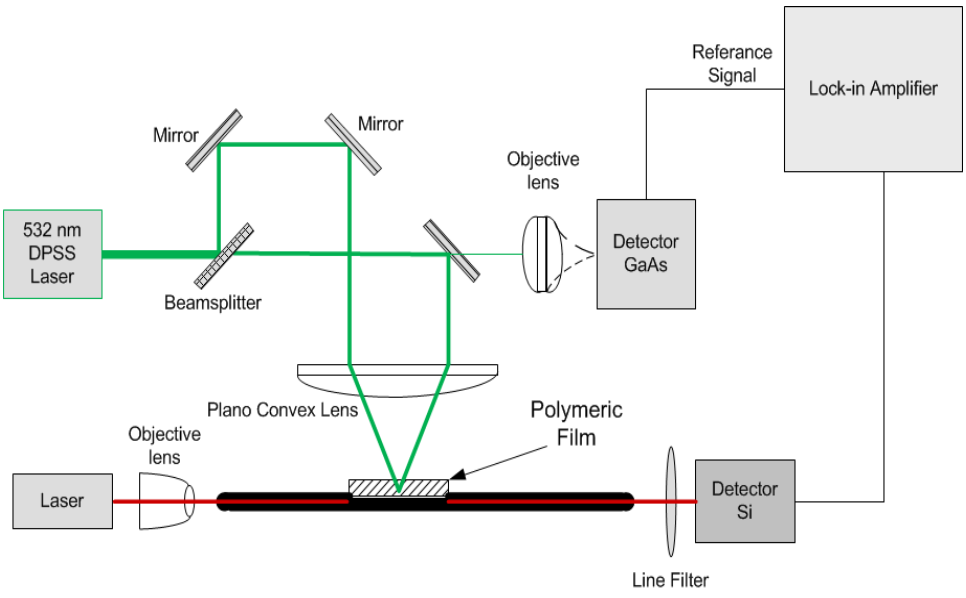

Figure 5.11. Switching with a transient grating

Experimental setup, which is constructed considering the structure given in figure 5.1, is depicted in figure 5.11. To test the structure, three different types of light sources are launched into the fiber, separately. In all cases, we ensure the nearly single mode excitation by recording the fiber output with a CCD camera (576x768 pixels with dimensions of $11\mu m \times 11\mu m$, as given in figure 5.12.

In order to demonstrate the switching capability and setup transient grating, DPSS laser with 532 nm wavelength, a pulse width of 14 ns , a repetition rate of about 25 kHz and beam peak power of 1.994 kW is employed. The light output of the laser is split by a 50% beam splitter into two excitation beams and those beams are crossed on the polymer to form a transient grating. Plano Convex lens with 5 cm diameter and 7.5 cm focal length is used to focus the pump beams. The pump beams are sent parallel to each other and separation distance between the parallel beams is used to modify the interference angle. The spot size of each beam is about 1 mm in diameter. The effect of transient grating is measured using high speed Silicon PIN detector connected to Lock-In Amplifier.

The mathematical model of the system was given in chapter 2. By crossing the two pump beams with Gaussian profile on the polymeric film, a non-periodic interference structure is formed. This structure is transferred to the polymer as a refractive index pattern. Fiber mode propagating in the fiber core is interacted with the transient grating and Four Wave Mixing occurs if frequency and phase matching requirements, given by (2.31) and (2.32), are satisfied. Thus, according to the grating structure (grating period) the switching capability of the device is measured.

Firstly, He-Ne laser with 543 nm wavelength is used as a light source. The light emerged from this laser is coupled to the fiber with objective lens having NA value of 0.11. By utilizing Sellmeier approach, core and cladding refractive indices of the fiber at that wavelength is estimated as $n_{core} = 1.46372$ and $n_{cl} = 1.46151$, respectively. We estimated that fiber supports two modes: LP_{01} mode with effective index 1.4627176 and LP_{11} mode with effective index of 1.4615364. The profile of launched beam at far field is recorded by CCD and given at the right side of the figure 5.12. In this case the power at the output of the fiber is measured as 100 nW using power meter. When the pump beams are applied on the film, the grating is formed. The power variation as function of the half intersection angle (grating period) is given in figure 5.13.

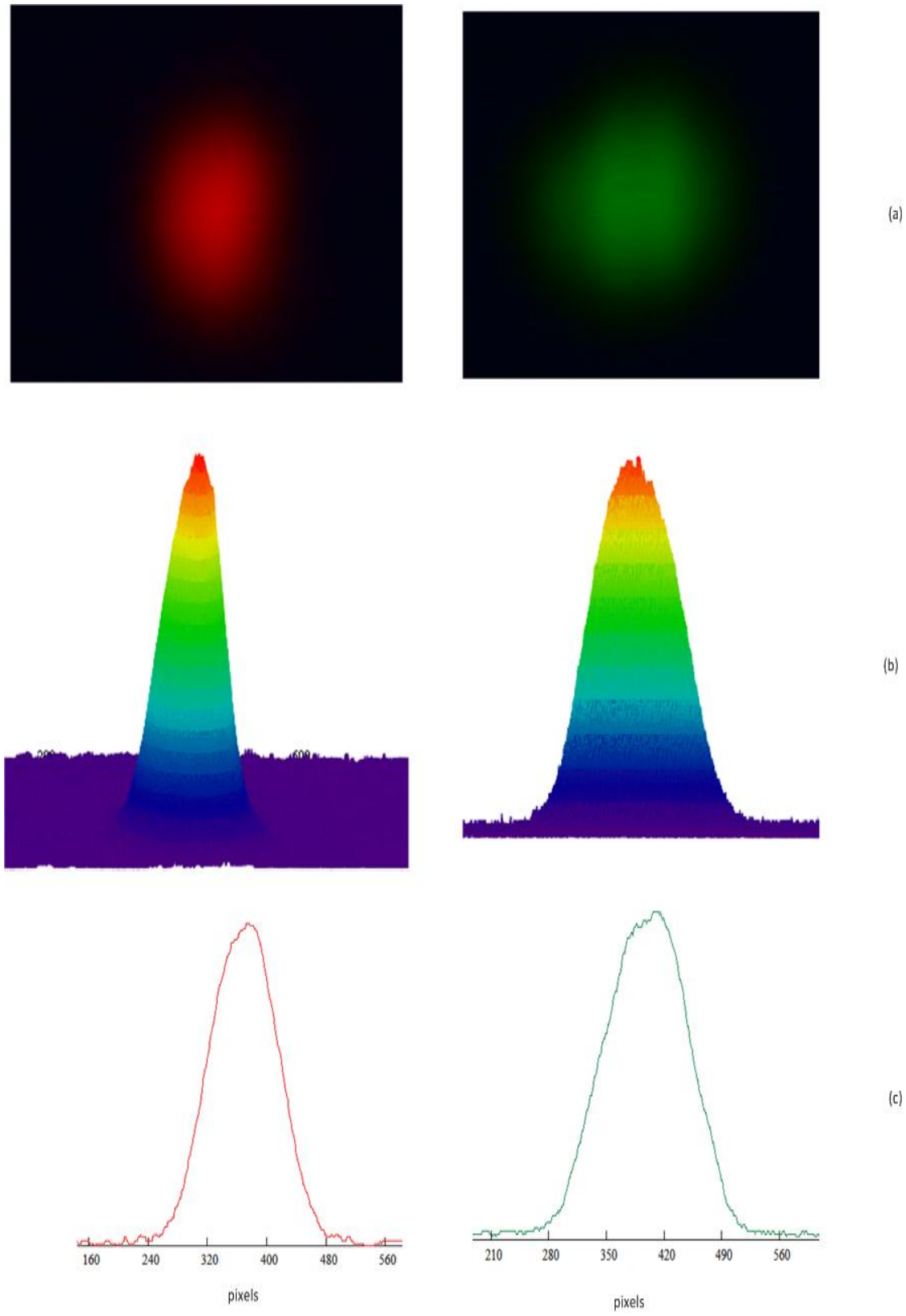

Figure 5.12. a) Far field profile of the beam radiated from fiber end b-) 3D visualization of the measured data c) 2D profile of the measured data. Left side: 632.8 nm, Right Side: 543 nm

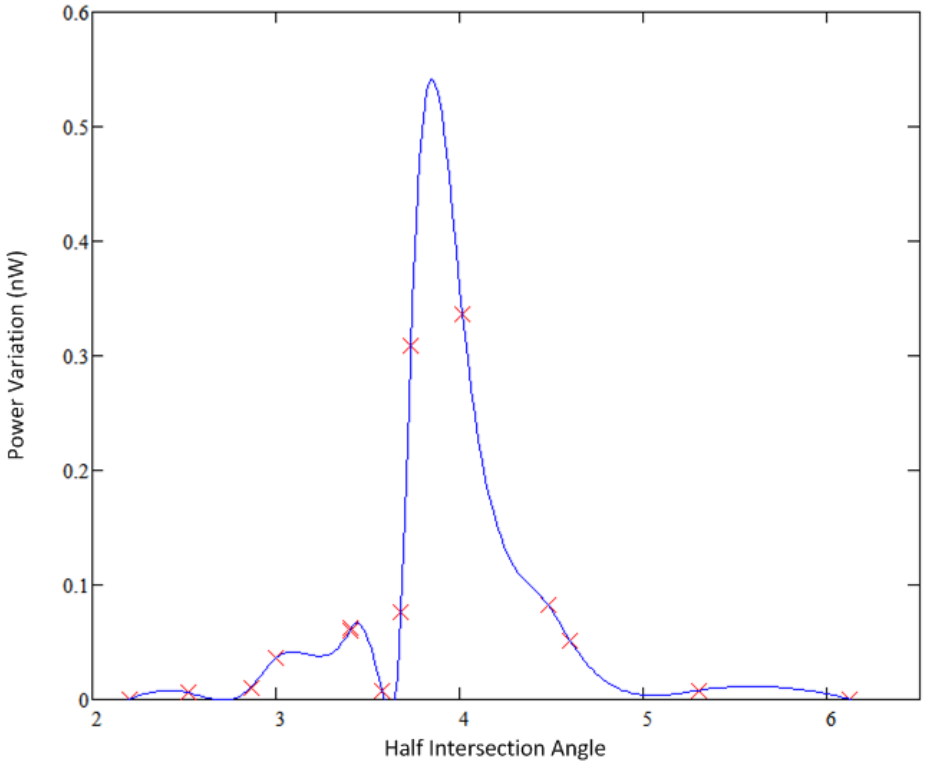

Figure 5.13. Output power variation as a function of interference angle at 543 nm

For half intersection angle θ of about $3.731^{\circ}$and 4.014°, power variation of 0.309nW and 0.336 nW, respectively, is observed at the fiber output. In the figure 5.13, dots represent real experimental data, while the line is obtained by linear interpolation of the data.

Subsequently, He-Ne laser with 632.8 nm wavelength and 15 mW output power is employed as light source. Core and cladding refractive indices of the fiber at that wavelength is estimated as as $n_{core} = 1.46277$ and $n_{cl} = 1.45757$, respectively. It is estimated that fiber supports two modes: LP_{01} mode with effective index of 1.4611506 and LP_{11} mode with effective index of 1.4588856. The profile of launched beam at far field is recorded by CCD and given at the left side of the figure 5.12. In this case the power at the output of the fiber is measured as 342 nW using power meter. For half intersection angle θ of about 5.2° corresponding to 1.957 μm grating period, 0.078 nW power variation is measured at the fiber output as shown in figure 5.14. In this figure dots represent real experimental data and line is obtained by linear interpolation of the experimental data.

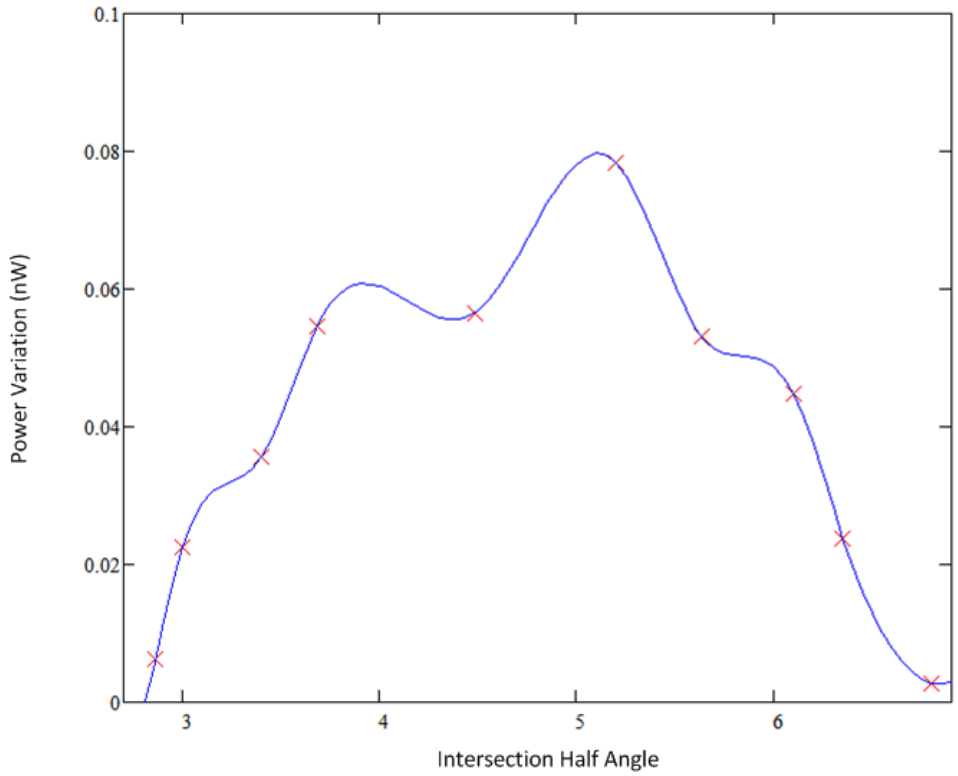

Figure 5.14. Output power variation as a function of interference angle at 632.8 nm

To proceed with, another source with 852 nm wavelength laser is utilized to launch the light into the fiber. The CCD we have is not much sensitive at 852 nm to observe the mode profile at far field, thus the power meter is used as a only tool and it reads 75 nW. Core and cladding refractive indices of the fiber at that wavelength is estimated as $n_{core} = 1.4588$ and $n_{cl} = 1.45248$, respectively. It is estimated that fiber supports two modes: LP_{01} mode with effective index of 1.4561920 and LP_{11} mode with effective index of 1.4528941. For half intersection angle θ of about 7.2°, 0.418 nW power variation is measured at the fiber output as shown in figure 5.15.

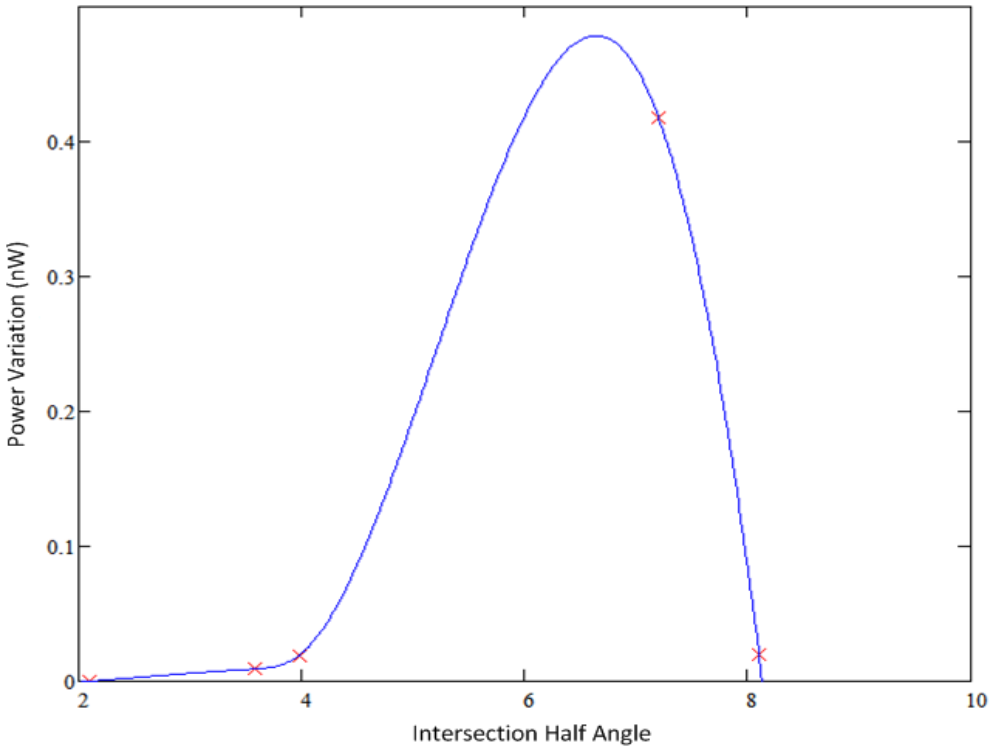

Figure 5.15. Output power variation as a function of interference angle at 852 nm

5.3.2 All Optical Switching by Wavelength Conversion

One way of measuring the mode conversion switching capability of the system is to observe the far field radiation pattern of the fiber output using CCD detector array. However, the recording speed of the CCD array is too slow to measure the nanosecond pulse response of the switching mechanism. Instead of CCD, we used a measurement system that allows only wavelength of interest to be measured and consists of band pass filter, detector and lock-in amplifier. In order to observe the switching capability of the system, two different laser sources were employed with center wavelengths $\lambda_1 = 663\,nm$ and $\lambda_2 = 440\,nm$, respectively. These light waves with distinct wavelengths were launched into the fiber simultaneously and control pump beams were applied on the nonlinear material at the same time. According to the FWM theory given in chapter 2, power exchange between propagating modes was expected. The power variations at each wavelength were measured using Lock-in amplifier as shown in figure 5.16. Band

pass filter was utilized before the detector to block the wavelength that was out of measurement issue.

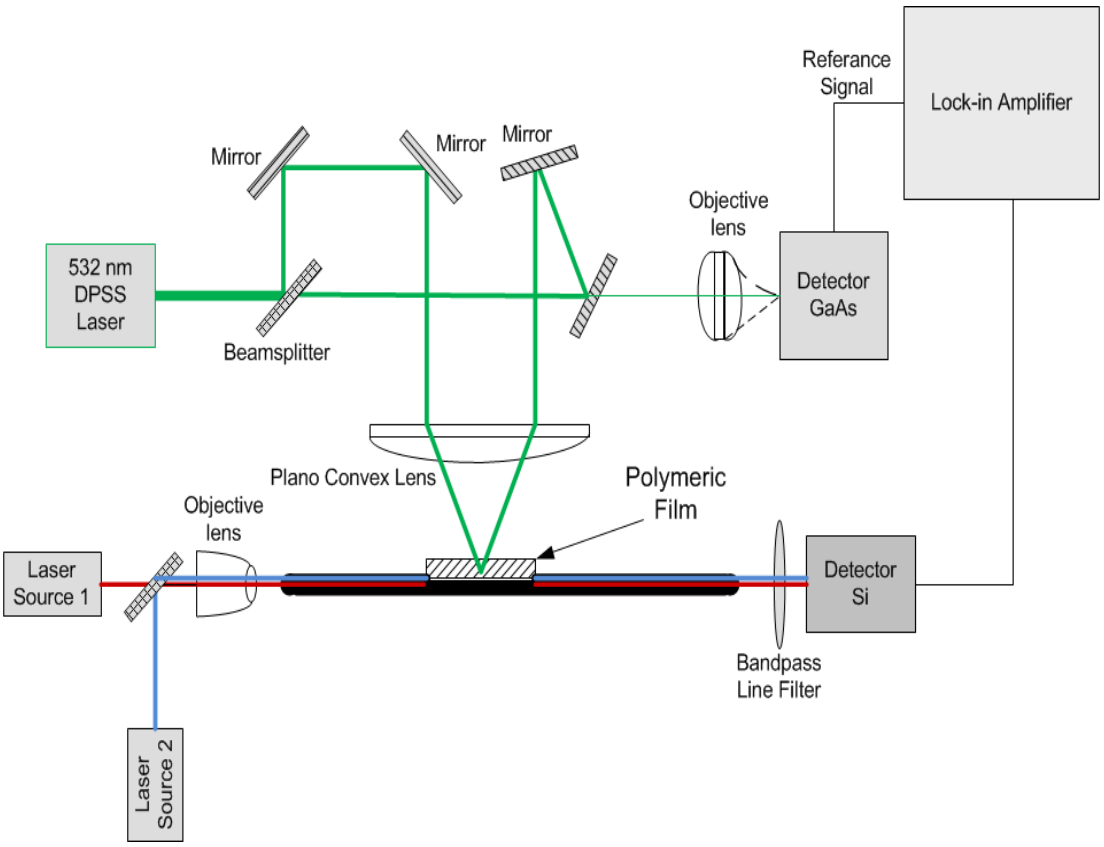

Figure 5.16. Wavelength switching with a transient grating

The spectrum of the laser sources was measured using Optical Spectrum Analyzer and given in figure 5.17. The light beams from the two sources were combined with beamsplitter and launched into the fiber using objective lens with NA = 0.11. Nearly single mode excitation was provided for each of the laser sources. To begin with, the effect of grating on each wavelength was observed using detector and lock-in amplifier at the fiber output. When only laser source 1 was launched, at half intersection angle of 7.1°, maximum power increase of 0.04 nW was observed at the fiber output as shown in figure 5.18. This angle corresponds to the grating period of $\Lambda = 1.435\ \mu m$ and 1 mm grating length.

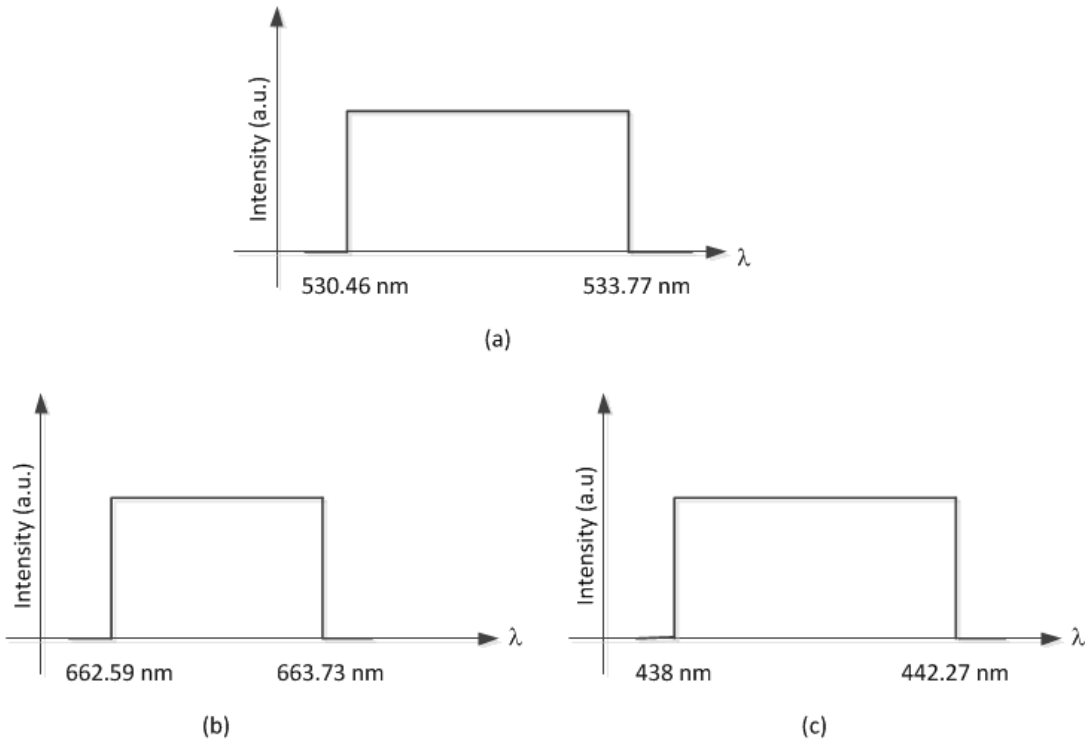

Figure 5.17. Laser source bandwidth a) 532 nm DPSS laser b-)Laser source 1- Red Laser diode c-) Laser source 2-Single mode blue laser diode

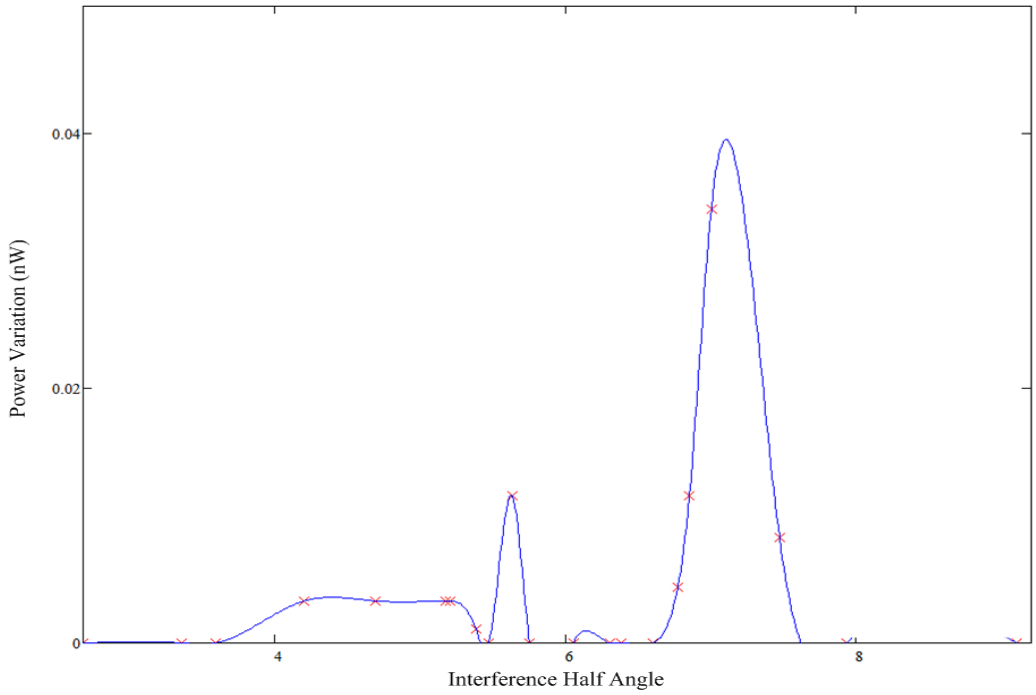

Figure 5.18. Output power variation as a function of interference angle at 663 nm

In the second step, laser source 1 was turned off and laser source 2 with wavelength λ_2 was launched into fiber and single mode was excited. In this case maximum power increase of 0.035 nW was observed at 5.06°. This angle corresponds to grating period of $2.01\ \mu m$ and grating length is about 1 mm. The power variation according to the interference angle (grating period) is given in figure 5.19

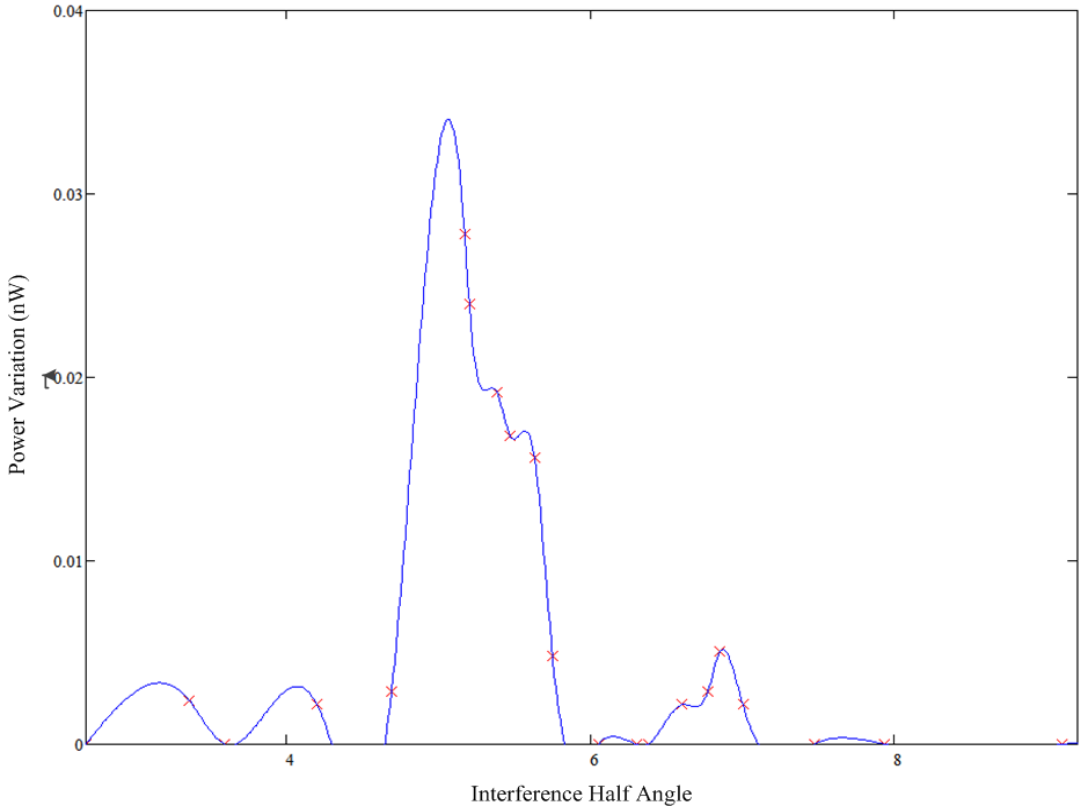

Figure 5.19. Output power variation as a function of interference angle at 440 nm

As a final step, two laser sources were launched at the same time as pictured in figure 5.16. The output of the fiber was measured as a function of interference angle (grating period). At a half interference angle of 6.6°, the phase and frequency matching conditions for Four Wave Mixing were satisfied and power transfer of about 0.25 nW from signal with wavelength λ_1 into the signal with λ_2 was observed as illustrated in figure 5.20. The grating period was $1.548\ \mu m$ and grating length was measured as 1mm and the power transfer occurred from the stronger signal to the weaker one.

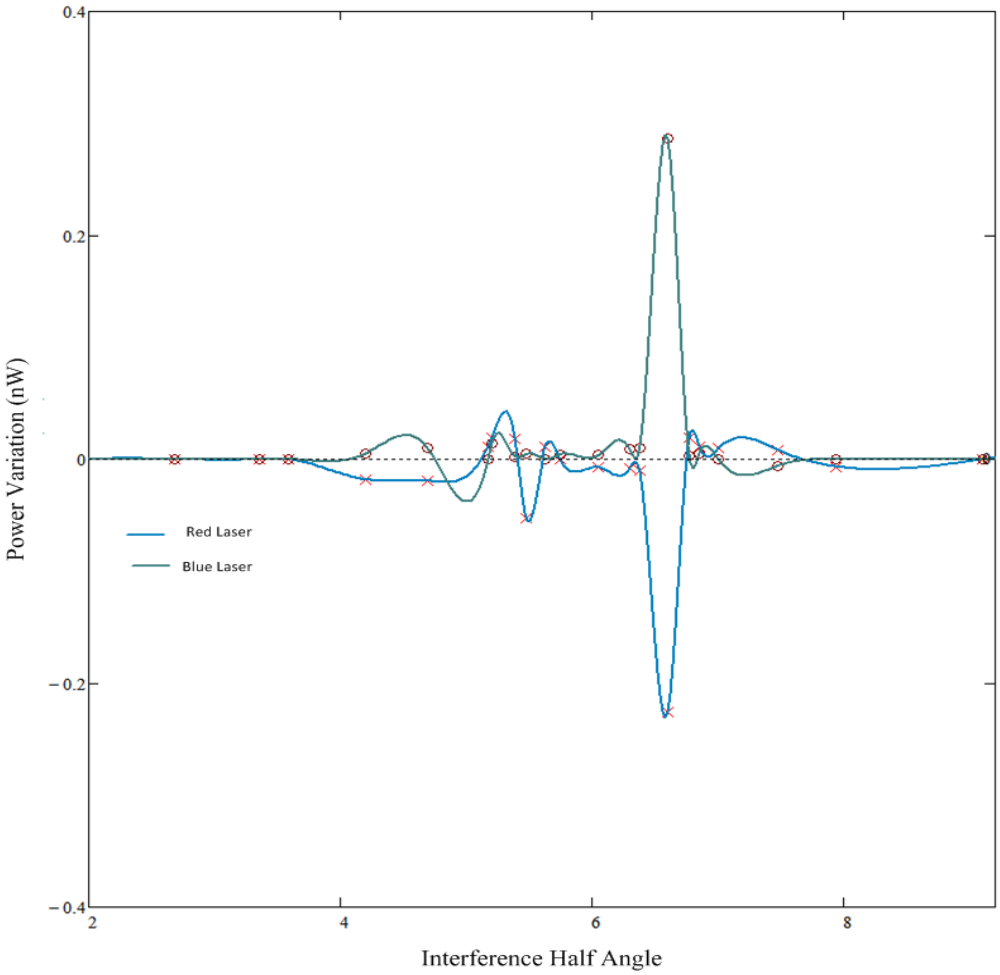

Figure 5.20. Wavelength conversion

These results show that switching structure examined in this dissertation is achieved for all optical switching devices. However, the structure performance should be improved by considering the core-flat side distance, Kerr coefficient of the polymer and polymer linear refractive index.

CHAPTER 6

DISCUSSION ON EXPERIMENTAL RESULTS

6.1 General Discussion on Four Wave Interactions

According to the the mathematical model and experimental procedure, the propagating waves and transient power interact with each other in the polymeric film of the fiber device. These interactions may be considered as a FWM or a Grating Assisted Coupling depending on relative powers of the waves as explained in the Mathematical Model (Chapter 2). In this chapter, the experimental results for the various interaction cases are discussed and compared with estimations of the mathematical model.

The Four Wave Mixing processes are described in detail through out the previous chapters for the switching device structure as given a simplified version in figure 6.1. In the figure where k_3 and k_4 are wave vectors of the propagating modes in the evanescent region, k_1 and k_2 are the wave vectors of the pump beams, these four waves undergo various interactions as explained below.

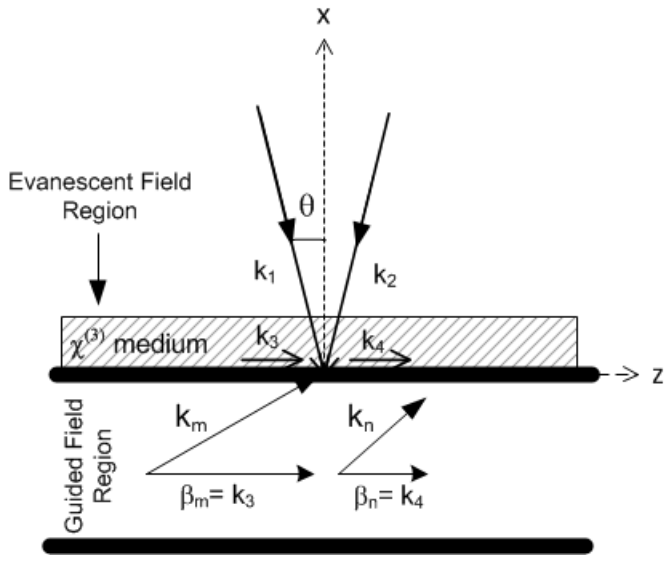

Figure 6.1. FWM in the evanescent region of the waveguide

In order for the waves to be mixed by the medium and to generate the forth wave with wave number k_4, frequency and phase matching requirements given by eq. (6.1) and eq. (6.2), respectively, have to be satisified.

$$\omega_4 = \pm\omega_1 \pm \omega_2 \pm \omega_3 \tag{6.1}$$

$$\overrightarrow{k_4} = \pm\overrightarrow{k_1} \pm \overrightarrow{k_2} \pm \overrightarrow{k_3} \tag{6.2}$$

k_1 and k_2 emerge from the same source that yields $\omega_1 = \omega_2 = \omega_0$ and $|k_1| = |k_2| = k_0$.

These matching requirements produce eight distinct conditions at which FWM may take place.

Case 1

$$\omega_4 = \omega_1 + \omega_2 + \omega_3 \tag{6.3}$$

$$\overrightarrow{k_4} = \overrightarrow{k_1} + \overrightarrow{k_2} + \overrightarrow{k_3} \tag{6.4}$$

Considering the propagating wave vectors components in z-direction and identical pump beams yields

$$\omega_4 = 2\omega_0 + \omega_3 \tag{6.5}$$

$$k_4 = k_3 \tag{6.6}$$

This interaction result in a mode with frequency ω_4. This mode has the same propagation constants with the signal wave with wave vector k_3 in the cladding. However, the resulting wave with wave vector k_4 can not be guided because ω_4 is too high and not supported by the waveguide.

Case 2

$$\omega_4 = \omega_1 + \omega_2 - \omega_3 \tag{6.7}$$

$$\overrightarrow{k_4} = \overrightarrow{k_1} + \overrightarrow{k_2} - \overrightarrow{k_3} \tag{6.8}$$

Considering the propagating wave vectors components in z-direction and identical pump beams yields

$$\omega_4 = 2\omega_0 - \omega_3 \tag{6.9}$$

$$k_4 = -k_3 \tag{6.10}$$

These two waves with symmetrical frequencies around ω_0 are propagating in the reverse direction as shown in figure 6.2. They may be different (higher) modes or the same fundamental modes of the two different frequencies.

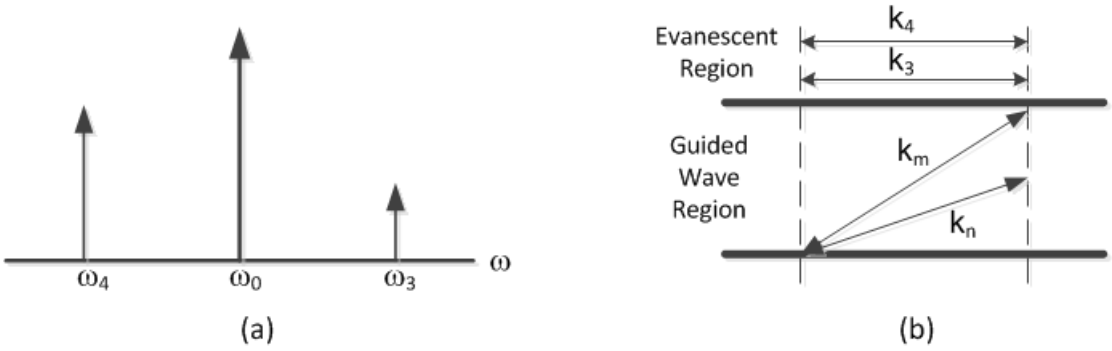

Figure 6.2. Illustration of a-) frequency matching b-) phase matching

Case 3

$$\omega_4 = \omega_1 - \omega_2 + \omega_3 \tag{6.11}$$

$$\overrightarrow{k_4} = \overrightarrow{k_1} - \overrightarrow{k_2} + \overrightarrow{k_3} \tag{6.12}$$

Considering the propagating wave vectors components in z-direction and identical pump beams yields

$$\omega_4 = \omega_3 \tag{6.13}$$

$$k_4 = k_3 + 2k_0 \sin\theta \tag{6.14}$$

As a result of interaction, the waves have the same frequency but magnitudes of the propagation vectors have different values due to impact of the transient grating. This

situation refers to the mode conversion switching among the modes (fundamental-higher order) of the same frequency.

Case 4

$$\omega_4 = \omega_1 - \omega_2 - \omega_3 \tag{6.15}$$

$$\overrightarrow{k_4} = \overrightarrow{k_1} - \overrightarrow{k_2} - \overrightarrow{k_3} \tag{6.16}$$

Considering the propagating wave vectors components in z-direction and identical pump beams yields

$$\omega_4 = -\omega_3 \tag{6.17}$$

$$k_4 = -k_3 + 2k_0 \sin\theta \tag{6.18}$$

The resulting wave have the same frequency with the incident wave and the modes mediated by the laser induced grating propagates at different directions. Minuse sign at the front of ω_3 is due to the wave vector direction.

Case 5

$$\omega_4 = -\omega_1 - \omega_2 + \omega_3 \tag{6.19}$$

$$\overrightarrow{k_4} = -\overrightarrow{k_1} - \overrightarrow{k_2} + \overrightarrow{k_3} \tag{6.20}$$

Considering the propagating wave vectors components in z-direction and identical pump beams yields

$$\omega_4 = -2\omega_0 + \omega_3 \tag{6.21}$$

$$k_4 = k_3 \tag{6.22}$$

This interaction is similar to case 2 but pump beams are reversed as shown in figure 6.3.

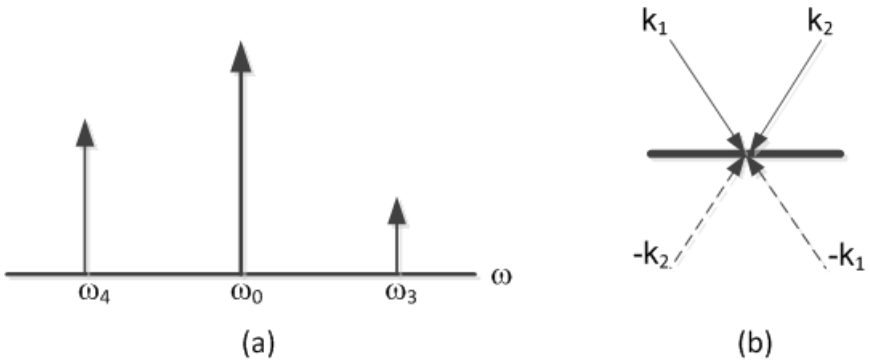

Figure 6.3. Illustration of interaction in case 5 a-) Frequency matching b-) Pump beams

Case 6

$$\omega_4 = -\omega_1 + \omega_2 - \omega_3 \tag{6.23}$$

$$\overrightarrow{k_4} = -\overrightarrow{k_1} + \overrightarrow{k_2} - \overrightarrow{k_3} \tag{6.24}$$

Considering the propagating wave vectors components in z-direction and identical pump beams yields

$$\omega_4 = -\omega_3 \tag{6.25}$$

$$k_4 = -k_3 - 2k_0 \sin\theta \tag{6.26}$$

This case is similar to case 4. The waves mediated by grating propagates in the opposite directions.

Case 7

$$\omega_4 = -\omega_1 - \omega_2 - \omega_3 \tag{6.27}$$

$$\overrightarrow{k_4} = -\overrightarrow{k_1} - \overrightarrow{k_2} - \overrightarrow{k_3} \tag{6.28}$$

Considering the propagating wave vectors components in z-direction and identical pump beams yields

$$\omega_4 = -2\omega_0 - \omega_3 \tag{6.29}$$

$$k_4 = -k_3 \tag{6.30}$$

This interaction is similar to case1. However, the resulting wave travels in opposite direction according to signal wave with frequency ω_3 and their wave vectors are of equal magnitude. On the other hand, the mode with wave vector k_4 can not be guided

because ω_4 is too high and not supported by the waveguide used ın "*fiber switching device"*.

Case 8

$$\omega_4 = -\omega_1 - \omega_2 - \omega_3 \tag{6.31}$$

$$\overrightarrow{k_4} = -\overrightarrow{k_1} + \overrightarrow{k_2} + \overrightarrow{k_3} \tag{6.32}$$

Considering the propagating wave vectors components in z-direction and identical pump beams yields

$$\omega_4 = \omega_3 \tag{6.33}$$

$$k_4 = k_3 - 2k_0 \sin\theta \tag{6.34}$$

In this case k_4 may take several forms. According to the magnitude of the k_0 and interference angle θ, k_4 may take the form of the higher order mode propagating in the same direction with k_3. On the other hand, if $2k_0 \sin\theta \gg k_3$, this case may be interpreted as a contradirectional mode coupling as depicted in figure 6.4

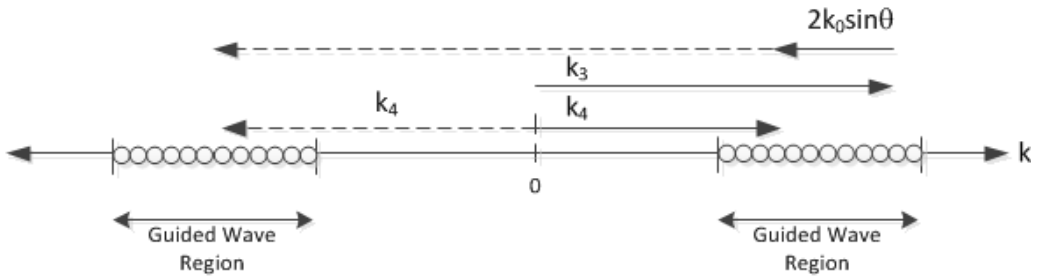

Figure 6.4. Illustration of mode coupling by a transient grating

All of the interaction cases described above can be grouped into three main categories according to the frequency and phase matching conditions. In this classification, described in table 6.1, switching action can be defined as Mode Conversion Switching and Wavelength Conversion Switching according to the resultant interaction. It is not possible to detect the "*Group 3"* interaction from the experimantal studies carried out in this thesis, because the fiber does not allow the propagation of k_4 resulted from the interaction in this group.

Table 6.1. Classification of FWM interaction processes

Group	**Frequency Matching Condition**	**Phase Matching Condition**	**Switching Type**
I	$\omega_4 = \lvert\omega_3\rvert$	$k_4 = k_3 \pm 2k_0 \sin\theta$ $k_4 = -k_3 \pm 2k_0 \sin\theta$	Mode Conversion Switching
II	$\omega_4 = \lvert 2\omega_0 - \omega_3\rvert$	$k_4 = \pm k_3$	Wavelength Conversion Switching
III	$\omega_4 = \lvert 2\omega_0 + \omega_3\rvert$	$k_4 = \pm k_3$	Wavelength Conversion Switching

6.2 Discussion on Optical Switching by Mode Conversion

In the presence of a grating, in general, the coupling of mode with propagation constant β_m into mode with propagation constant β_n occurs when

$$\beta_n \pm \beta_m = \pm p \frac{2\pi}{\Lambda} \tag{6.35}$$

where Λ is the grating period and p is a positive integer number. The propagation constants can be written in terms of effective index n_{eff} as

$$\beta = \frac{2\pi}{\lambda} n_{eff} \tag{6.36}$$

Thus, according the equation (6.35), the resonant Bragg wavelength for reflection and transmission gratings can be generalized by

$$m\lambda_{Bragg} = \left(n_{effm} \pm n_{effn}\right)\Lambda \tag{6.37}$$

where positive and negative signs refer to the reflection and transmission, respectively.

In order to understand the coupling mechanism, the phase matching conditions for aperiodic transient grating was derived in chapter 2, where interaction requirements are given by (2.31), (2.32) and (2.58). Because of lack of analytical solution for the aperiodic structures, the grating function was extended into Fourier series and coupling efficiency was derived. When complete phase matching requirements are satisfied, strong coupling is expected between the fiber modes. However, phase matching requirements may also be satisfied only for some fourier components, which results in a

weak coupling. This weak coupling mechanism is related with the shape (Gaussian-apodized, raised-cosine-apodized, etc.) and length of the transient grating rather than the grating period.

To investigate the optical switching mechanism by means of mode conversion, we used three different laser sources with wavelengths $\lambda_1 = 543\,nm$, $\lambda_2 = 632.8\,nm$ and $\lambda_3 = 852\,nm$. And the grating has been generated by the 532 nm laser source as shown in figure 5.11.

Considering the switching structure, for the source with $\lambda_1 = 543\,nm$, fiber supports two modes with effective indices of $n_{eff01} = 1.4627176$ and $n_{eff11} = 1.4615364$. From the experimental data taken for the setup in figure 5.11, the maximum efficiency is obtained at interference angle of 4.014° which corresponds to the grating period of $2.534\,\mu m$ and the grating length is about 1.1 mm. For the given effective indices and grating period, Bragg wavelength is calculated as $7.41\,\mu m$ for the reflected mode which is far away of the working wavelength λ_1. The coupling mechanism in this interaction can be explained considering the group I classification in table 6.1. This type of the wave interaction is described in "case 3" and "case 8". In this structure weak coupling is observed. Although frequency matching condition is met, phase matching requirement is partially satisfied only for one of the Fourier components ($p = 2$) of the grating which has a spatial frequency of $^{4\pi}/_{Lg}$. For the specified matching condition, mode conversion efficiency of %0.46 has been calculated theoretically which refers to 0.46 nW power variation at fiber output.

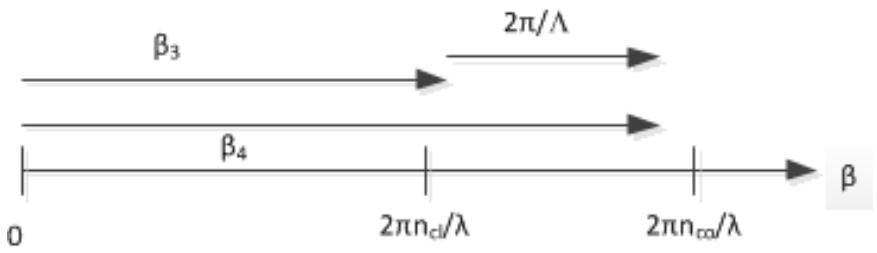

Figure 6.5. Demonstration of coupling using propagation constants

On the contrary, the measured value given in figure 5.13 is 0.336 nW which is in good agreement with theoretical result. Figure 6.5 illustrates the energy coupling of a mode with effective indice n_{eff01} into a mode propagating in the same direction with effective index n_{eff11}.

To continue with another source with wavelength of $\lambda_2 = 632.8\,nm$, the fiber supports two modes $n_{eff01} = 1.4611506$ and $n_{eff11} = 1.4588856$. From the experimental data taken for the setup in figure 5.12, the maximum efficiency is obtained at interference angle of 5.2° which corresponds to the grating period of $1.957\,\mu m$ and the grating length is about 1 mm. For the given effective indices and grating period, Bragg wavelength is $5.715\,\mu m$ for the reflection, which is away of the working wavelength λ_2. This case suits group I processes, described in table 6.1. In theoretical calculations, for $p = 4$ the phase matching condition is satisfied for grating harmonic with frequency $8\pi/L_g$ and node conversion efficiency of 0.27% is obtained, that corresponds to the 0.09 nW power transfer. These theoretical calculations are in good agreement with experimental data where 0.08 nW power varation has been measured.
According to the "case 3" interaction, the fundamental mode propagating in the optical fiber can be coupled or transferred to the higher order modes.

In this experiment, the result of the FWM interaction beween propagating mode and the pump beams was observed as a power increment at the output for certain intersection angle. However, the power transfer among the beams has been observed as an overall power change at the device output because the power of individual modes can not been identified due to practical problems. The mode pattern at far field observation is restricted by pump pulse duration which is too short (nanoseconds) to detect or record by the CCD detector array.

6.3 Discussion on Optical Switching by Wavelength Conversion

In the previous section, the switching efficiency by means of mode conversion results in weak power transfer between modes because phase matching is satisfied only for one of the higher order harmonics of Fourier components of the grating function. Theoretically, for pump wavelength λ_p and interference angle θ, phase matching condition may be satisfied considering the energy transfer between the fundamental

mode and higher order modes $LP_{l\mu}$ $(l > 5)$. Nevertheless, due to practical consideration in our case, the fiber we use supports only LP_{01} and LP_{11} modes and does not allow higher order modes to propagate at given wavelengths. For the two modes supported by the fiber phase matching can be achived at very small angles that the grating is practically ineffective.

On the other hand, if the phase and frequency matching conditions for FWM are satisfied, the coupling between two wavelengths is possible. The strong control pulses with wavelength λ_p forms the grating and two light signals with wavelengths λ_1 and λ_2 are launched into fiber. For each light waves the fundamental mode excitation is ensured. Considering the structure in figure 5.16, the matching conditions given by eq. (6.1) and eq.(6.2) have to be satisfied. This type interaction corresponds the case 2, where two distinct frequencies around the pump frequency and the equal propagation vectors in the cladding as depicted in the case 2 in figure 6.2. The frequency matching condition, given by (6.9) yields the following relation between the wavelengths

$$\lambda_2 = \frac{1}{\frac{2}{\lambda_p} - \frac{1}{\lambda_1}} \tag{6.38}$$

Considering the laser bandwidths given in figure 5.17, using $\lambda_p = 530.6\, nm$ and $\lambda_1 = 663.5\, nm$, λ_2 is calculated as $\lambda_2 = 442.06\, nm$. All of the values are within the measured limits of the laser bandwidths. The process also requires phase matching. Considering the geometry in figure 5.16, the phase matching condition can be written as

$$\overrightarrow{k_{p1}} + \overrightarrow{k_{p2}} = \overrightarrow{k_3} + \overrightarrow{k_4} \tag{6.39}$$

where $k_{p1}$and k_{p2} are the wave vectors of pump beams, k_3 and k_4 are the wave vectors of the source waves. The components of k_{p1} and k_{p2} in the propagation direction of source wave cancel each other that implies

$$k_{3z} = -k_{4z} \tag{6.40}$$

Considering the experimental data taken for the setup given in figure 5.20, we may conclude that as a result of the interaction, two photons with frequency ω_0 are annihilated to create two photon with frequencies ω_3 and ω_4, travelling in opposite directions. This causes decrease in amplitude of wave with wavelenght λ_1 and increase in the amplitude of the wave with wavelength λ_2 as observed in the experimental data.
On the other hand, the situation can also be regarded as a grating assistant coupling, in which the propagating wave is affected by the grating. The grating can be considered as a quasi-stationary due to strong pump power and the interaction turns into the grating assisted coupler where the coupling is realized given the following condition

$$\beta_4 \pm \beta_3 \pm m\frac{2\pi}{\Lambda} = 0 \tag{6.41}$$

where Λ is the grating period, $\beta_3 = |k_{3z}|$ and $\beta_4 = |k_{4z}|$ are propagation constant of the source wave and m is an integer number.

From to the experimental data shown in figure 5.20, there is a power transfer from signal λ_1 to signal with wavelength λ_2 and this process occurs only when grating

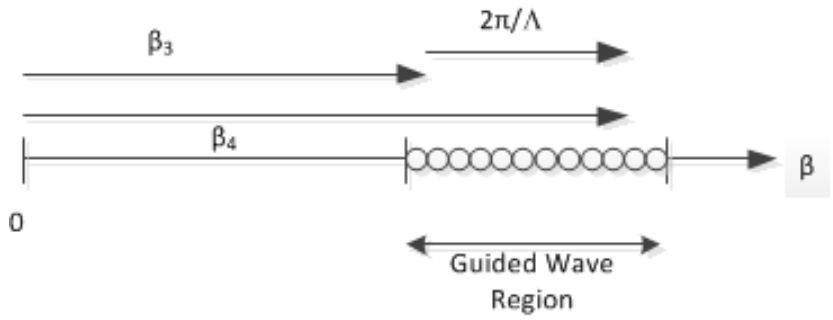

Figure 6.6. Demonstration of coupling with transient grating

period Λ=1.543 μm. For m=2 the phase matching condition given by (6.22) is satisfied and illustrated in figure 6.6.

In general, the experimental results are in good agreement with the expectation of the mathematical model proposed in this thesis. Also, the device has proved that it functions as an all-optical switch and further as an router for potential implementation in future all-optical networks.

CHAPTER 7

CONCLUSION

This thesis has been demonstrated proof-of-concept in-fiber all optical switching device controlled by a transient grating formed in the evanescent region of the fiber. This study consists of two parts; in the first part mathematical model has been developed and subsequently, experimental verification of the model has been provided.

In the theoretical part, the introduced switching structure has been analyzed with FWM and Coupled Mode Theory. The simulations presented for the mathematical model shows that 67% mode power coupling can be achieved without critical length adjustment under perfect phase matching condition. However, for the lack of phase matching, the power coupling is around 33 %. The model used in the simulations also shows that the phase matching can be tuned to match by means of the total power of the grating forming beams. When the device performance is compared with transient sinusoidal grating, the proposed device performs better both at low and high nonlinear susceptibilities. Furthermore, its transmission characteristic does not exhibit oscillation at all, which confirms inessentiality of the critical length.

In the experimental part of the thesis, firstly, polymeric materials have been investigated for their material properties and characterized for absorption and third order optical nonlinearity. The ultrafast switch has been fabricated using highly nonlinear material, PVA doped MR films, with low absorption at 532 nm and fast response time. The linear refractive index and Kerr coefficient of PVA doped MR was measured as 1.4995 and $n_2 = -4.02 \times 10^{-11}\ {}^{cm^2}/_{W}$, respectively. To prove the capability of the material as a switching device layer, laser induced gratings were formed and diffraction ability of the dynamic gratings is characterized using pump probe technique. Solution consisting of 9.09% w/v PVA and 0.018% w/v MR was found to be the most suitable mixture as a polymeric film layer by providing nearly 10% diffraction efficiency in pump probe experiment.

The successful switching structure that has been firstly demonstrated in this thesis is the coupler based all optical switch/modulator. Ultrafast cladding index

modulation has been realized by means of direct beam application on the nonlinear material, which results in power transfer from propagating mode into radiation modes. The modulating capability of the system has also been proved. However, the efficiency is very sensitive to linear refractive index of the polymer; thus, the structure needs optimization in terms of polymeric material refractive index and buffer thickness to increase the modulation contrast at the device output. The second system that has been fabricated is the all optical coupler based switch. This device relies on the power coupling between propagating modes where the coupling process is regulated by the phase and frequency matching specifications of FWM interaction. In this structure the interaction of pump beams forms a dynamic transient grating that has an effect of a stationary grating. The influence of the laser induced grating parameters on the power transfer capability of the system has been observed.

Finally, a novel ultrafast wavelength switch has been fabricated. By generating an interaction in the nonlinear cladding region, the wavelength switching/routing principle of the device based on FWM interactions has been verified. This observation proved the dynamic switching capability of the dynamic transient gratings in optical fiber devices.

Considering the all optical switching device, setting the optimal structure parameters is very important in terms of minimum power requirement, switching response time and switching efficiency. Switching power is crucial for Kerr-type nonlinear integrated optical switching devices when the optical control signal is not very strong. However, for the minimum power requirement it is not easy to give a rate at that point since only the fraction of the pump power is usefully involved into the operation. The switching response time fundamentally depends on the nonlinear material response time which is in the order of femtoseconds for Kerr-type nonlinear materials due to electronic transitions; therefore the switching time is virtually limited only by material excitation dynamics. Finally, the complete device operation may need some other components to be integrated such as addres extracter, spectral filter, optical buffer, etc.

This type of a device seems especially promising for all-optical network switches, routers and DWDM devices, where the optical packets need to be switched or routed in fiber among a few output ports. This study has mostly consantrated on provement of the principle and it needs optimization for the better performans before practical applications.

The dynamical nature of the device operation makes it attractive for many other applications such as light-by-light switch that may also be regarded as an counterpart of the transistor in the electronics. This makes the device very attractive for applications like tunable filters; add/drop channels for DWDM and wavelength recognizing switching, etc.

REFERENCES

[1] R. Driad, R. E. Makon, V. Hurm et al., "INP DHBT-based ICs for 100 Gbit/s data transmission," in the International Conference on Indium Phosphide and Related Materials (IPRM '08), May 2008.

[2] T. S. El-Bawab, Optical Switching. New York: Springer, 2006.

[3] G. P. Agrawal, Lightwave Technology: components and Devices. Wiley-Interscience, 2004.

[4] S. A. Haque, J. Nelson, "Toward Organic All-Optical Switching," Science, Vol. 327, No. 5972, pp.1466-1467, Mar. 2010.

[5] A. M. C. Dawes, D. J. Gauthier, S. Schumacher, N. H. Kwong, R. Binder, and A. L. Smirl, "Transverse optical patterns for ultra-low-light level all-optical switching," Laser & Photon. Rev., 2009.

[6] V. Lal, M.L. Masanovic, J.A. Summers, G. Fish, and D.J. Blumenthal, "Monolithic Wavelength Converters for High-Speed Packet-Switched Optical Networks," IEEE Journal of Selected Topics in Quantum Electronics, vol. 13, No. 1, Jan/Feb. 2007.

[7] A. Martinez et al., "Ultrafast All-Optical Switching in a Silicon-Nanocrystal-Based Silicon Slot Waveguide at Telecom Wavelengths," Nano Lett. , vol. 10, pp. 1506-1511, 2010.

[8] A.Y. Elezzabi, Z. Han, S. Sederberg, and V. Van, "Ultrafast all-optical modulation in silicon-based nanoplasmonic devices", Optics Express, Vol. 17, No. 13, 2009.

[9] L. Liu, R. Kumar, K. Huybrechts, T. Spuesens, G. Roelkens, E. J. Geluk, T. de Vries, P. Regreny, D. Van Thourhout, R. Baets, G. Morthier, "An ultra-small, low-power, all-optical flip-flop memory on a silicon chip", Nature Photonics 4, 2010.

[10] I.V. Kabakova, B. Corcoran, J.A. Bolger, C.M. de Sterke, and B.J. Eggleton, "All-optical self-switching in optimized phase-shifted fiber Bragg grating," Optics Express, Vol. 17, No. 7, Mar. 2009.

[11] I. Glesk, P. Bock, P. Cheben, J. Schmid, J. Lapointe, and S. Janz, "All-optical switching using nonlinear subwavelength Mach-Zehnder on silicon," Opt. Express 19, 14031-14039, 2011.

[12] B.E.A. Saleh and M.C. Teich, Fundamentals of photonics. Wiley & Sons, 2007.

[13] N. Chen, B. Yun, Y. Cui, "Cladding index modulated fiber grating," Optics Communications, vol. 259, 2006.

[14] T. Schneider, D.Wolfframm, J. Reif, "Ultrafast laser–induced index grating in transparent insulators," Nuclear Instruments and Methods in Physics Research

Section B, Beam Interactions with Materials and Atoms, vol. 166-167, pp. 809-814, May. 2000.

[15] H. T. Hsieh et. Al., "Femtosecond holography in lithium niobate crystals," Opt. Lett., vol. 30, 2005.

[16] T. Schneider et. Al., "Ultrafast optical switching by instantaneous laser–induced grating formation and self-diffraction in barium fluoride," Applied Physics B Lasers and Optics, vol. 68, issue 4, pp. 749-751, Apr. 1999.

[17] B. J. Eggleton, R. E. Slusher, J. B. Judkins, J. B. Stark, and A. M. Vengsarkar, "All-optical switching in long-period fiber gratings," Opt. Lett., vol. 22, issue 12, pp. 883-885, Jun. 1997.

[18] K.O. Hill, B. Malo, K.A. Vineberg, F. Bilodeau, D.C. Johnson, L. Skinner, "Efficient mode conversion in telecommunication fibre using externally written gratings," IEEE Electronics Letters, 1990.

[19] P. Poornesh, P.K. Hegde, G. Umesh, M.G. Manjunatha, K.B. Manjunatha, A. V. Adhikari , "Nonlinear optical and optical power limiting studies on a new thiophene-based conjugated polymer in solution and solid PMMA matrix," Optics & Laser Technology, vol. 42, pp. 230-236, 2010.

[20] R.W Boyd, Nonlinear Optics. San Diego, CA: Academic Press, 1992.

[21] A. Yariv, "Coupled-mode theory for guided-wave optics," IEEE J. of Quantum Electronics, Vol. QE-9, issue 9, pp. 919, Sep. 1973.

[22] M. S. Dinleyici, O. Akin, "3-D Switching Fabric Node Design," Proc. of IASTED Communication Systems and Networks (CSN 2004), September 1-3, 2004, Spain.

[23] M. Yamada and K. Sakuda, "Analysis of almost-periodic distributed feedback slab waveguides via a fundamental matrix approach," Appl. Opt., vol. 26, pp. 3474-3478, 1987.

[24] K. A. Winick, "Effective-index method and coupled-mode theory for almost-periodic waveguide gratings: a comparison," Appl. Opt., vol. 31, issue 6, 1992.

[25] E. Peral and J. Capmany, "Generalized Bloch wave analysis for fiber and waveguide gratings," Journal of Lightwave Technology, vol. 15, issue 8, 1997.

[26] L. A. Weller-Brophy and D. G. Hall, "Analysis of waveguide gratings: application of Rouard's method," J. Opt. Soc. Am. A, vol. 2, issue 6, pp. 863-871, June 1985.

[27] A. E. Siegman, "Bragg diffraction of a Gaussian beam by a crossed-Gaussian volume grating," J. Opt. Soc. Am., vol. 67, issue 4, pp. 545-550, Apr. 1977.

[28] A Kulagin et al., "Components of the third-order nonlinear susceptibility tensors in KDP, DKDP and LiNbO nonlinear optical crystals," Quantum Electronics, vol. 34, issue 7, pp. 657, Jul. 2004.

[29] X. Zhan, Y. Liu, D. Zhu, X. Liu, G. Xu, P. Ye, “Large third-order nonlinear optical response of a conjugated copolymer consisting of 2,5-diethynylthiophene and carbazole units,” Chemical Physics Letters, Vol. 343, issue 5-6, Aug. 2001.

[30] L. Brzozowski, E. H. Sargent, “Azobenzenes for photonic network applications: Third order nonlinear optical properties,” Journal of Materials Science: Materials in Electronics, vol. 12, 2001.

[31] T. He, Y. Cheng, Y. Du, Y. Mo, “Z-scan determination of third-order nonlinear optical nonlinearity of three azobenzenes doped polymer films,” Optics Communications, Volume 275, Issue 1, 1 July 2007.

[32] Ortuno et. al, “Optimization of a 1 mm thick PVA/Acrylamide recording material to obtain holographic memories: method of preparation and holographic properties,” Appl. Phys. B 76, 851-857, 2003.

[33] A. Sabatyan and M. T. Tavassoly "Application of Fresnel diffraction to nondestructive measurement of the refractive index of optical fibers", Opt. Eng. 46(12), 128001, December 18, 2007.

[34] M. S. Dinleyici, C. Sümer, “Characterization and estimation of refractive index profile of laser-written photopolymer optical waveguides”, Optics Communications, Volume 284, Issue 21, 1 October 2011.

[35] M. Sheik-Bahae, A.A. Said, T.-H. Wei, D.J. Hagan, E.W. Van Stryland, "Sensitive measurement of optical nonlinearities using a single beam," Quantum Electronics, IEEE Journal of , vol.26, no.4, pp.760-769, Apr. 1990.

[36] S.L Gomez, F.L.S. Cuppo, A.M. Figueiredo Neto, “Nonlinear optical properties of liquid crystals probed by Z-scan technique,” Braz. J. Phys., vol.33, n.4, 2003.

[37] “Z-Scan for the Characterization of Transparent Optical Materials”, Newport Application Note.

[38] M. H. Nayfeh, G. Belomoin, N. Barry, O. Akcakir, “Silicon nanoparticle microcrystal nonlinear optical devices”, US Patent No: 6456423, 2000

[39] A Stampanoni-Panariello, B Hemmerling, W Hubschmid, “Electrostrictive generation of nonresonant gratings in the gas phase by multimode lasers”, Physical Review A, 51(1), 655-662, 02/1995.

[40] P. Günter, Nonlinear Optical Effects and Materials, Springer Series in Optical Sciences, 2000

[41] B. Sturman et al., “Femtosecond recording and time-resolved readout of spatial gratings in lithium niobate crystals”, J. Opt. Soc. Am. B, Vol. 24, No. 3, 2007.

[42] Dinleyici, M. S., and Patterson, D. B., “Vector Modal Solutions of Evanescent Couplers", IEEE/OSA Journal of Lightwave Technology, Vol. 15, No. 12, pp. 2316, 1997.

[43] L. N. Binh, S. Zheng, “Generalized analysis of nonlinear optical guided-wave coupled systems”, J. Opt. Soc. Am. B., Vol. 18, No. 11, November 2001.

[44] C. H. Lee, C. Kim, J. H. Park, S. W. Kang, “Light-Coupling Characteristics of a Fiber-Slab Coupler Using a Buffer Layer Based on Coupled-Mode Theory”, Journal of the Korean Physical Society, vol. 54, issue 2, p. 603, 2008.

[45] C. Kim, H. Cherl, J. H. Park; D. M. Choi, “Optimization of the Buffer Layer of a Side-polished Fiber-slab Coupler Based on 3-D Alternating Direct Implicit Beam Propagation Method”, Journal of the Korean Physical Society, vol. 56, issue 11, p. 329, 2009.

[48] M. Cooper, S. Mookherjea, "Numerically-assisted coupled-mode theory for silicon waveguide couplers and arrayed waveguides," Opt. Express 17, 1583-1599 (2009).

[49] S. Tseng, C. Chen, "Side-polished fibers," Appl. Opt. 31, 3438-3447 (1992)

[50] C. Vassallo, “Rigorous theory for modes of optical fibers with cladding limited by a plane,” 22, p. 944–945 (1986)

[51] T. Erdogan, "Fiber grating spectra," Lightwave Technology, Journal of, vol.15, no.8, pp.1277-1294, 1997.

[52] M. Samoc, A. Samoc, B. Luther-Davies, Z. Bao, L. Yu, B. Hsieh, and U. Scherf, "Femtosecond Z-scan and degenerate four-wave mixing measurements of real and imaginary parts of the third-order nonlinearity of soluble conjugated polymers," J. Opt. Soc. Am. B 15, 817-825 (1998).

[53] G. Boudebs, F. Sanchez, C. Duverger, B. Boulard, “Improvement of Mach–Zehnder interferometry technique for third-order susceptibility measurement,” Optics Communications, Volume 199, Issues 1–4, 15 November 2001.

[54] R. Volle, V. Boucher, K.D. Dorkenoo, R. Chevalier, X. Nguyen Phu, “Local polarization state observation and third-order nonlinear susceptibility measurements by self-induced polarization state changes method,” Optics Communications, Volume 182, Issues 4–6, 15 August 2000.

[55] H. J. Eichler, P. Gunter, D.W. Pohl, Laser-induced dynamic gratings, Springer-Verlag, Berlin ; New York, 1986.

[56] S. Hvilsted, C. Sánchez, Rl Alcalá, “The volume holographic optical storage potential in azobenzene containing polymers,” J. Mater. Chem., 19, 2009.

[57] Y. Enami, J. Hong, C. Zhang, J. Luo, A. K. Jen, "Optical Transmission Stability of Hybrid Sol–Gel Silica/Electrooptic Polymer Waveguide Modulators," Photonics Technology Letters, IEEE , vol.23, no.20, 2011.

VITA

Osman Akın was born in Kırcaali, Bulgaria on April 20, 1977. He received his Bachelor of Science degree in Electrical and Electronics Engineering from Ege Univeristy in 2001. He earned his MSc degree in Electronics and Communications Engineering from Izmir Institute of Technology, Izmir, Turkey in 2005. He received a Ph.D. in Electronics and Communications Engineering from Izmir Institute of Technology in December 2012.